Analysis and modeling of the behavior of hydrogels-based systems for biomedical and agro-food applications

Diego Caccavo

Unione Europea

UNIVERSITÀ DEGLI
STUDI DI SALERNO

Department of Industrial Engineering

Ph.D. Course in Industrial Engineering

(XV Cycle-New Series)

ANALYSIS AND MODELING OF THE BEHAVIOR OF HYDROGELS-BASED SYSTEMS FOR BIOMEDICAL AND AGRO-FOOD APPLICATIONS

Supervisor
Prof. Gaetano Lamberti

Ph.D. student
Diego Caccavo

Scientific Committee
Prof. Anna Angela Barba
Prof. Anette Larsson
Prof. Juergen Siepmann

Ph.D. Course Coordinator
Prof. Ernesto Reverchon

If the facts don't fit the theory, change the facts.

(Albert Einstein)

Table of Content

List of Figures

List of Tables

List of Publications

Journal papers concerning these activities:

ABRAHMSEN-ALAMI, S., **CACCAVO, D.**, LAMBERTI, G., BARBA, A. A., VIRIDÉN, A. & LARSSON, A. **2015**. Hydrogel-based drug delivery systems (HB-DDSs): a combined experimental-modeling approach AstraZeneca Internal Journal.

CACCAVO, D., CASCONE, S., LAMBERTI, G. & BARBA, A. A. **2015**. Controlled drug release from hydrogel-based matrices: Experiments and modeling. International Journal of Pharmaceutics, 486, 144-52.

CACCAVO, D., CASCONE, S., LAMBERTI, G. & BARBA, A. A. **2015**. Modeling the Drug Release from Hydrogel-Based Matrices. Molecular Pharmaceutics, 12, 474-483.

CACCAVO, D., CASCONE, S., LAMBERTI, G., BARBA, A. A. & LARSSON, A. **2017**. Drug delivery from hydrogels: a general framework for the release modeling Current Drug Delivery, 14 (2), 179-189.

CACCAVO, D., CASCONE, S., POTO, S., LAMBERTI, G. & BARBA, A. A. **in press**. Mechanical and transport phenomena in agarose-based hydrogels studied by compression-relaxation tests. Carbohydrate Polymers, doi: 10.1016/j.carbpol.2017.03.027.

CACCAVO, D. & LAMBERTI, G. **2017**. PoroViscoElastic model to describe hydrogels' behavior. Materials Science and Engineering: C, 76, 102–113.

CACCAVO, D., LAMBERTI, G., BARBA, A. A., ABRAHMSÉN-ALAMI, S., VIRIDÉN, A. & LARSSON, A. **submitted**. Effects of HPMC substituent pattern on water up-take, polymer and drug release; an experimental and

modelling study. European Journal of Pharmaceutical Sciences.

CACCAVO, D., CASCONE, S., LAMBERTI, G., BARBA, A. A. & LARSSON, A. **2016**. Swellable Hydrogel-based Systems for Controlled Drug Delivery. In: SEZER, A. D. (ed.) Smart drug delivery system, Intech.

Conference proceedings concerning these activities:

CACCAVO, D., CASCONE, S., LAMBERTI, G. & BARBA, A. A. Experimental and modeling description of hydrogel-based controlled release systems. 10TH WORLD MEETING on Pharmaceutics, Biopharmaceutics and Pharmaceutical Technology, **2016** Glasgow, United Kingdom.

CACCAVO, D., CASCONE, S., LAMBERTI, G. & BARBA, A. A. Mathematical modeling of hydrogels' poro-visco-elastic behavior. GRICU MEETING 2016, **2016** Anacapri (NA), Italy. 1-4.

CACCAVO, D., APICELLA, P., CASCONE, S., DALMORO, A., LAMBERTI, G. & BARBA, A. A. Hydrogels-based systems for controlled release in agricultural applications 42nd Annual Meeting & Exposition of the Controlled Release Society, **2015** Edinburgh, United Kingdom. 1-1.

CACCAVO, D., CASCONE, S., BOCHICCHIO, S., LAMBERTI, G., DALMORO, A. & BARBA, A. A. Hydrogels-based matrices behavior: experimental and modeling description 42nd Annual Meeting & Exposition of the Controlled Release Society, **2015** Edinburgh, United Kingdom. 1-1.

CASCONE, S., **CACCAVO, D.**, LAMBERTI, G., TITOMANLIO, G., D'AMORE, M. & BARBA, A. A. MODELING THE BEHAVIOR OF SWELLABLE HYDROGELS-BASED MATRICES FOR PHARMACEUTICAL APPLICATIONS 13th European Symposium on Controlled Drug Delivery, **2014** Egmond aan Zee, The Netherlands. ESCDD 3-4.

CACCAVO, D., CASCONE, S., LAMBERTI, G. & BARBA, A. A. Testing and modelling of hydrogels behavior for pharmaceutical and biomedical applications. Proceedings of CHISA **2014**, 2014 Prague, Czech Republic. CHISA 2014, 1-1.

CACCAVO, D., CASCONE, S., LAMBERTI, G. & BARBA, A. A. Hydrogel-Based CRSs Analyses: Testing And Modeling. 1st International Congress of Controlled Release Society - Greek Local Chapter, **2015** Athens (Greece). 1st International Congress of Controlled Release Society, 1-1.

Other publications:

BARBA, A. A., CASCONE, S., **CACCAVO, D.**, LAMBERTI, G., CHIARAPPA, G., ABRAMI, M., GRASSI, G., GRASSI, M., TOMAIUOLO, G., GUIDO, S., BRUCATO, V., CARFÌ PAVIA, F., GHERSI, G., LA CARRUBBA, V., ABBIATI, R. A. & MANCA, D. **in press**. Engineering approaches in siRNA delivery. *International Journal of Pharmaceutics*, doi: 10.1016/j.ijpharm.2017.02.032.

BARBA A.A, BOCHICCHIO S., DALMORO A., **CACCAVO D.**, CASCONE S., LAMBERTI G., **submitted**. Polymeric and lipid-based systems for controlled drug release: an engineering point of view, Pharmaceutical Nanotechnology, Volume IX: Sustained and controlled delivery systems.

CACCAVO, D., CASCONE, S., AMOROSO, M. C., APICELLA, P., LAMBERTI, G. & BARBA, A. A. **2015**. Hydrogel-based Granular Phytostrengtheners for Prolonged Release: Production and Characterization. Chemical Engineering Transaction, 44, 235-240.

CACCAVO, D., CASCONE, S., APICELLA, P., LAMBERTI, G. & BARBA, A. A. **submitted**. HPMC-based granules for prolonged release of phytostrengtheners in agriculture, Chemical Engineering Communications.

CACCAVO, D., CASCONE, S., LAMBERTI, G., DALMORO, A. & BARBA, A. A. **in press**. Modeling of the behavior of natural polysaccharides hydrogels for bio-pharma applications. Natural Product Communications.

CACCAVO, D., LAMBERTI, G., CAFARO, M. M., BARBA, A. A., KAZLAUSKE, J. & LARSSON, A. **in press**. Mathematical modeling of the drug release from an ensemble of coated pellets. British Journal of Pharmacology, doi: 10.1111/bph.13776.

CACCAVO, D., LAMBERTI, G., CASCONE, S., BARBA, A. A. & LARSSON, A. **2015**. Understanding the adhesion phenomena in carbohydrate-hydrogel-based systems: Water up-take, swelling and elastic detachment. Carbohydrate Polymers, 131, 41-49.

CACCAVO, D., STRÖM, A., LARSSON, A. & LAMBERTI, G. **2016**. Modeling capillary formation in calcium and copper alginate gels. Materials Science and Engineering: C, 58, 442-449.

CASCONE, S., APICELLA, P., **CACCAVO, D**., LAMBERTI, G., BARBA, A. A., **2015**, Optimization of Chelates Production Process for Agricultural

Administration of Inorganic Micronutrients, Chemical Engineering Transaction, 44, 217-222.

CHIARAPPA, G., GRASSI, M., ABRAMI, M., ABBIATI, R. A., BARBA, A. A., BOISEN, A., BRUCATO, V., GHERSI, G., **CACCAVO, D.**, CASCONE, S., CASERTA, S., ELVASSORE, N., GIOMO, M., GUIDO, S., LAMBERTI, G., LAROBINA, D., MANCA, D., MARIZZA, P., TOMAIUOLO, G. & GRASSI, G. **2017**. Chemical Engineering in the "BIO" world. Current Drug Delivery, 14 (2), 158-178.

LAMBERTI, G., BARBA, A. A., CASCONE, S., DALMORO, A. & **CACCAVO, D. 2016**. An Engineering Point of View on the Use of the Hydrogels for Pharmaceutical and Biomedical Applications. In: MAJEE, S. B. (ed.) Emerging Concepts in Analysis and Applications of Hydrogels. Intech.

KAZLAUSKE, J., CAFARO, M. M., **CACCAVO, D.**, MARUCCI, M. G., LAMBERTI, G., BARBA, A. A. & LARSSON, A. **submitted**. Determination of the release mechanism of Theophylline from pellets coated with Surelease - a water dispersion of Ethyl cellulose. International Journal of Pharmaceutics.

Abstract

Hydrogels are three-dimensional, hydrophilic, polymeric networks capable of imbibing large amounts of water or biological fluids. Depending on the type of polymer, number of cross-links, presence of ionic species the swelling/shrinking behavior can be greatly modified. This peculiar behavior, which has led to define this soft matter as "smart materials", makes hydrogels and hydrogel-based systems very attractive by several frontier fields, such as biomedical applications, as well as for sectors that are less demanding technology, i.e. agro-food applications.

The general aim of this Ph.D. thesis is to analyze, with ad hoc experiments, and to describe/simulate, through mathematical modeling, the behavior of hydrogels and hydrogel-based systems.

A first question to answer when approaching hydrogels is: "are they multiphasic or monophasic systems"? The answer cannot be taken for granted. Despite in most experimental cases the response is simply avoided, it become fundamental when the aim is to develop a mechanistic mathematical model of the system. The most natural approach is to consider hydrogels as single-phase matter, in which several components can coexist, like it would be indisputably done for polymeric solutions (hydrosols). Another vision is to consider hydrogels as made of different phases, i.e. the water phase is separated from the polymeric phase, and these can exchange momentum. During this work a general modeling framework has been proposed to which several models from literature, multiphasic or monophasic, can be traced back or, vice versa, depending on the chosen approach the framework can be particularized to give the multiphasic or the monophasic balance equations. In this thesis, in light of its thermodynamic and numerical robustness, the monophasic approach, which is more consistent, has been chosen.

Another important question is related to the need of modeling/analyze the full behavior, mass transport plus mechanics, or just one aspect, mass transport only. The difficulties related to the solution/analysis of the full hydrogels behavior have led many researchers to describe hydrogel-based systems with a "mass transport only" approach. This is, in example, common in drug delivery applications. During this PhD a mechanistic model based on a "mass

transport only" approach for drug release from hydrogel-based system has been developed and validated against experimental data. HPMC-based tablets, loaded with Theophylline have been studied. Differently to what is normally done in dissolution tests, in this work besides the evaluation of the drug release via spectrophotometric analysis, the water and polymer residue have been determined by gravimetric analysis. This has been done on the entire tablets, as well as on portion of them, obtaining internal profiles of the components. The partially swollen tablets have been also subjected to indentation tests, which after an opportune calibration have allowed obtaining information on the water distribution inside the system. A 2D-axisymmetric model has been built on the water and drug mass transport equations; the polymer has been obtained from the mass fraction constraint. The deformations have been described with an ALE moving mesh method, whose boundaries move in relation to the amount of water and drug entering or leaving the system. The comparison between the detailed experimental results and the modeling results has shown a good agreement, in terms of masses, shape and components distribution, demonstrating that the main features had been correctly described.

Such a formulated model has been applied to describe commercial-like tablets (in which excipients were present), with two type of HPMC with different substitution pattern (i.e. different degree of cross-links) and tested in non-standard apparatus (NMR cell). Despite after a proper tuning the model has been able to describe the drug and polymer release, the shape and the water distribution inside the system (experimentally taken from MRI technique) have not been correctly described. This application demonstrated the limits of a "mass transport only" approach. In the analyzed case the forces acting on the swelling tablet (shear, centrifugal, gravitational) could have a relevant impact, but most of all the different degree of cross-links of the HPMC played the major role.

In order to consider the hydrogel mechanics, the pure hydrogel behavior has been studied. Hydrogels normally couple solvent mass transport to system deformation and vice versa. This phenomenon is generally called poroelasticity and it is characteristic also of other materials (i.e. biological tissues, soils etc.). Another peculiarity of hydrogels is that the constituent polymeric network can have viscoelastic characteristics (i.e. like polymeric melts), which eventually translate in an overall hydrogel viscoelastic behavior. Depending on the time interval of interest and on the characteristic times of relaxation and diffusion, hydrogels can behave viscoelastically, poroelastically or poroviscoelastically (when the diffusion time is comparable with the relaxation time). A 3D model describing the poroviscoelastic behavior of hydrogels, still scarcely implemented in literature, has been developed within the field of non-equilibrium thermodynamics and non-linear solid mechanics (large deformations) and implemented in a commercial FEM-

based software. The results of such kind of model permit to discriminate between and to study the poroelastic and viscoelastic regime as well as it permits to study the poroviscoelastic behavior. Experimental unconfined stress-relaxation tests have been performed on agarose-gels at different concentrations with radius and height of 1 cm, and imposing a deformation of 10%. In the time range analyzed (1200 s) the agarose-gel has shown a predominant viscoelastic behavior, releasing only little amount of water. The model, after an initial tuning of the parameters, has been able to fairly predict the experimental data. Characteristic of the developed approach is that, once the model parameters are derived, it is possible to describe the hydrogel subjected to different stimuli (mechanicals or chemicals).

The proposed poroviscoelastic model is extendable to multicomponent diffusion systems, which could be, in example, controlled release systems based on hydrogels. For the first time, to the author's knowledge, in the hydrogel-based systems modeling literature, in this thesis it has been shown how to extend the poroviscoelastic model to consider the presence of another diffusing species. The transport and constitutive model equations, opportunely modified, have been implemented in a commercial FEM-based software and, as an example, the drug release from a swelling system has been reported.

Sommario

Gli idrogel sono dei reticoli polimerici idrofilici tridimensionali capaci di assorbire grosse quantità di acqua o di fluidi biologici. A seconda del tipo di polimero, numero di reticolazioni, presenza di specie ioniche, la capacità di rigonfiamento/restringimento può essere ampiamente modificata. Questo peculiare comportamento, che ha portato a definire questi materiali morbidi come "materiali intelligenti", rende gli idrogel e i sistemi basati su idrogel molto attraenti per diversi settori di frontiera, come per applicazioni biomedicali, così come per settori non altamente tecnologici, in esempio applicazioni agro-alimentari.

Lo scopo generale di questa tesi di dottorato è l'analisi, con esperimenti ad hoc, e la descrizione/simulazione, attraverso la modellazione matematica, del comportamento di idrogel e sistemi basati su idrogel.

Una prima domanda da porsi quando si approcciano questi materiali è: "sono dei sistemi multifasici o monofasici?". La risposta non è scontata. Sebbene in molti studi sperimentali chiarire questo aspetto non è di fondamentale importanza, quando lo scopo è sviluppare un modello meccanicistico la risposta diviene fondamentale. L'approccio più naturale è quello di considerare l'idrogel come un materiale a singola fase, in cui più specie possono coesistere, così come sarebbe fatto per una soluzione polimerica (idrosol). Un'altra visione consiste nel considerare l'idrogel come un sistema multifasico, per esempio la fase liquida acquosa è separata dalla fase solida polimerica, e queste possono scambiare momento. Durante questo lavoro un *framework* generale per la modellazione di sistemi basati su idrogel è stato proposto, al quale possono essere ricondotti diversi lavori di letteratura o, viceversa, a seconda dell'approccio scelto il *framework* può essere particolarizzato per dare le equazioni di bilancio per un sistema multifasico o monofasico. In questa tesi è stato adottato un approccio monofasico date le sue forti basi termodinamiche e la sua robustezza numerica.

Un'altra domanda importante è correlata al bisogno di modellare/analizzare il comportamento completo, trasporto di massa e meccanica, o solo un aspetto, il solo trasporto di massa. Sebbene questa domanda da un punto di vista puramente teorico non avrebbe senso, le difficoltà legate alla soluzione/analisi del comportamento "completo" dell'idrogel hanno portato molti ricercatori a descrivere questi sistemi con approcci basati sul solo trasporto di massa. Questo è, ad esempio, molto

comune in applicazioni di sistemi di rilascio di farmaci basati su idrogel. Durante questo lavoro di dottorato un modello meccanicistico basato sul "solo trasporto di massa" è stato sviluppato, implementato e validato contro dati sperimentali. Sono state studiate compresse di HPMC caricate con teofillina. Differentemente da quanto fatto nei normali test di dissoluzione, in questo lavoro oltre alla valutazione del rilascio di farmaco attraverso analisi spettrofotometrica, sono state anche determinate le quantità di acqua e polimero nella compressa attraverso analisi gravimetriche. Questo è stato fatto su compresse intere, così come su loro porzioni, ottenendo i profili interni di concentrazione dei componenti. Le compresse parzialmente rigonfiate sono state sottoposte a prove di indentazione che, dopo un opportuna calibrazione, hanno consentito di ottenere informazioni sulla distribuzione di acqua all'interno del sistema. Il modello 2D-assialsimmetrico è stato costruito sulle equazioni di trasporto di acqua e farmaco; il polimero è stato ottenuto dal vincolo sulle frazioni massiche. La deformazione è stata descritta con un metodo a *mesh* mobile ALE, i cui contorni si muovono in relazione alla quantità di acqua e farmaco entrante/uscente dal sistema. Il confronto tra i risultati sperimentali e di modellazione ha mostrato un buon accordo, in termini di massa, forma e distribuzione dei componenti, dimostrando che le principali caratteristiche erano state correttamente descritte.

Il modello così formulato è stato utilizzato per descrivere il comportamento di compresse simil-commerciali (in cui sono presenti eccipienti), con due tipi di HPMC con differente distribuzione di reticolazioni, e testate in apparati non standard (NMR cell). Sebbene dopo un opportuna messa a punto iniziale il modello sia stato capace di descrivere il rilascio di farmaco e polimero, la forma e la distribuzione di acqua nel sistema (valutata sperimentalmente con la tecnica MRI) non sono state correttamente descritte. Questa applicazione ha dimostrato i limiti dell'approccio modellistico basato sui soli bilanci di massa. Nei casi analizzati, le forze agenti sulla compressa rigonfiata (di taglio, centrifuga, gravitazionale) potrebbero avere impatti rilevanti ma, più di tutti il diverso grado di reticolazione dell'HPMC può giocare il ruolo fondamentale.

Allo scopo di considerare la meccanica dell'idrogel, è stato studiato il comportamento di idrogel puri. Gli idrogel normalmente accoppiano il trasporto di solvente con la deformazione del sistema, e viceversa. Questo fenomeno è generalmente chiamato "poroelasticità", ed è caratteristico anche di altri materiali (ad esempio tessuti biologici, terreni, etc.). Un'altra peculiarità degli idrogel è che le catene polimeriche possono presentare caratteristiche viscoelastiche (ad esempio come i fusi polimerici), che eventualmente si traduce in un comportamento viscoelastico dell'idrogel. A seconda dell'intervallo temporale di interesse e dei tempi caratteristici di rilassamento e diffusione, gli idrogel possono comportarsi in maniera viscoelastica, poroelastica o poroviscoelastica (quando il tempo di diffusione è comparabile con il tempo di rilassamento). Un modello 3D capace di

descrivere il comportamento poroviscoelastico degli idrogel, ancora scarsamente implementato in letteratura, è stato sviluppato all'interno del campo della termodinamica di non-equilibrio e la meccanica non lineare dei solidi (grosse deformazioni) e implementato in un software commerciale basato sull'analisi FEM. I risultati di questo tipo di modello permettono di discriminare e studiare il comportamento poroelastico, viscoelastico così come il comportamento poroviscoelastico. Prove sperimentali di compressione-rilassamento sono state effettuate su gel cilindrici di agarosio a differenti concentrazioni, con raggio e altezza di 1 cm, e imponendo una deformazione del 10%. Nell'intervallo temporale analizzato (1200 s) i gel di agarosio hanno mostrato un predominante comportamento viscoelastico, rilasciando solo piccole quantità di acqua. Il modello, dopo una messa a punto iniziale dei parametri, è stato capace di predire ragionevolmente i dati sperimentali. Caratteristica dell'approccio modellistico utilizzato è che, una volta derivati i parametri, è possibile descrivere l'idrogel sottoposto a differenti stimoli (meccanici e chimici).

Il modello poroviscoelastico proposto è estendibile a sistemi con multiple specie diffondenti, che potrebbero essere ad esempio i sistemi di rilascio controllato basati su idrogel. Per la prima volta, a conoscenza dell'autore, nella letteratura di modellazione dei sistemi basati su idrogel, in questa tesi è stato mostrato come estendere il modello poroviscoelastico per considerare altre specie diffondenti. Le equazioni di trasporto e costitutive, opportunamente modificate, sono state implementate in un software commerciale basato sull'analisi FEM e, come esempio, il rilascio di farmaco da un sistema rigonfiante è stato riportato.

Chapter One

Introduction

In this chapter the definition of hydrogel will be given. The peculiar properties of these materials along with their application as delivery systems will be shown. A brief overview on the modeling approaches will be done. Finally the aims of this PhD thesis will be stated.

Part of this work has been reported in:

- **CACCAVO, D.**, CASCONE, S., LAMBERTI, G., BARBA, A. A. & LARSSON, A. **2016**. Swellable Hydrogel-based Systems for Controlled Drug Delivery. In: SEZER, A. D. (ed.) Smart drug delivery system.
- **CACCAVO, D.,** CASCONE, S., LAMBERTI, G., BARBA, A. A. & LARSSON, A. **2017**. Drug delivery from hydrogels: a general framework for the release modeling Current Drug Delivery, 14 (2), 179-189.

1.1 Hydrogels

Hydrogels are three-dimensional, hydrophilic, polymeric networks capable of imbibing large amounts of water or biological fluids (Peppas et al., 2000). A distinction has to be done between hydrosols and hydrogels: with the first are indicated solutions in which polymers are dissolved in water, instead, with the term hydrogels cross-linked hydrosols are identified (Siepmann et al., 2011). These last, due to the presence of chemical or physical cross-links (junctions, tie-points, entanglements) in the polymeric network, are unable to dissolve in water but they can absorb it increasing their volume. The system so formed is very complex and generally can be considered as made of three different parts: the solid polymer network matrix, the interstitial water or biological fluid and the ionic species (**Figure 1**) (Li, 2009).

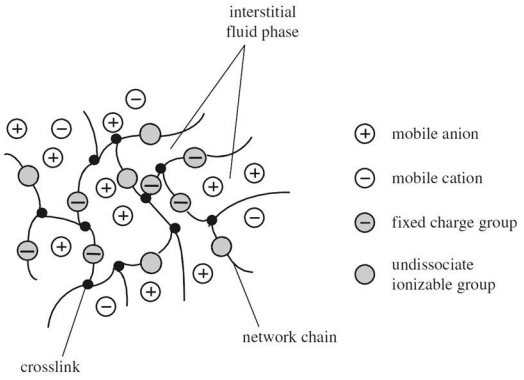

Figure 1. *Schematic microscopic structure of charged hydrogel (Li, 2009).*

The behavior of these systems is the result of the interaction of all three parts (polymeric network, water, ions) with the external environment. Indeed the water adsorption due to diluting force (the entropy of the system increases, like in the normal solubilization process of linear polymers) causes the network swelling. Therefore, the chains between network junctions are required to assume elongated configurations generating an elastic force. As swelling proceeds, this force increases and the diluting force decreases. Ultimately, a state of equilibrium swelling is reached in which these two forces are in balance. When these polymers have an ionic network with ionizable groups, the swelling ability may be greatly increased as a result of the localization of charges that, setting up an electrostatic repulsion, tend to expand the network. However, the fixed charges are not the only ions present in the gel, at least a stoichiometric amount of mobile counterions has to be considered. These, by screening effect, reduce the ideal swelling capacity due to the repulsion. Moreover, the swollen ionic gel can exchange ions with the solvent closely resembling a Donnan membrane equilibrium. The polymer

acts as its own membrane preventing the charged substituents from diffusing into the outer solution (Flory, 1953).

This peculiar behavior, which has led to define this soft matter as "smart materials", makes hydrogels and hydrogel-based systems very attractive by several frontier fields, such as biomedical applications, as well as for sectors that are less demanding technology, i.e. agro-food applications.

1.2 Structure-properties relationships

1.2.1 Interaction between mass transport and structure mechanics

It is clear, from the previous paragraph, that the structure mechanics influence the water absorption/desorption and viceversa. This mutual relation gives rise to different mass transport regimes, reported in literature as "Fickian" and "non-Fickian" (or "Anomalous") diffusion. The first transport is characteristic of a concentration gradient driven processes, whereas the latter deviate from a standard diffusion problem due to the influence of the polymer network relaxation. Vrentas et al. (Vrentas et al., 1975, Vrentas and Duda, 1977) have suggested a simple way to establish the regions in which Fickian and non-Fickian transports take place, on the basis of the *diffusional Deborah number*, $N_{De.D}$, defined according to equation (1.1), in which τ is the characteristic stress-relaxation time of the polymer–solvent system and τ_D is the characteristic time for the diffusion of the solvent in the polymer:

$$N_{De.D} = \frac{\tau}{\tau_D} = \frac{\int_0^\infty sG(s)ds \Big/ \int_0^\infty G(s)ds}{L_{Ch}^2/D_{1.s}} \qquad (1.1)$$

The stress-relaxation time, τ, can be evaluated by integrals of the shear relaxation modulus, $G(t)$, over the entire relaxation time spectrum; the diffusion time, τ_D, is given by the ratio between the second power of a characteristic diffusional path length (for the solvent), L_{Ch}, and the diffusion coefficient of the solvent in the swollen network, $D_{1.s}$ (Davidson and Peppas, 1986). If the change in solvent concentration during the swelling process is limited, average values for each characteristic time have to be used, and then the full process can be characterized by a single value of the Deborah number. If the change in solvent concentration is large, the Deborah number have to be calculated for both the initial and final stages, and their order of magnitude will be used to characterize the behavior of the system.

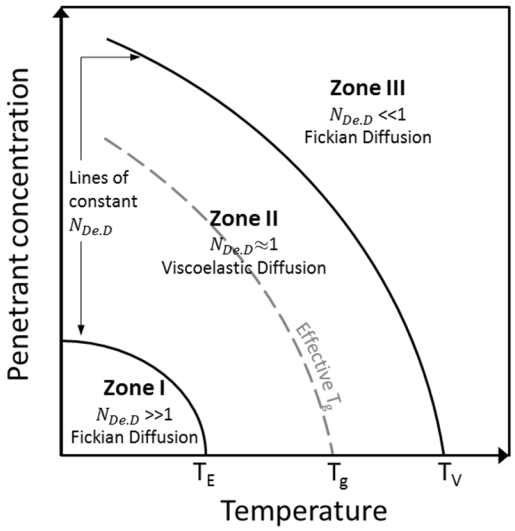

***Figure 2**. Schematic illustrating the different zones of diffusion, function of the temperature, and penetrant concentration. The solid lines represent lines at constant diffusional Deborah number, $N_{De.D}$; the dashed gray line represents the effective glass transition temperature, T_g. The temperatures T_E and T_V represent the temperatures at which the polymer behaves like an elastic solid and viscous fluid, respectively. Figure redrawn on the basis of the suggestions in (Vrentas et al., 1975, Davidson and Peppas, 1986).*

The value of the diffusional Deborah number, $N_{De.D}$, discriminates the nature of the diffusive phenomena, as schematized in **Figure 2**:

- Large values of the Deborah number ($N_{De.D} \gg 1$) identify **Zone I**, where the characteristic relaxation time, τ, is long with respect to characteristic diffusion time, τ_D: the polymer structure does not change during the water diffusion process, i.e., the polymer remains in its glassy state. The diffusion phenomenon is usually described by the conventional Fick's law, using coefficients of diffusion constant and independent from water/polymer concentrations.
- Small values of the Deborah number ($N_{De.D} \ll 1$) identify **Zone III**, where the relaxation phenomenon is much faster than the diffusion phenomenon. Practically, it is a diffusion through a viscous mixture (the swollen, rubbery hydrogel), a process which can be described again by the conventional Fick's law, using coefficients of diffusion which are a strong function of water/polymer concentrations.
- Intermediate values of the Deborah number ($N_{De.D} \approx 1$) identify **Zone II**, when the two characteristic times are of the same order

of magnitude, i.e., the relaxation and the diffusion phenomena take place on the same time scale. This is the transition zone in which the polymer experiences its glass–rubber phase change, the mixture has a viscoelastic nature, and the diffusion is an anomalous transport (and its limit, the Case-II transport), which is non-Fickian.

1.2.2 Diffusion in hydrogels

The diffusion of molecules in hydrogel is never an easy task, also when the mass transport is only driven by concentration gradients (Fickian regime). This is due to the sieving effect exerted by the polymeric network on the diffusing molecules, which results in non-constant diffusion coefficients.

Generally, the models useful to predict the diffusivity of a molecule "i" in a swollen network "s," $D_{i.s}$, with respect to the diffusivity of the same molecule in the solvent "1," have the following general form (Lin and Metters, 2006) (the ratio $D_{\mathrm{i}.s}/D_{\mathrm{i}.1}$ is sometimes called "the retardation effect"):

$$\frac{D_{\mathrm{i}.s}}{D_{\mathrm{i}.1}} = f(\xi, \phi_2, r_s) \tag{1.2}$$

Where, ξ and ϕ_2 are, respectively, the network mesh size (is a measure of the space available between the macromolecular chains) and the polymer volume fraction, while the parameter r_s is the size of the diffusing molecule. The mechanistic theories which are used to build the left-hand side of equation (1.2) are known as hydrodynamic theories, obstruction theories, and theories based on free volume. The hydrodynamic theory assumes that the solute molecules, depicted as hard spheres, move through the liquid phase of the network, the diffusion coefficient being dependent upon the drag force exerted by the liquid molecules on the spheres. The obstruction theories are based on the sieve effect due to the presence of an impenetrable polymer network. The diffusion takes place through the holes in the network; therefore, the path length is increased with respect to the diffusion in pure solvent. The retardation effect is thus calculated on the basis of the sieve effect. According to the free volume theory, a molecule diffuses through the hydrogel by "jumping" into voids that are present in the network. The free volume is the volume of the holes, formed on statistical bases due to random thermal motions. All these theories have been thoroughly reviewed in the following references (Grassi et al., 2007a, Amsden, 1998b, Amsden, 1998a, Masaro and Zhu, 1999).

1.3 Modeling hydrogels and hydrogel-based systems behavior

Modeling hydrogels and Hydrogel-Based Systems (HBSs) behavior is of great interest for everyone who deals with this complex matter. This is related to the deep understanding that a descriptive/predictive mathematical model

would lead, necessary to the correct design of these systems, as well as to the cost reduction that it would generate (i.e. faster and cheaper experimental campaign).

The wide spreading of hydrogels and HBSs, across several sectors (from the biomedical to the agro-food to the construction industry) has led several researchers, with different backgrounds, to deal with hydrogel-based systems, producing a vast and fragmented literature on the possible mathematical modeling approaches. Indeed, since the 1961 (Higuchi, 1961) several models have been proposed, going from the empirical to the mechanistic treatment of the problem, often emphasizing single aspects that characterize the hydrogels behavior.

1.3.1 Empirical models

The first modeling attempts were mainly related to describe the release of an active ingredient (i.e. a drug) from hydrogel-based systems. They can be traced back to the semi-empirical model of Higuchi (Higuchi, 1961), where the fractional drug release from an ointment (thin film) was related to the square root of the time.

$$\frac{M_t}{M_\infty} = k\sqrt{t} \tag{1.3}$$

M_t is the cumulative amount of drug released at time t. M_∞ is the mass of drug released at infinite time (equal to the initial drug loading) and k is a constant reflecting the design variables of the system.

A generalization of the Higuchi equation was proposed by Peppas and coworkers in the 1985 (Peppas, 1985) where the fractional drug release was related to the power "n" of the time, where the exponent "n" was an index, function of the kind of drug transport regime.

$$\frac{M_t}{M_\infty} = k\, t^n \tag{1.4}$$

For a thin film, with a values of n of 0.5, 1 or a value between them, were respectively described a purely diffusion process (the same as the Higuchi's), a swelling-controlled drug release (also known as case-II transport) or an intermediate behaviors (also called anomalous transport).

To distinguish between the relative importance of the Fickian release and the swelling-controlled release, Peppas and Sahlin (Peppas and Sahlin, 1989) proposed the model:

$$\frac{M_t}{M_\infty} = k_1\, t^m + k_2 t^{2m} \tag{1.5}$$

Where k_1, k_2 and m are constants. The first term on the RHS represents the Fickian diffusional contribution, F, whereas the second term the swelling-controlled (case II) contribution, R. The relative importance of the two transport mechanisms can be highlighted by the ratio:

$$\frac{R}{F} = \frac{k_2 t^m}{k_1} \tag{1.6}$$

Bettini et al. (Bettini et al., 1994) used this equation to investigate the effect of the (HydroxyPropyl)Methyl Cellulose (HPMC) molecular weight on the kinetic of drug release. No significant difference was found within the different grades of HPMC and the value of the ratio R/F was smaller than 0.1, suggesting that the drug transport is mainly Fickian diffusion driven.

Due to their simplicity these equations have been used countless times to analyze the experimental results, often without taking into account that these equations are based on very strict assumptions among which constant diffusion coefficients and negligible swelling, that for swellable systems are very far from real behavior (Siepmann and Peppas, 2001, Lin and Metters, 2006). Therefore, these models can only give a limited insight into the release mechanism and caution should be paid when they are applied to swelling systems.

1.3.2 Mechanistic models

A first question to answer when approaching hydrogels is: "are they multiphasic or monophasic systems?". The answer cannot be taken for granted. Despite in most experimental cases the response is simply avoided, it become fundamental when the aim is to develop a mechanistic mathematical model of the system.

The most natural approach is to consider hydrogels as single-phase matter, in which more components can coexist, like it would be indisputably done for polymeric solutions (hydrosols).

Another vision is to consider hydrogels as made of different phases, i.e. the water phase is separated from the polymeric phase, and these can exchange momentum. Despite this approach could seem odd to many experimental researchers, it has been the most used in literature when modeling hydrogels. The reasons of such "incoherence" are related to the absence, for decades, of a proper theory. Therefore the multiphasic approach, even if without strong thermodynamic basis, has spread and permitted to describe anyway hydrogels (at cost of a major number of partial differential equations and some non-physical parameters). More recently a monophasic theory, which couples the water diffusion along with the system mechanics, has been developed (Hong et al., 2008). Therefore the modeling gap has been compensated and nowadays the choice of the approach is left to the researcher, which in my opinion should prefer the monophasic approach that is more thermodynamically and numerically robust.

Another important question is related to the need of modeling/analyze the full behavior, mass transport plus mechanics, or just one aspect, mass transport only. Despite this question would have theoretical no sense, the difficulties (along with the previously mentioned absence of a theory) related to the solution/analysis of the full hydrogels behavior have led many researchers to describe hydrogel-based systems with a "mass transport only" approach. This is, for example, a common approach in drug delivery applications, where no one used a "full" monophasic model.

1.3.2.1 A general framework for the HBSs modeling

All the mechanistic models have to be based on mass and momentum balances, correlated with proper constitutive equations. In (Caccavo et al., 2016, Caccavo et al., 2017) a general framework for the mechanistic modeling of HBSs have been proposed, where both the multiphasic and monophasic approach can be treated (in **Figure 3**).

As it can be seen, equations (A) and (G) represent the general expressions of a mass and linear momentum (neglecting transient and inertial terms) conservation equations.

The multiphasic approach particularizes the mass conservation in terms of volume fractions (of water and polymer (B)) and eventually in the concentration of ions/active ingredients etc. (C). The momentum balance (G) can be rewritten for both the phases, accounting for the chemical potential contribution, internal stresses, electric field, and friction forces between phases and components. The momentum balances on the ions/active ingredients can be seen as equations defining their mass flux (Feng et al., 2010). Accompanying these equations with the electro-neutrality conditions (ionic gels only) and proper constitutive equations, it is (in principle) possible to solve for the volume fractions, the ions/active ingredients concentrations and for the velocities of each phase and component. However some unphysical parameters (like the friction coefficients between phases and phase/component) are needed and several Partial Differential Equations (PDEs) have to be numerically solved. In particular, this last issue has always led to implement simplified versions of the presented approach.

Following the monophasic (multicomponent) approach, instead, the general mass balance (A) can be rewritten in term of species densities or in term of mass fractions. The momentum balance (G) remains fundamentally the same (I), where the stress tensor should be derived considering the monophasic nature of the system and accounting for the polymer and solvent presence. Also in this case accompanying the mass and momentum balances with electro-neutrality equation (ionic gels only) and proper constitutive equations, it is possible to solve for the species densities (or mass fractions) and the mixture velocity (or system deformation).

Multiphasic approach	Multicomponent approach
Mass conservation:	
$\frac{\partial \rho_i}{\partial t} = -\boldsymbol{\nabla} \cdot (\rho_i \boldsymbol{v}_i) \quad i = 1 \dots N_C$ (A)	
$\begin{cases} \frac{\partial \phi_i}{\partial t} = -\boldsymbol{\nabla} \cdot (\phi_i \boldsymbol{v}_i) & i = 1, 2 \\ \frac{\partial \phi_1 c_i}{\partial t} = -\boldsymbol{\nabla} \cdot (\phi_1 c_i \boldsymbol{v}_i) & i = 3 \dots N_C \\ \phi_1 + \phi_2 \cong 1 \end{cases}$ (B) (C)	$\frac{\partial \rho_i}{\partial t} = -\boldsymbol{\nabla} \cdot (\rho_i \boldsymbol{v_{mix}}) - \boldsymbol{\nabla} \cdot \boldsymbol{j_i} \quad i = 1 \dots N_C$ (D) *or* $\rho \frac{\partial \omega_i}{\partial t} = -\rho \boldsymbol{v_{mix}} \cdot \boldsymbol{\nabla} \omega_i - \boldsymbol{\nabla} \cdot \boldsymbol{j_i} \quad i = 1 \dots N_C$ (E) $\sum_{i=1}^{N_C} \omega_i = 1$ (F)
Momentum conservation: $\boldsymbol{\nabla} \cdot (\boldsymbol{\sigma}_H - p\boldsymbol{\delta}) = \boldsymbol{0}$ (G)	
$\begin{cases} \boldsymbol{0} = \boldsymbol{\nabla} \cdot (-\phi_1 p\boldsymbol{\delta} + \mu_1 \dot{\boldsymbol{\gamma}}) + \phi_1 RT \sum_{i=3}^{N_C} \boldsymbol{\nabla} c_i + \boldsymbol{f}_{12} + \sum_{i=3} \boldsymbol{f}_{1i} & i = 1 \\ \boldsymbol{0} = \boldsymbol{\nabla} \cdot (-\phi_2 p\boldsymbol{\delta} + \boldsymbol{\sigma}_2) - \phi_1 (z_F c_F F) \boldsymbol{\nabla} \psi + \boldsymbol{f}_{21} & i = 2 \\ \boldsymbol{0} = -\phi_1 RT \boldsymbol{\nabla} c_i - \phi_1 (z_i c_i F) \boldsymbol{\nabla} \psi + \boldsymbol{f}_{i1} & i = 3 \dots N_C \end{cases}$ (H)	$\boldsymbol{\nabla} \cdot (\boldsymbol{\sigma_{mix}} - p\boldsymbol{\delta}) = \boldsymbol{0}$ (I)
Distribution of the ionic species:	
$\nabla^2 \psi = -\frac{F}{\varepsilon \varepsilon_0} \left(\sum_{i=4}^{N_C} z_i c_i - z_F c_f \right), \quad \overbrace{\nabla^2 \psi = 0}^{electroneutrality}$ (J)	
Constitutive equations:	
$\{p_{osm}, \boldsymbol{\sigma_H}\} = g(A_{el}, A_{mix}, A_{ion})$ (K) $p = p' + p^{osm}$ (L)	
$\boldsymbol{f}_{ij} = -\boldsymbol{f}_{ji} = \boldsymbol{f}_{ij}(\zeta, \boldsymbol{v}_i, \boldsymbol{v}_j)$ (M)	$\boldsymbol{j_i} = -\rho_i (\boldsymbol{v}_i - \boldsymbol{v_{mix}}) \propto -\rho D_i \boldsymbol{g} (\mu_i, x_i, \omega_i, M, p_{osm}, \psi, \dots)$ (N) $D_i = g(\rho_1 \text{ or } \rho_2)$
Unknowns to solve for:	
$\phi_1, \phi_2, c_3 \dots c_{N_C}, \boldsymbol{v}_1 \dots \boldsymbol{v}_{N_C}$	$\omega_i, \boldsymbol{v_{mix}}$

*Hydrogel (H) = Solvent ($i = 1$) + Polymer ($i = 2$) + Drug ($i = 3$) + Ions ($i = 4 \dots N_C$)

***Figure 3**. A general framework for the HBSs modeling (Caccavo et al., 2016, Caccavo et al., 2017).*

The constitutive equations in this case are most of the time derived from non-equilibrium thermodynamics, using as thermodynamic potential the Helmholtz free energy (a comprehensive review can be find in (Liu et al., 2015)). Moreover, differently from the multiphasic approach, in this case are not required unphysical/immeasurable parameters and less PDEs are needed.

Several literature models, based on the multiphasic or monophasic approach, can be traced back to this framework. Some example of multiphasic models for hydrogel behavior can be find in (Birgersson et al., 2008, Doi, 2009, Feng et al., 2011, Kurnia et al., 2011, Kurnia et al., 2012b, Kurnia et al., 2012a, Xu et al., 2013), where in (Xu et al., 2013) it is also dealt with hydrogel-based drug delivery systems.

At the same manner several model based on the multicomponent (monophasic) approach can be find in (Barba et al., 2009b, Caccavo et al., 2015b, Caccavo et al., 2015a, Chirico et al., 2007, Galdi and Lamberti, 2012, Kaunisto et al., 2010, Kaunisto et al., 2013, Kiil and Dam-Johansen, 2003, Lamberti et al., 2011, Siepmann et al., 1999a, Siepmann and Peppas, 2001), where the models are based on the mass transport only and describe also the drug release from hydrogels. In (Achilleos et al., 2001, Achilleos et al., 2000, Chester, 2012, Chester and Anand, 2010, Hong et al., 2009, Hong et al., 2010, Hong et al., 2008, Lucantonio et al., 2013, Wang and Hong, 2012) the mass transport is coupled with the mechanics to describe pure hydrogels behavior.

1.4 General aim

General aim of this PhD thesis is to analyze, with ad hoc experiments, and to describe/simulate, through mathematical modeling, the behavior of hydrogels and hydrogel-based systems.

Chapter Two

Analysis and modeling hydrogel-based systems

In this chapter, the analysis and modeling of hydrogel-based systems for active ingredient delivery applications will be treated. A model drug delivery system (made of polymer and drug only) and a commercial-like tablet behavior will be analyzed. Following the common literature approach, a monophasic model based on "mass transport only" equations will be developed, implemented and validate against experimental tests, highlighting pro and cons of such kind of approach.

Part of this work has been reported in:

- **CACCAVO, D.**, CASCONE, S., LAMBERTI, G. & BARBA, A. A. **2015**. Modeling the Drug Release from Hydrogel-Based Matrices. Molecular Pharmaceutics, 12, 474-483.
- **CACCAVO, D.**, CASCONE, S., LAMBERTI, G. & BARBA, A. A. **2015**. Controlled drug release from hydrogel-based matrices: Experiments and modeling. International Journal of Pharmaceutics, 486, 144-52.
- **CACCAVO, D.**, LAMBERTI, G., BARBA, A. A., ABRAHMSÉN-ALAMI, S., VIRIDÉN, A. & LARSSON, A. **submitted**. Effects of HPMC substituent pattern on water up-take, polymer and drug release; an experimental and modelling study. European Journal of Pharmaceutical Sciences.

2.1 Introduction

The hydrogels' characteristics make them perfect substances to formulate Active Ingredient (AI) delivery systems responsive to temperature, pH, and particular solutes variations.

When a dry hydrogel-polymer-based, loaded with an AI, is immersed in a physiological fluid, the solvent starts to penetrate inside the polymeric matrix. If the polymer shows a glass transition temperature higher than the room/physical temperature, when the solvent concentration exceed a threshold value, polymeric chains unfold so that the glass-rubbery transition occurs and a gel-like layer, surrounding the matrix dry core appears (Grassi et al., 2007b). The moving front at which this process takes place is called "swelling front", which separates the swollen from non-swollen matrix (Colombo et al., 1999). In the swollen region the polymeric chains assume an elongated configuration that allows the contained AI molecules to easily diffuse toward the outer dissolution medium, once that they are dissolved. Indeed depending on the drug solubility, in the swollen layer there could be zones in which the drug coexist in the dissolved and dispersed form (Grassi et al., 2010). The front that separates the swollen matrix, containing only dissolved drug, from the swollen part that contains both dissolved and dispersed drug, is called "diffusion front". Additionally, on the zone at which the swollen matrix is in contact with the outer medium a third front can be defined: the "erosion front". On this boundary the polymer network became extremely hydrated and process like chains disentanglement can take place, "eroding" the matrix (Siepmann and Siepmann, 2008).

All these regions are shown in **Figure 4**, where a picture of a swollen tablet subjected to radial dissolution test is compared to a scheme of a hydrogel-based matrix hydration behavior.

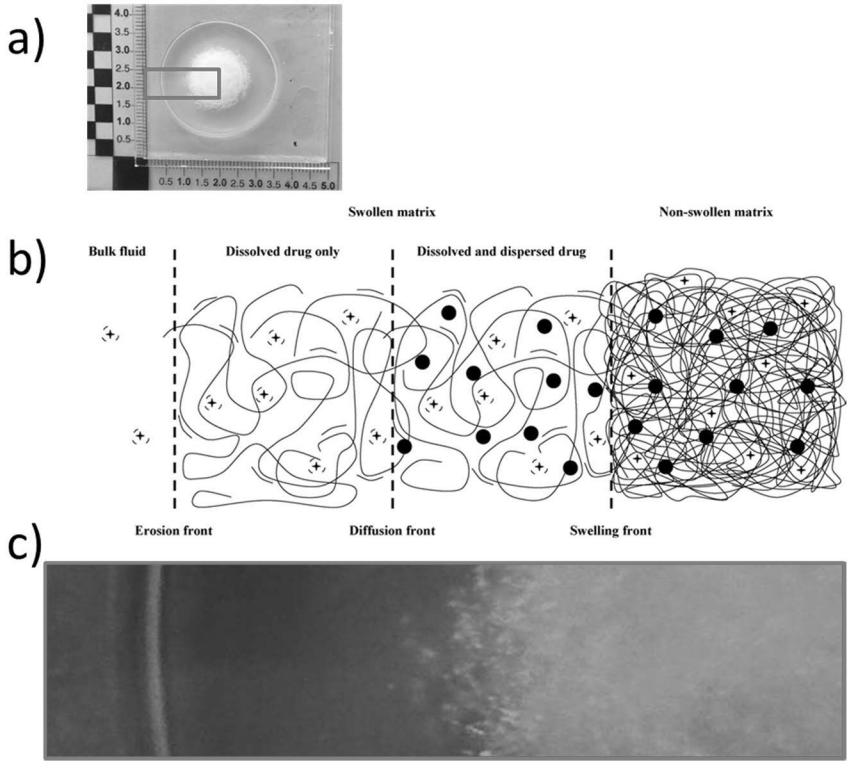

Figure 4. *An (HydroxyPropyl)Methyl Cellulose (HPMC) plus theophylline swollen tablet picture (a); a schematic representation of a partially swollen drug delivery system with the erosion, diffusion and swelling front (b) (Siepmann and Siepmann, 2008), a zoom of the swollen tablet picture readily comparable with the upper scheme (c).*

Mathematically model these systems is of great interest, fact that is testified by a large number of literature works. Disregarding the empirical models, which can only give limited insights in the release mechanisms, a milestone in drug release modeling is represented by the works of Siepmann et al. (Siepmann et al., 1999b, Siepmann et al., 1999a, Siepmann and Peppas, 2000) in which a 3D model, accounting for drug release from a swelling HPMC matrix, including erosion phenomena, was developed. The so called "sequential layer" model was able to describe the drug release and water uptake through the Fick's second law in dilute systems with "Fujita-type" (Fujita, 1961) diffusion coefficients, whereas the polymer mass was obtained from a macroscopic balance with a constant dissolution rate. However, the model was based on the hypothesis of affine deformations; therefore, the initial cylindrical shape was maintained during the dissolution process whereas the volume was able to increase accordingly to the amount of substances transported through the system.

The assumption of affine deformations was first implemented in a general code (Barba et al., 2009b), and then removed by Lamberti et al. (Lamberti et al., 2011) considering the swelling as driven by the water flux. In particular it was considered that part of the total inlet water flux was responsible for the tablet swelling whereas the rest was responsible for the inner layers hydration. This, with the introduction of an additional parameter, namely the swelling constant "k_{swe}", allowed to obtain a local swelling velocity on the erosion front that, coupled with an ALE (Arbitrary Lagrangian-Eulerian) moving mesh method was used to describe the observed swelling behavior along with the drug release. The evolution of the polymer mass, similarly to Siepmann's model, was derived from a macroscopic balance. However, with this approach the system was not constrained in terms of mass fractions, possibly leading to unrealistic results in some domain points.

Kaunisto et al. (Kaunisto et al., 2013) analyzed the behavior of an HPMC matrix loaded with a poorly soluble drug, under the assumption of constant density, coupling the polymer mass description with the transport equations for drug and water through the mass fraction constrain. The transport equations were based on a simplified version of the generalized Fick equation (Bird et al., 2007) where the driving force was the species gradient concentration. Despite the elegant approach, all the multicomponent interactions, except those with the solvent, were assumed to be zero and the multicomponent Fick diffusivities were interpreted as "pseudo-binary". For the water-polymer diffusivity a "Fujita-type" form was used. Even in this case, like in Lamberti's model, the swelling was described through an ALE moving mesh method but the swelling velocity was derived from a polymer/solid drug mass balance on the erosion boundaries

It is worth noting that all these modeling approaches can be traced back to the framework of **Figure 3** using a monophasic model based on mass transport only equations.

2.2 Aims

Aim of this part of the thesis is to develop a mathematical model able to describe the behavior of hydrogel loaded with an active ingredient and subjected to dissolution. To fulfill this goal a monophasic approach based on the "mass transport" only equation is used, and the system deformation is described with a moving mesh (ALE) method driven by local mass balances.

Further aim is to characterize experimentally the HPMC-based tablets behavior, first with model tablets (HPMC plus drug) and then with commercial-like tablets (HPMC plus drug plus excipients), with techniques that allows characterizing several aspect of the system behavior and not only the drug release.

Final aim is to describe the experimental recorded behavior with the mathematical model developed.

2.3 Materials and Methods

In this part of the thesis, the HydroxyPropyl MethylCellulose (HPMC) has been used as hydrogel forming material to produce and analyze tablets for controlled release applications. Theophylline (TP) has been used as model drug due to its easy quantification via spectrophotometric analyses and high solubility. In case of commercial-like tablets (project in collaboration with Chalmers and AstraZeneca) two different batch of HPMC (different in heterogeneity of substitution) have been used, in conjunction with MicroCrystalline Cellulose (MCC) and Lactose (LAC) as excipients.

2.3.1 HydroxyPropyl MethylCellulose (HPMC)

HydroxyPropyl MethylCellulose (HPMC) is a nonionic semi-synthetic polymer obtained from methylcellulose modified with a small amount of propylene glycol ether groups attached to the anhydroglucose of the cellulose **(Figure 5)**.

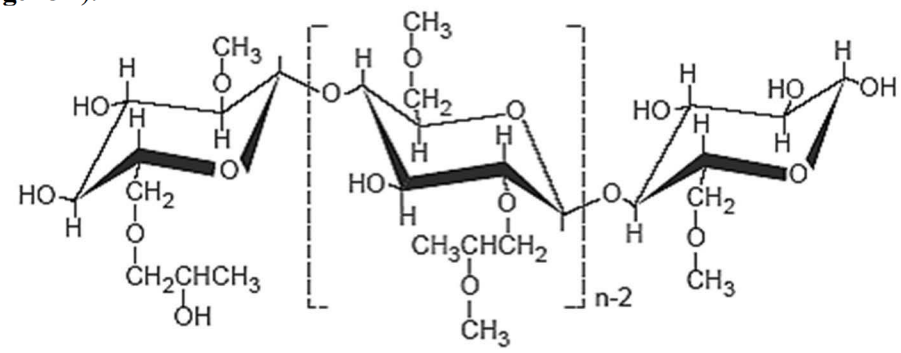

Figure 5. *Chemical structure of HPMC (Dow, 2000).*

In the manufacture of HPMC the alkali cellulose reacts with methyl chloride to produce methyl cellulose (MC) and sodium chloride. The MC is then further reacted with the staged addition of an alkylene oxide, which in the case of HPMC is propylene oxide. After this reaction, MC and HPMC are purified in hot water, where they are insoluble. Drying and grinding completes the process (Majewicz and Podlas, 2000). The particles obtained present the structure of long-fibrous particle, classified as “very fine powders” in terms of particle size distribution.

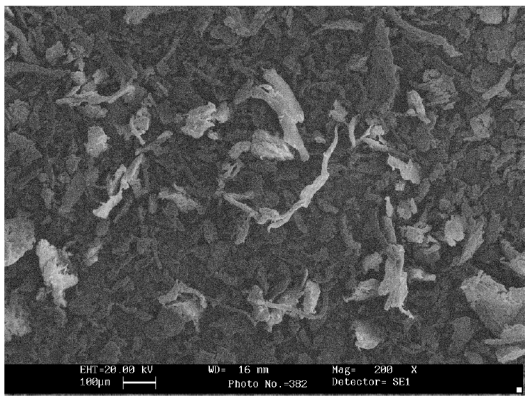

Figure 6. *SEM image of a sample of HPMC K4M.*

Premium grades of HPMC meet requirements of United States Pharmacopeia (USP), European Pharmacopeia (EP), Japanese Pharmacopeia (JP), Food Chemicals Codex (FCC) and FDA (21 CFR 172.874), that allow their use in pharma as well as in food applications.
The USP classified the HPMC according to the amount of substituents:

- HPMC 1828;
- HPMC 2208;
- HPMC 2906;
- HPMC 2910.

Where the first two numbers indicate the average percentage of methoxyl, $-OCH_3$, (MeO) groups and the second two the average percentage of hydroxypropoxyl, $-OCH_2CHOHCH_3$, (HPO) groups.

The Dow's HPMC products (used in this work), identified by the producer with the letters "K", "E", "F" can be related to the USP classification according to **Figure 7**.

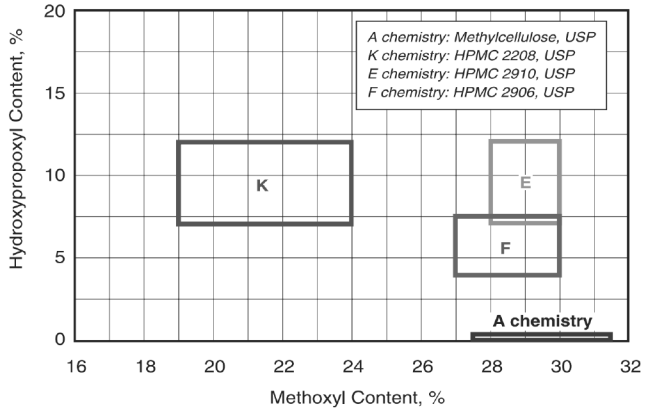

Figure 7. *Substitution levels in Dow's HPMC products (Dow, 2000).*

The substitution has a very significant impact on the performance of

hydroxypropyl methylcellulose in hydrophilic matrix systems. A useful way to examine how substitution affects polymer properties is the phenomenon of thermal gelation. When aqueous solutions of HPMC are heated, they form reversible gels at certain temperatures, that are specific for each product type. The gelation phenomenon has been mainly attributed to hydrophobic transient crosslinks between HPMC molecules (Viridén et al., 2010), that in turns are influenced by the degree of substitution as well as by the heterogeneity of substitution (Viridén et al., 2011).

Another important parameter is the degree of polymerization (DP), that is varied in production to obtain a polymer with the desired properties. Normally, for controlled release application, the DP is adjusted to a range between 100 and 1500 (Dow, 2000). The different DPs generate HPMC products different in molecular weight, that in turns produce different aqueous solution viscosities. Normally, referring to HPMC, with the term "viscosity grade" is intended the viscosity of a 2% w/w aqueous solution at 20°C. Values between 80-120000 cP can be obtained.

2.3.1 Tablet preparation

HPMC and TP powders were mixed (TP/HPMC 50% w/w) and compressed using a cylindrical tableting machine (Specac PN3000, equipped with flat-faced punches), applying a loading force of 50 kN, kept for 5 min by a press. For the "radial" dissolution and "overall" dissolution tests, the matrices dimensions were: radius 6.5 mm, thickness 2 mm, weight 350 ± 5 mg; for the "semi-overall" dissolution tests: radius 6.5 mm, thickness 1 mm, weight 175 ± 2 mg.

The commercial-like tablets were produced in AstraZeneca with a composition in weight of 10% of TP, 45% of HPMC, 15% of MCC and 30% of LAC. The powders were blended in a mortar for 5 min to obtain a well-mixed composition before tableting. A single punch tableting machine (Kilian SP300, Kilian & Co. GmbH, Germany) equipped with 10 mm flat-faced punches was used. The compression force was 10 ± 0.5 kN, and the powder was pre-weighed for each tablet using a Mettler Toledo AX205 Delta Range to get a tablet weight of about 300 ± 5 mg.

2.3.2 Dissolution conditions and release determination

The "radial" dissolutions was performed on matrices confined between two glass slides to ensure only the lateral uptake of water. Using this method, the matrix swells only in radial direction and preserves its thickness.

The "semi-overall" dissolution tests was performed on matrices glued in a small center-part on a glass slab. The matrix is free to swell both in axial and in radial direction, and the glass slide could be seen as the symmetry plane orthogonal to the z-axis (the cylinder axis) of a double-sized tablet.

The "overall" dissolutions was performed on tablets immersed in the bath at the bottom of the USP vessel. An homemade sample holder was used, composed by a wire basket with a large mesh size. The basket was conceived

to have size (both diameter and height) larger than the size of swollen tablet. The system was provided of metal weights to guarantee the stability of the holder at the bottom of the vessel and to ensure the reproducibility of the fluid dynamic conditions. The medium (phosphate buffer water solution: pH 1 for the first 2 hour and pH 6.8 for the following time) during all the tests was kept at 37°C and at constant rotation speed of 100 rpm in a USP II apparatus (AT7Smart, Sotax, Allschwil, Switzerland). The amount of theophylline in the dissolution medium (drug released) was determined spectrophotometrically.

The release of drug (theophylline) and polymers from the commercial like tablets was studied by the AstraZeneca partners, as in a previous work (Viridén et al., 2011). Briefly the release of drug and polymer from the tablets was done by using an USP II dissolution apparatus (Dissolutest, Prolabo, France), equipped with baskets for the tablets, and using a paddle speed of 50 rpm and 900 ml release medium (phosphate buffer, pH 6.8) at 37°C. The tablets were also subjected to dissolution (with same dissolution medium) in a release cell (Abrahmsen-Alami et al., 2007) inside a NMR equipment. The medium was pumped (about 3 ml/min) between the NMR release cell and an external container (500 ml) to achieve sink-condition. The tablets were glued to the center of a rotating disc, which was positioned in the NMR release cell (**Figure 8** to the right) and inserted into the NMR probe for imaging. The amount of theophylline in the dissolution medium (drug released) was determined spectrophotometrically. The amount of HPMC released was determined by using size exclusion chromatography with a refractive index detection (SEC-MALS/RI), see reference (Viridén et al., 2011).

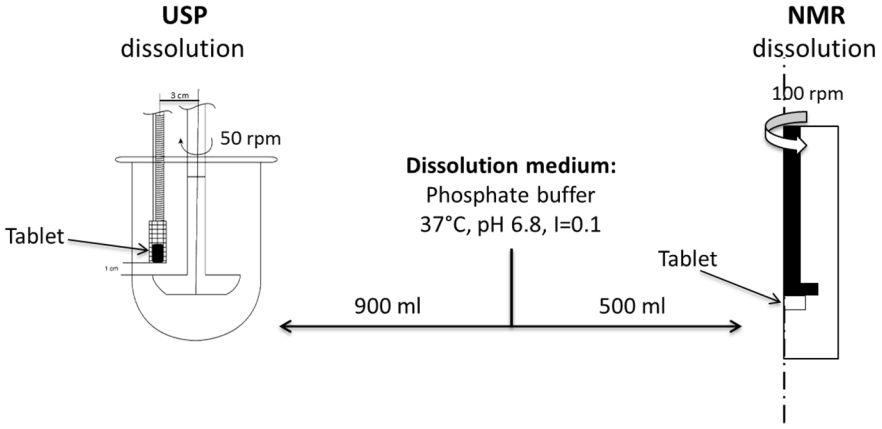

***Figure 8**. Dissolution methods used for the commercial-like tablets, (left) USP dissolution and (right) NMR dissolution*

2.3.3 Gravimetric analysis

2.3.3.1 Whole tablet analysis

The total mass amounts of the components after the hydration were evaluated. To evaluate the water up-take of the matrix, it was weighted, dried, and then weighted again, from the difference between the two weights, the water mass entered in the matrix during the dissolution was evaluated. The dried matrix was completely dissolved, to determine the drug content by the use of spectrophotometric analysis. The residual polymer mass was easily obtained knowing the total weight after the hydration and the drug and water masses. Repeating these analyses for several hydration times, the drug, the polymer and the water masses evolution inside the tablet, function of the hydration time, were obtained.

2.3.3.2 Components distribution inside the swollen tablet

The gravimetric method was used to evaluate the mass amounts of the three components (polymer, drug, and water) in the swollen matrix according to a previously developed technique (Barba et al., 2009a). At given immersion times, the sample was withdrawn from the bath and the swollen matrix was cut by several thin-walled metallic punches ("hollow punches"). Each portion was recovered and quantitatively transferred on a glass holder. The cutting procedures were repeated by using punches of decreasing radius, obtaining several annuli and a central core, which were placed on different glass holders. All the samples were dried till reaching a constant weight to obtain the amount of water in each section. Then, the dried tablet sections were completely dissolved, to allow the determination of the drug content and thus the determination of the polymer fraction. These operations were repeated for all the considered dissolution times, obtaining the evolutions of mass fractions with both the time and the radial direction. All the runs were performed in triplicate.

2.3.4 Image analysis

To evaluate the swollen matrix size, an image analysis technique was applied. Once withdrawn from the dissolution medium, the matrix was carefully removed and an overhead photo was taken. From this image the diameter of the matrix after erosion and swelling phenomena was measured. To measure the thickness and evaluate the shape of the hydrated matrix, after each dissolution time, the matrix was carefully cut along a diameter and photographed from the side. The characteristic dimensions were evaluated with the commercial software Image-Pro® Plus 6.0 (Media Cybernetics).

2.3.5 Texture analysis

The mechanical tests were performed according to a previously described procedure (Cascone et al., 2014). Indentation tests using a texture analyzer

(TA.XT Plus Stable Micro System Godalming, UK equipped with a needle probe and a 5 kg loading cell) were performed on swollen matrices for both the radial and semi-overall systems.

Matrices were penetrated axially at several distances from the center. The indentation test velocity was kept constant at 0.03 mm/s, and the instrument measures the force necessary to penetrate into the swollen matrix. Data acquisition starts when the probe touches the sample (this means that the sample offers a not negligible force to penetration) and it ends when the probe reaches the 90% of the total sample thickness with a recording rate of 100 points/s.

The force recorded, in particular the slope of the force-displacement plots $(\mathrm{dF}/\mathrm{ds})$, has been related to the amount of water using the equation proposed by (Cascone et al., 2014):

$$H_2O\ \%_{(w/w)} = -24.37 \times \log_{10}\left(\frac{\mathrm{dF}}{\mathrm{ds}}\right) + 33.97 \qquad (2.1)$$

With a range of confidence comprised between 20-90% of water.

To ensure reproducibility of the data, every test was performed in triplicate.

2.3.6 Nuclear magnetic resonance microimaging

Tablets subjected to dissolution in the NMR apparatus, where analyzed by the Magnetic Resonance Imaging technique by the AstraZeneca parteners. The signal intensity was weighted according to the proton spin–spin (T2) and spin–lattice (T1) relaxation times by using the original multi-spin pulse sequence (called m_msme). Presented images were probed at 20 different echo times (10–200 ms). A detailed description can be find in (Viridén et al., 2011).

In this work the resulting NMR images (128×128 pixel) were analyzed to give the water distribution inside the swollen tablets. Each pixel is associated with a numerical value that, with the proper scaling factor (given by the instrument), can be related to the proton T2 relaxation. The proton T2 relaxation in turn is mainly attributed to the signal from water protons, therefore, it can be related to the amount of water in each pixel of the image. Calibration curves were obtained by analyzing water solutions with known concentrations of different solutes. In particular, solutions with pure HPMC from batch A or B, HPMC plus mannitol, and pure mannitol were prepared and analyzed (the experimental data are from (Tajarobi et al., 2009)). Data in terms of mass percentage of water versus the T2 relaxation are shown in **Figure 9**. The effect on water proton T2 relaxation was similar regardless of solute (HPMC or mannitol) and depended only on the concentration of the solute. Therefore, the effect of lactose with HPMC were assumed to be the same as for mannitol mixed with HPMC and the calibration curve in **Figure 9** was used utilized in this work to obtain the water concentration in each pixel. The obtained fitted equation for the calibration curve was an exponential decay function of the second order (R^2=0.98):

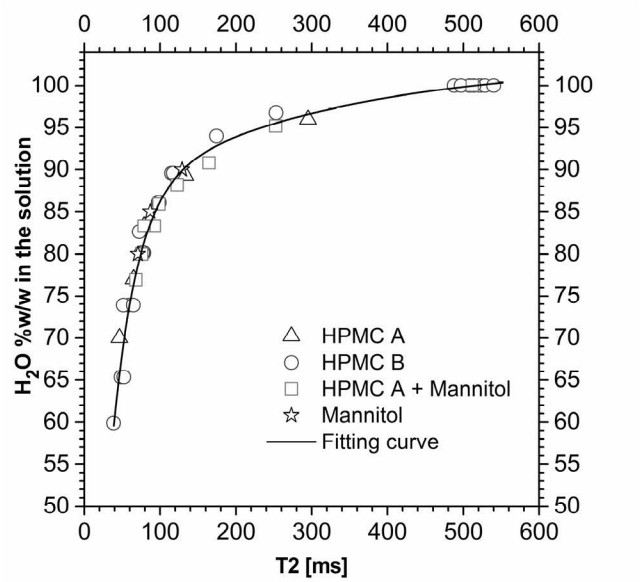

***Figure 9**. Water content-T2 relaxation time relationship for the solutions of two batches (A and B) of pure HPMC, solutions of HPMC mixed with mannitol, or pure mannitol solutions. The experimental data are from (Tajarobi et al., 2009).*

$$H_2O\ \%_{(w/w)} = 103 - 17.9\exp\left(-\frac{T2}{283}\right) - 94.9\ \exp\left(-\frac{T2}{32}\right) \quad (2.2)$$

2.4 Modeling

2.4.1 Model development

Similarly to what is commonly done in literature for HBSs, in this part of the Ph.D. thesis a monophasic model based on the "mass transport" only approach has been developed, implemented and compared with experimental data. In the following the subscript 1 is used for water, 2 for drug, 3 for polymer i ≥ 4 for other species.

The tablet geometry (cylinder) is suitable to study the system in the 2D-axial symmetric configuration, where a cylinder is represented by a rectangle.

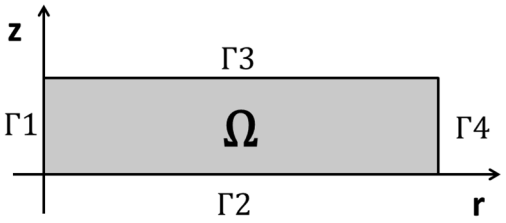

Figure 10. *Computational domain representing a cylindrical tablet.*

In **Figure 10** it is possible to distinguish the system boundaries whose physical meaning is explained in **Table 1**.

Table 1. Physical meaning of the domain boundaries

	Model tablets			**Commercial-like tablets**	
Boundary	**Radial**	**Semi-overall**	**Overall**	**USP dissolution**	**NMR**
$\Gamma 1$	Axial symmetry	Axial symmetry	Axial symmetry	Axial symmetry	Axial symmetry
$\Gamma 2$	Plane of symmetry	In contact with the glass slab	Plane of symmetry	Plane of symmetry	In contact with the NMR probe
$\Gamma 3$	In contact with the glass slab	Erosion front	Erosion front	Erosion front	Erosion front
$\Gamma 4$	Erosion front	Erosion front	Erosion front	Erosion front	Erosion front

The domain dimension (radius and thickness) were properly chosen to describe the real analyzed system.

Initially all the tablets are completely dry, being formed by drug and polymer (and eventually excipients) perfectly mixed and pressed. As the time passes, the water penetrates inside the tablet generating the swelling of the polymeric network, the drug release and the matrix erosion. All these phenomena were described through the transport equations treated in the next paragraphs with the following assumptions:

- there is no volume change upon mixing ($\Delta V_{mix} = 0$, ideal thermodynamic behavior);
- the drug dissolution within the matrix is fast compared to drug diffusion;

- perfect sink conditions for drug and constant critical solvent concentration on the erosion front are maintained;
- negligible mass average velocity (convection) contribution to the species transport;
- the relocation of the polymer due to the water inlet and drug outlet generate the tablet swelling and shape variation without contribute to the polymer release;
- the erosion mechanism is function of the external fluid dynamics and of physicochemical interactions between tablet and external fluid that remain the same during the dissolution tests.

2.4.1.1 Mass transport equations

The species transport inside the system has been considered as a pseudo-diffusion phenomenon. Starting from the equation of continuity for the i^{th} components or species (Bird et al., 2007):

$$\frac{\partial \rho_i}{\partial t} = -(\nabla \cdot \rho_i \mathbf{v}) - (\nabla \cdot \mathbf{j_i}) + r_i \qquad (2.3)$$

Where ρ_i is the mass concentration (density) of the i^{th} component, $\mathbf{v}$ is the mixture mass-average velocity, $\mathbf{j_i}$ is the diffusive mass flux and r_i is the source term of the i^{th} component. Considering that $\rho_i = \rho\, \omega_i$ (where ρ is the system density and ω_i the mass fraction of the i^{th} component) and the equation of continuity for a multicomponent mixture (Bird et al., 2007), equation (2.3) can be rewritten as:

$$\rho \frac{\partial \omega_i}{\partial t} = -\rho \mathbf{v} \cdot \nabla \omega_i - (\nabla \cdot \mathbf{j_i}) + r_i \qquad (2.4)$$

In the system described there is no chemical reaction ($r_i = 0$) and the diffusion-induced convection contribution to the species transport is not considered ($\rho \mathbf{v} \cdot \nabla \omega_i = 0$), as reported in most of the literature (Siepmann and Peppas, 2000, Lamberti et al., 2011, Kaunisto et al., 2013). This last hypothesis has been shown to be reasonably true when the apparent species densities are similar in magnitude and when the mixture can be considered ideal (therefore the volume change on mixing is negligible) (Alsoy and Duda, 2002) . Therefore equation (2.4) becomes:

$$\rho \frac{\partial \omega_i}{\partial t} = -(\nabla \cdot \mathbf{j_i}) \qquad (2.5)$$

Equations (2.5) describe the mass fraction evolution (in time and space) of the i^{th} component. The mass fractions are related trough the mass fraction constraint ($\sum_i \omega_i = 1$), which makes only N-1 balance equations (where N is the number of components) independent. In this work the polymer mass fraction distribution was derived from the mass fraction constraint, the other species from equations (2.5).

The initial conditions for equations (2.5) are the initial mass fractions:

$$@t = 0 \quad \forall \mathbf{x} \in \Omega \quad \omega_i(t = 0, \mathbf{x}) = \omega_{i,0} \tag{2.6}$$

The boundary conditions employed are known mass fractions on the boundaries in contact with the external medium and no flux on the impermeable surfaces. In particular the water mass fraction on the boundaries was fixed to $\omega_{1,eq} = 0.97$ (experimental evidence of (Chirico et al., 2007)), whereas all the other (except the polymer) were set to zero (perfect sink condition $\omega_{2,eq} = 0$).

$$\begin{aligned} &@\mathbf{x} \in \Gamma_{external} \quad \forall t > 0 \quad \omega_i(t > 0, \mathbf{x} \in \Gamma(t)) = \omega_{i,eq} \\ &@\mathbf{x} \in \Gamma_{impermeable} \quad \forall t > 0 \quad \mathbf{j_i} = \mathbf{0} \end{aligned} \tag{2.7}$$

2.4.1.2 Constitutive equations

2.4.1.2.a The system density

The density of the partial hydrated matrix has been calculated considering ideal mixing rule, which has been written for the specific volume:

$$\frac{1}{\rho} = \sum_i \frac{\omega_i}{\rho_{i0}} \tag{2.8}$$

Where ρ_{i0} are the pure species densities.

2.4.1.2.b The mass fluxes

The mass fluxes can be derived from the multicomponent mass fluxes (Bird et al., 2007):

$$\mathbf{j_i} = \rho_i \sum_{\beta=1}^{N} \mathbb{D}_{i\beta} \mathbf{d_\beta} \tag{2.9}$$

Where $\mathbf{d_\beta}$ are called diffusional driving forces and $\mathbb{D}_{i\beta}$ are the multicomponent Fick diffusivities, which can be related to the Maxwell-Stefan diffusion coefficient $\mathcal{D}_{i\beta}$. Assuming a pure concentration driven diffusion transport:

$$\mathbf{d_\beta} = x_\beta \boldsymbol{\nabla} \ln(a_\beta) = x_\beta \boldsymbol{\nabla} \ln(\gamma_\beta x_\beta) \sim x_\beta \boldsymbol{\nabla} \ln(x_\beta) = \boldsymbol{\nabla} x_\beta \tag{2.10}$$

So that:

$$\mathbf{j_i} = \rho_i \sum_{\beta=1}^{N} \mathbb{D}_{i\beta} \boldsymbol{\nabla} x_\beta \tag{2.11}$$

Where a_β and γ_β are respectively the activity and the activity coefficient of the species β. Using the mixture-average approximation, so that the mass flux of the i^{th} component depends on a single concentration gradient and is proportional to a diffusion coefficient D_i^m. This last diffusion coefficient describes the diffusion of species i relative to the remaining mixture ("m").

The general expression for the mass flux of the i^{th} component assumes the form (in the following the superscript "m" will be dropped):

$$\mathbf{j_i} = -\rho_i D_i \frac{\boldsymbol{\nabla} x_i}{x_i} \tag{2.12}$$

The equation (2.12) can be further simplified considering that $x_i = \omega_i M/M_i$, where M_i is the i^{th} component molar mass and $M = (\sum_i(\omega_i/M_i))^{-1}$ is the system average molar mass:

$$\begin{aligned}\mathbf{j_i} &= -\frac{\rho\,\omega_i}{\frac{\omega_i M}{M_i}} D_i \boldsymbol{\nabla}\left(\frac{\omega_i M}{M_i}\right) = -\frac{\rho}{M} D_i \boldsymbol{\nabla}(\omega_i M) \\ &= -\left(\rho D_i \boldsymbol{\nabla}\omega_i + \rho D_i \omega_i \frac{\boldsymbol{\nabla} M}{M}\right)\end{aligned} \tag{2.13}$$

Which is the mass flux expression employed in this work.

To elucidate the steps that lead from the multicomponent mass fluxes (equation (2.11)) to the Fick's law type expression (equation (2.12)) a binary system example will be reported. For a binary systems:

$$\mathbf{j_1} = \rho_1(\mathbb{D}_{11}\boldsymbol{\nabla} x_1 + \mathbb{D}_{12}\boldsymbol{\nabla} x_2) \tag{2.14}$$

Knowing that:

$$\begin{aligned}\mathbb{D}_{11} &= -\frac{\omega_2^2}{x_1 x_2}\mathcal{D}_{12}. \\ \mathbb{D}_{12} &= \frac{\omega_1\omega_2}{x_1 x_2}\mathcal{D}_{12}\end{aligned} \tag{2.15}$$

Equation (2.14) can be rewritten as:

$$\mathbf{j_1} = \rho_1\left(-\frac{\omega_2^2}{x_1 x_2}\mathcal{D}_{12}\boldsymbol{\nabla} x_1 + \frac{\omega_1\omega_2}{x_1 x_2}\mathcal{D}_{12}\boldsymbol{\nabla} x_2\right) \tag{2.16}$$

Being the mixture-average diffusivities defined as:

$$D_i^m = \frac{1-\omega_i}{\sum_{k\neq i}^{N}\frac{x_i}{\mathcal{D}_{ik}}} \rightarrow D_1^m = D_1 = \frac{\omega_2\mathcal{D}_{12}}{x_2} \rightarrow \mathcal{D}_{12} = \frac{D_1 x_2}{\omega_2} \tag{2.17}$$

That can be substituted in equation (2.16) along with $x_2 = 1 - x_1$, which leads, after simplifications to:

$$\mathbf{j_1} = -\rho_1 D_1 \frac{\boldsymbol{\nabla} x_1}{x_1} \tag{2.18}$$

2.4.1.2.c The diffusion coefficients

The pseudo-diffusion coefficients, D_i (for $i = 1, 2$), have been described with a "Fujita-type" equation. This approach, based on the free volume concept (Fujita, 1961, Muhr and Blanshard, 1982, Neogi, 1996, Masaro and Zhu, 1999), has been intensively utilized in literature to describe HPMC-based systems during diffusion-swelling processes (Gao and Fagerness, 1995, Siepmann et al., 1999a, Siepmann and Peppas, 2000, Siepmann et al., 1999b,

Siepmann et al., 2002, Kaunisto et al., 2013, Lamberti et al., 2011). In this manner it has been possible to consider low diffusivity values in the dry matrix core and increasing values along with the water concentration:

$$D_i = D_{i,eq} \exp\left[-\beta_i\left(1 - \frac{\omega_1}{\omega_{1,eq}}\right)\right] \quad (2.19)$$

Where $D_{i,eq}/\exp(\beta_i)$ are the values of the effective pseudo-diffusion coefficients in the dry matrix ($\omega_1 = 0$), and $D_{i,eq}$ are the values of the effective pseudo-diffusion coefficients in the fully swollen matrix ($\omega_1 = \omega_{1,eq}$).

2.4.1.3 Swelling/shrinking description

The swelling phenomenon, increasing the length of diffusion pathways and changing the matrix morphology (mobility), greatly contribute to the final drug release kinetics (Siepmann and Siepmann, 2008). On the other hand, the surface erosion has to be included as well, since this mechanism accounts for the polymer release, mainly due to disentanglements, leading to matrix shape modifications and in turn to modified drug release behavior. Both these mechanisms can be mathematically translated in a deformable domain, therefore Ω is treated as $\Omega(t)$.

In this work the ALE (Arbitrary Lagrangian Eulerian) method has been applied to describe the tablet/domain deformation: $\Omega(t)=\left\{\left(r(R,Z,t), z(R,Z,t)\right)\Big|_{(R,Z)\,\epsilon\,\Omega_0}\right\}$. Briefly with "R" and "Z" are indicated the reference coordinate of the mesh/material frame (mesh and material frame are identical in this application), fixed to their original position, and with "r" and "z" are specified the spatial coordinates of the spatial frame in which all the previous equations have been defined. The domain deformation has been modeled considering that the domain is freely deformable and the deformation is driven by the movements of the boundaries exposed to the external medium. These boundaries move with a certain velocity, which is a net velocity obtained considering a swelling (positive) velocity and a shrinking /erosion (negative) velocity.

The swelling velocity has been derived through a polymer mass balance on the erosion front. It has been considered that the polymer movements, due to the water inlet and drug outlet, contributes only to the swelling phenomenon, without resulting in a polymer release. Therefore the polymer flux reaching the erosion front goes to increase the outer layers dimension, without being released (a scheme in **Figure 11**).

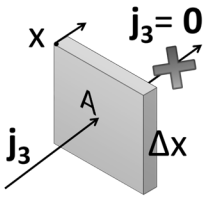

***Figure 11**. Sketch of a boundary element*

Mathematically:

$$\mathbf{j_3} A = \rho\, \omega_3 A \frac{\mathrm{d}\mathbf{x}}{\mathrm{dt}} \tag{2.20}$$

Therefore:

$$\mathbf{v_{swe}} = \frac{\mathrm{d}\mathbf{x}}{\mathrm{dt}} = \frac{\mathbf{j_3}}{\rho\, \omega_3} = -\frac{\sum_{i,i\neq 3} \mathbf{j_i}}{\rho\, \omega_3} \tag{2.21}$$

Where the definition $\sum \mathbf{j_i} = 0$ has been applied. This swelling formulation is different from the theoretical hypothesis in which the swelling occurs on the swelling front causing the movement of the hydrated external layer (the ones between the swelling and erosion fronts) toward the external environment. However it has been equally able to capture all the features of the system, not requiring for any fitting parameter.

The erosion phenomenon is related to the system fluid dynamics and to physicochemical interaction between the tablet interface and the outer medium. If these features are constant during the dissolution process and uniform around the swelling matrices, the erosion velocity can be accounted for using a constant value (which is a fitting parameter):

$$\mathbf{v_{er}} \cdot \mathbf{n} = -\,\mathrm{k_{er}} \tag{2.22}$$

Where **n** is the unit normal vector (outward-pointing) to the boundary

The relocation of the internal mesh nodes has been obtained accordingly to Laplace smoothing equations (COMSOL, 2013, Jin et al., 2014):

$$\begin{aligned} \frac{\partial^2}{\partial \mathrm{R}^2}\left(\frac{\partial \mathrm{r}}{\partial \mathrm{t}}\right) + \frac{\partial^2}{\partial \mathrm{Z}^2}\left(\frac{\partial \mathrm{r}}{\partial \mathrm{t}}\right) = 0 \\ \frac{\partial^2}{\partial \mathrm{R}^2}\left(\frac{\partial \mathrm{z}}{\partial \mathrm{t}}\right) + \frac{\partial^2}{\partial \mathrm{Z}^2}\left(\frac{\partial \mathrm{z}}{\partial \mathrm{t}}\right) = 0 \end{aligned} \tag{2.23}$$

It is worth to specify that the mesh convection induced by equations (2.23) does not have any physical meaning in the current model. Equations (2.23) have been solved with the following initial condition:

$$@\,\mathrm{t} = 0 \quad \Big(\mathrm{r}(\mathrm{R},\mathrm{Z},\mathrm{t}),\ \mathrm{z}(\mathrm{R},\mathrm{Z},\mathrm{t})\Big) = (\mathrm{R},\mathrm{Z}) = (\mathrm{r_0},\mathrm{z_0}) \tag{2.24}$$

The boundary conditions imposes the net velocity ($\mathbf{v_{swe}} + \mathbf{v_{er}}$) on the surface exposed to the dissolution medium and no movements on the surface where the tablet is fixed.

2.4.2 Code solving

The computational domain has been built, due to the symmetry, in the 2D-axial symmetric configuration.

The previous Partial Differential Equations (PDEs), along with all the initial and boundary conditions, have been solved with the Finite Element Methods (FEM) using the commercial software COMSOL Multiphysics® 5.0. The development and the implementation of the simulations have been carried out using a workstation based on the processor Intel® Core™ i7-4820K with a clock rate of 3.7 GHz and a RAM of 64 GB.

2.5 Results and discussion

The following sections have been divided in "whole-matrix" and in "distributed" results to emphasize the model ability to describe aspects related to the whole matrix (macroscopic), like global drug release, as well as distributed (microscopic) aspects, like the mass fraction profiles inside the tablet.

2.5.1 Overall release system

All the model parameters are reported in **Table 2**. Some of them have been obtained by direct measurements, some others have been estimated from previous works and, few of them, have been used as fitting parameters, starting from literature values and optimizing the model prediction on the experimental data. In particular the transport parameters and the erosion constant ($D_{1,eq}$, $D_{2,eq}$, β_1, β_2, k_{er}) were optimized against the macroscopic results: water, drug and polymer masses in the tablet during the dissolution process. The initial guess values for the diffusivities in the fully swollen layers have been the self-diffusion coefficient of water in water (3.027×10^{-9} [m^2/s] @37°C (Holz et al., 2000)) for $D_{1,eq}$ and the diffusion coefficient of theophylline in water (8.21×10^{-10}[m^2/s] @37°C (Grassi et al., 2001)) for $D_{2,eq}$. However in a swelling hydrogel system the variables that could affect the species transport are several: presence of concentration gradients, polymer relaxation (Camera-Roda and Sarti, 1990), ionic species and so on. That is why, in this work, the simplest expressions for the diffusive fluxes modified with Fujita-type diffusivities have been chosen. In this manner a robust, but still simple, model has been built, leaving with the fitting parameters the necessary flexibility to deal with these complicate systems.

Table 2. *Values of the model parameters in the overall release system*

From experiments/literature		
r_0	Initial tablet radius [mm]	6.5
z_0	Initial tablet semi-thickness [mm]	1
ω_{10}	Initial water mass fraction [−]	0
ω_{20}	Initial drug mass fraction [−]	0.475
ω_{30}	Initial polymer mass fraction [−]	0.525
ρ_1	Water density [kg/m^3]	1000
ρ_2	Drug density [kg/m^3]	1200
ρ_3	Polymer density [kg/m^3]	1200
M_1	Water molecular weight [g/mol]	18
M_2	Drug molecular weight [g/mol]	180.16
M_3	Polymer molecular weight [g/mol]	120000
From experiments/hypotheses		
$\omega_{1,eq}$	Equilibrium water mass fraction [−]	0.97
$\omega_{2,eq}$	Equilibrium drug mass fraction [−]	0
From literature/optimization		
$D_{1,eq}$	Water effective diffusivity in the fully swollen matrix [m^2/s]	2.2×10^{-9}
$D_{2,eq}$	Drug effective diffusivity in the fully swollen matrix [m^2/s]	1×10^{-10}
β_1	Water Fujita-type equation coefficient [−]	5
β_2	Drug Fujita-type equation coefficient [−]	4
k_{er}	Erosion constant [m/s]	55×10^{-9}

It has to be specified that each of these fitting parameters affect more than one model outcomes and therefore they are not completely independent. For example "k_{er}" is the only responsible for the polymer erosion but it has even a direct impact on the tablet size and shape. In the same manner the diffusion coefficients, tuned on the mass of drug and water, influence the tablet shape and the internal mass fraction profiles. Therefore only the right combination of these parameters can be able to describe the whole system.

2.5.1.1 Whole matrix results

In **Figure 12** are reported the experimental results referred to the whole matrix, from Lamberti et al. (Lamberti et al., 2011), compared with the modeling results obtained in this work.

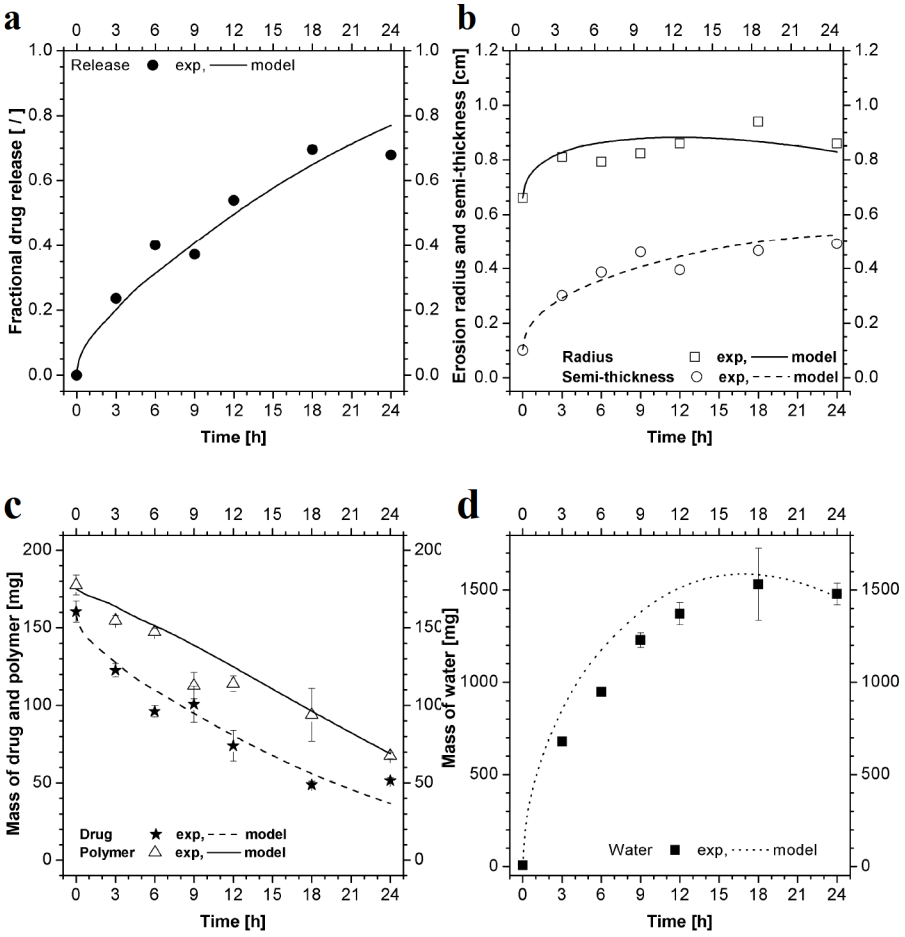

Figure 12. *Comparison between experimental and calculated results in the overall system, in terms of fractional drug release(a), erosion radius and semi-thickness (b), mass of drug and polymer (c) and water (d) inside the tablet at different dissolution times.*

The experimental fractional drug release (**Figure 12**/a), apart from the first instants, resembles a zero order release kinetic, releasing the drug at a constant rate. As it can be seen the modeling results, derived indirectly from the current drug mass inside the tablet, perfectly describe this release behavior.

In **Figure 12**/b the erosion radius and semi-thickness are shown, that correspond experimentally and from modeling point of view to the point on $\Gamma 4$ at $z=0$ and on $\Gamma 3$ at $r=0$, respectively (**Figure 10**). Even in this case the model is able to describe the "macroscopic" non-affine swelling. Indeed one of the strong points of this model is the possibility to describe tablet deformation different from the limiting assumption of affine swelling (like in Siepmann et al. (Siepmann and Peppas, 2000)). It can be seen that whereas the

semi-thickness still increases within the time analyzed, the radius starts to decrease. This can be explained considering that the water inlet driving force became smaller in the radial than in the axial direction, mainly due to a longer pathway generated by a thicker gel layer, letting the erosion to take over.

In **Figure 12**/c and **Figure 12**/d the drug and polymer masses, as well as the water mass inside the tablet *vs* time, are respectively represented. This modeling results have been obtained integrating the mass concentrations of the i^{th} species ($\rho\ \omega_i$) on the deformed domain:

$$m_i(t) = 2 \times \int_{\Omega(t)} \rho\ \omega_i\ d\Omega \qquad (2.25)$$

The model has been found able to correctly describe the evolution of the mass species, inside the tablet, during the dissolution process.

2.5.1.2 Distributed results

The model so formulated allows to know in each point of the domain the mass fractions of water, drug and polymer. Therefore it is able to describe microscopic aspect like the species distribution inside the swollen tablet or, defining a solvent concentration threshold value for the glass-rubber transition, it would able to describe the matrix core position and its movements.

In **Figure 13** the experimental and calculated mass fraction (averaged along the thickness direction) profiles inside the tablet are compared.

The experimental results have been obtained in this work with the "hollow punch" procedure described in the method section. The horizontal bars in **Figure 13** represent the radius of the tablet pieces (annulus or core) analyzed. To compare the experimental values with the calculated results, a mass fraction value averaged along the thickness direction, z, has to be defined:

$$\langle \omega_i \rangle(r) = \frac{\int_0^{H(r)} \omega_i dz}{\int_0^{H(r)} dz} \qquad (2.26)$$

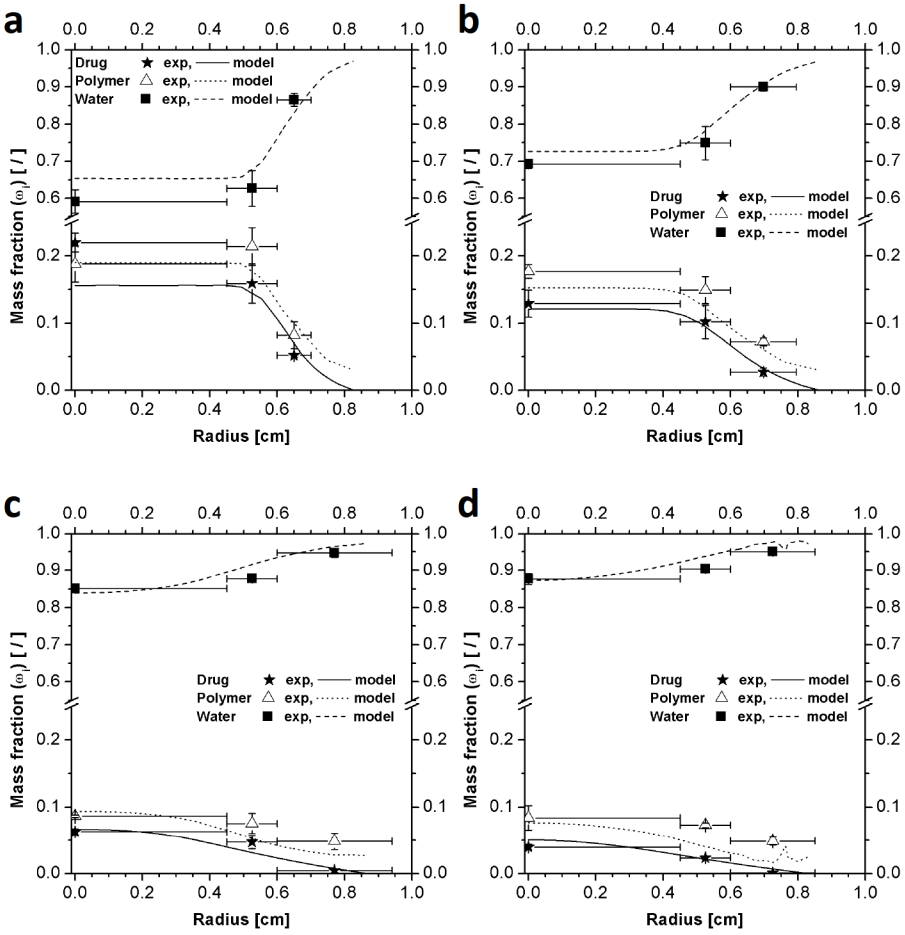

Figure 13. *Comparison between experimental and calculated results in terms of mass fraction (averaged along the thickness direction) profiles along the radial direction. Dissolution times of 3 h (a), 6 h (b), 18 h (c), 24 h (d).*

These are average mass fractions along the axial direction, as function of the radial position. As it can be seen in **Figure 13** the calculated profiles well describe the experimental data, confirming the model ability to reproduce the system behavior.

Other microscopic comparisons are shown in **Figure 14**. Tablets pictures (top part) are compared with the calculated water mass fraction contour plots (bottom right part) and with the calculated swollen tablet shapes (the black lines in top right part). In the graphs showing the tablet after 3 and 6 h of dissolution the reader should follow the bright reflection to individuate the right swollen tablet profile since the pictures include, due to inclination of the photos, a piece of the tablets top part. The modeling results even in this case seems to nicely describe the experimental results. The shape profiles close

resemble the experimental one and, just qualitatively on the basis of the data available, the contours of the water mass fraction seem to well describe the tablet hydration levels.

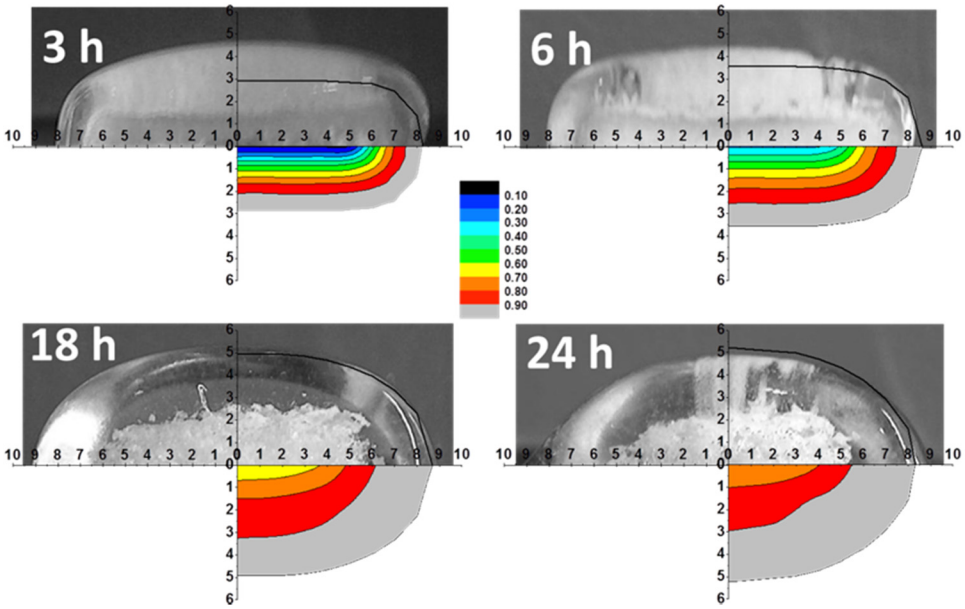

Figure 14. *Comparison between experimental and modeling results. In the top part of each graph: photos, and calculated shape of the swollen matrix as a black line. In the bottom right part of each graph: calculated water mass fraction as contour plot. All the spatial sizes are in mm; color scale is referred to water content fraction (black = dry matrix; light gray = fully hydrated matrix).*

2.5.2 Radial release system

2.5.2.1 Whole matrix results

In the radial dissolution tests, the matrices behavior was monitored for 4 days, gathering experimental data each 24 h. In **Figure 15** the total mass evolution of each component inside the swollen matrix is shown. The drug release is particularly slow in this configuration, where the surface through which the system can exchange matter is only the lateral one, reaching at maximum the 60% of theophylline release in 4 days. However the release rate seems to be higher in the first 24 h, sensibly decreasing after that time. This can be explained considering that in this configuration within the first day the drug close to the tablet lateral surface is promptly dissolved and released whereas after this first part the presence of a gel layer takes over and the drug transport and its release become more and more difficult, leading to a decrease

of the release rate. On the other hand even the polymer dissolution is very limited, especially in the first 48 hours, bringing to a final dissolution of about 20% of the initial polymer amount in the matrix. The water uptake considerably increases in the first 3 days, slowing down after that time.

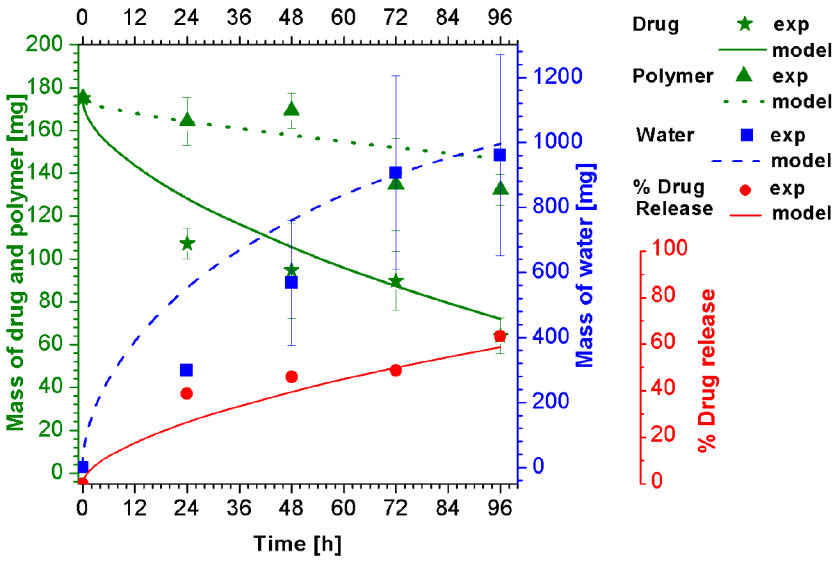

Figure 15. *Radial dissolution: mass of drug, polymer (green) and water (blue) inside the swollen tablet at different dissolution times. In red the percentage of drug release.*

The curves in **Figure 15** represent the modeling results. Most of the model parameters (**Table 3**) are the same of the overall release system with the exception of the water Fujita-type equation coefficient (β_1), that has been updated with experimental literature results from Gao et al. (Gao and Fagerness, 1995) and the drug effective diffusion coefficient that has been slightly increased to better describe the drug release. The erosion constant has been used as fitting parameter.

With this minimum parameters adjustment the model results seem to well describe all the "macroscopic" experimental results gathered.

Table 3. *Values of the model parameters in the radial and semi-overall release systems*

From experiments/literature		
r_0	Initial tablet radius [mm]	6.5
z_0	Initial tablet semi-thickness (radial) or thickness (semi-overall) [mm]	1
ω_{10}	Initial water mass fraction [−]	0
ω_{20}	Initial drug mass fraction [−]	0.5
ω_{30}	Initial polymer mass fraction [−]	0.5
ρ_1	Water density [kg/m^3]	1000
ρ_2	Drug density [kg/m^3]	1200
ρ_3	Polymer density [kg/m^3]	1200
M_1	Water molecular weight [g/mol]	18
M_2	Drug molecular weight [g/mol]	180.16
M_3	Polymer molecular weight [g/ mol]	120000
From experiments/hypotheses		
$\omega_{1,eq}$	Equilibrium water mass fraction [−]	0.97
$\omega_{2,eq}$	Equilibrium drug mass fraction [−]	0
From literature/optimization		
$D_{1,eq}$	Water effective diffusivity in the fully swollen matrix [m^2/s]	2.2×10^{-9}
$D_{2,eq}$	Drug effective diffusivity in the fully swollen matrix [m^2/s]	1.5×10^{-10}
β_1	Water Fujita-type equation coefficient [−]	3.53 (Gao and Fagerness, 1995)
β_2	Drug Fujita-type equation coefficient [−]	4
$k_{er_{radial}}$	Erosion constant [m/s]	10×10^{-9}
$k_{er_{semi-overall}}$	Erosion constant [m/s]	5×10^{-9}

2.5.2.1 Distributed results

The model so tuned has been compared to microscopic experimental results. In particular in **Figure 16** the data from the gravimetric and the texture analyses allow to completely characterize the system in terms of components distribution inside the swollen tablets. The horizontal bars represent the radius of the tablet pieces (annulus or core) analyzed, therefore the experimental point is a mean value of the piece examined. The texture data instead represent local water mass fraction that is constant along the tablet height (Lamberti et al., 2013). As it can be seen these two techniques are in good agreement and give precise information on the hydration of the swollen tablet. The other

gravimetric data, on drug and polymer mass fractions, close the balances on the whole system. After 24 h (**Figure 16**/a) the tablet core is almost not hydrated and as the dissolution time passes the inner part of the tablet get more and more hydrated, reaching the 50% w/w after 96 h (**Figure 16**/d) in the tablet core. The drug mass fraction profiles instead highlight the phenomenon of the faster drug release rate in the first 24 h with respect to greater dissolution times. Indeed the drug mass fraction close to the erosion front (**Figure 16**/a) shows the depletion of drug inside the swollen tablet for several millimeters, confirming the promptly dissolution and release of the theophylline close to the erosion front, whereas in the tablet core its mass fraction is still the original one. After the initial dissolution/release behavior, the inner tablet parts play the role of a drug storage, allowing its gradual release along with the tablet hydration (**Figure 16**/b-d). The polymer distribution, besides confirming the equilibrium polymer mass fraction at the erosion front (3% w/w), shows the gradual polymer dilution along with the tablet swelling.

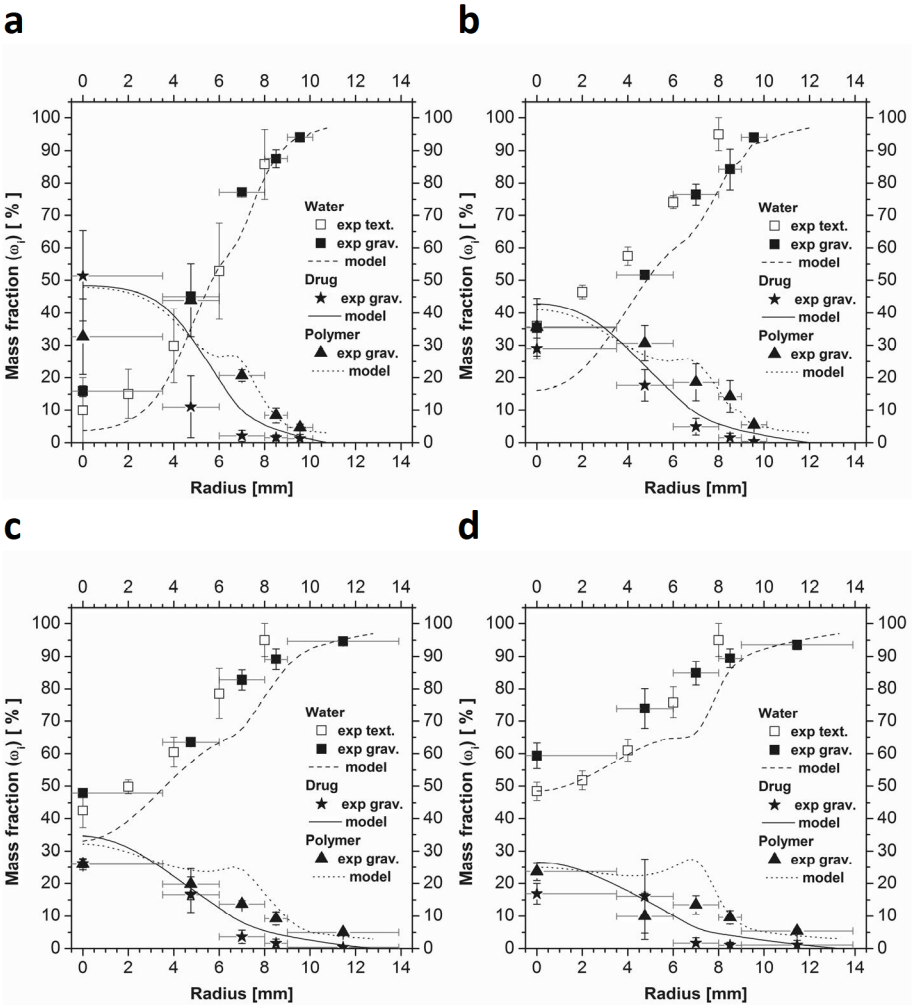

Figure 16. *Comparison between experimental and calculated results in terms of mass profiles along the radial direction. Dissolution times of 24 h (a), 48 h (b), 72 h (c), 96 h (d).*

The modeling results have been compared to the experimental results using the mass fraction profiles along the tablet radius (at any height) that, in this system, is equal to the $\langle\omega_i\rangle(r)$ since the mass fraction is constant along the axial direction. The modeling water mass fraction profiles in the first 48 h (**Figure 16**/a-b) slightly underestimate the experimental points whereas, at the same times, there is an overestimation in the macroscopic water uptake. This is explainable considering that a greater swollen tablet radius is predicted, and in the external layers the amount of water is predominant (97% of the total mass), bringing to an overestimation of the macroscopic water adsorption,

despite the underestimation of the internal mass fraction profiles. However with this null model parameters adjustment the experimental mass fraction profiles are satisfactorily well described (**Figure 16**).

2.5.3 Semi-overall release system

The "semi-overall" dissolution analyses, were set up to reproduce the behavior of the overall dissolution tests exploiting the plane of symmetry. Indeed half amount of components was utilized to form tablets, with respect to the normal tablets (e.g. the tablets employed for the radial tests), and the lower tablet part was centrally glued on a glass slab to reproduce the symmetry condition of the overall system: the null mass flux. With this expedient the system behavior can be easily characterized in terms of macroscopic data (e.g. residual masses and shape) and in terms of microscopic data (e.g. hydration via texture analyses).

2.5.3.1 Whole matrix results

In the semi-overall dissolution tests the tablets behavior was analyzed for 24 h. In **Figure 17**/a are reported the residual masses inside the swollen matrices as well as the percentage of drug release. In this configuration the surfaces through which the system can exchange matter are the lateral and the top part, substantially changing the release behavior with respect to the radial experiments. Indeed, after 24 h of dissolution the drug release is close to the 97% (just the 38% in the radial tests) and the water uptake is close to 1 g (less than 0.4 g in the radial tests). Instead the polymer dissolution/release, like in the radial experiments, is very limited in the dissolution time analyzed. In **Figure 17**/b the erosion radius and thickness obtained from the photos are shown, taking the maximum radius and the central height (at r=0). As it can be seen, the axial swelling is quite pronounced, increasing of almost 6 times with respect to the initial thickness, whereas the radial expansion is in somewhat less marked, despite the increment is of 1.5 times the initial radius. The model tuned on the macroscopic radial experiments has been applied with the same parameters (apart the erosion constant, the only fitting parameter) to the semi-overall configuration, changing the boundary conditions. The new value of k_{er} was $5 \times 10^{-9}[m/s]$ (see **Table 3**). As it can be seen all the experimental results in **Figure 17**/a-b are well predicted from the model, allowing the complete characterization of the macroscopic behavior of the tablet dissolution in the semi-overall configuration.

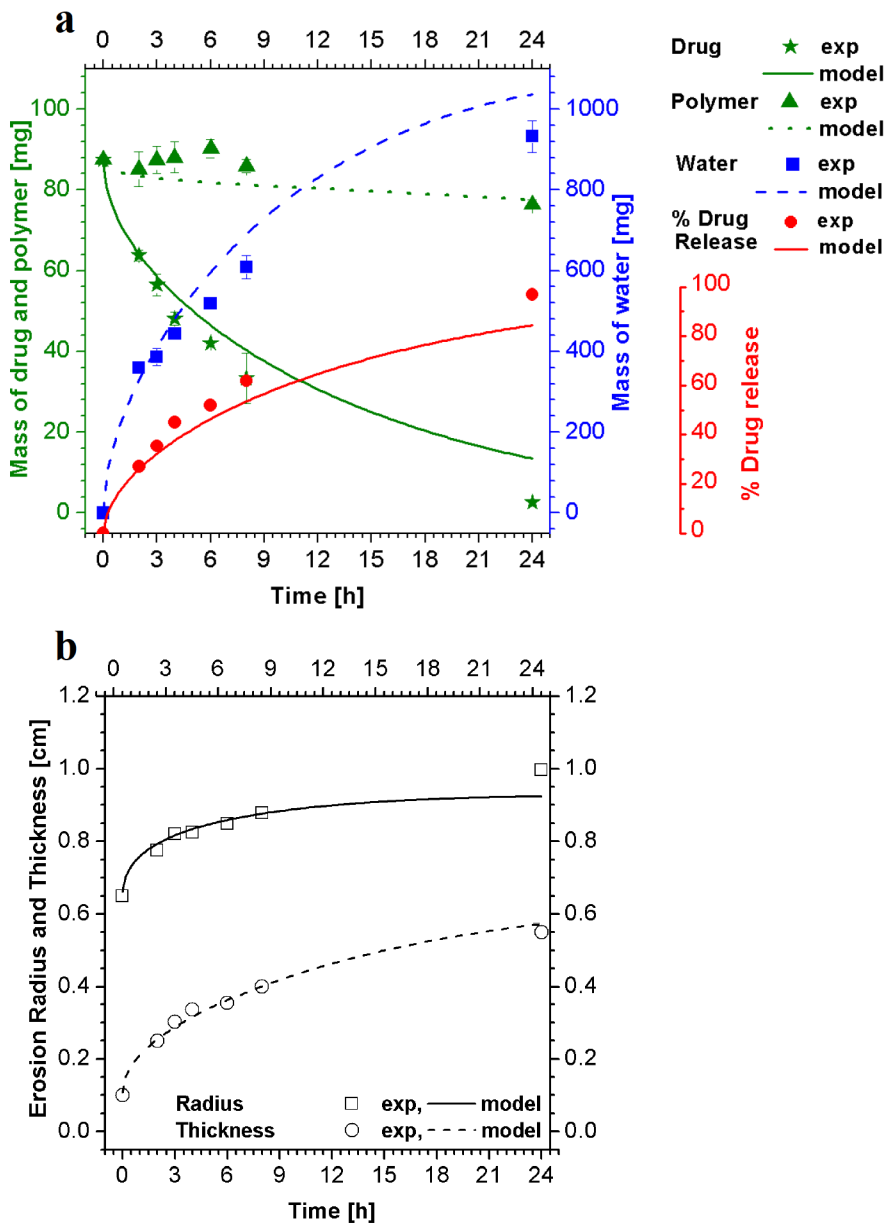

Figure 17. *Semi-overall dissolution: (a) mass of drug, polymer (green) and water (blue) inside the tablet at different dissolution times. In red the percentage of drug release. (b) Erosion radius and thickness of the swollen tablet.*

2.5.3.2 Distributed results

In order to completely investigate the matrix behavior, the swollen matrices have been subjected to texture analyses to obtain the hydration level. The technique gives information on the water content along the axial distance: repeating the analysis at several radii it is possible to build a contour plot that shows the hydration level in the whole swollen tablet. As explained in Cascone et al. (Cascone et al., 2014) this type of analysis is not able to detect the presence of the fully swollen layers (ω_1>0.9) due to their low resistance to the needle penetration. However these simple analyses give precious information on the internal water content that can be compared with pictures of the swollen tablet as well as with modeling results. In **Figure 18** swollen tablet pictures (top left part) with texture analysis results (top right part), and modeling water mass fraction distribution (bottom right part) at several dissolution times (2, 3, 6 and 8 h) are shown. Both the texture and the modeling data are expressed in terms of water mass fraction content, starting from zero (black) in the dry regions up to more than 0.9 in the fully swollen regions (light gray).

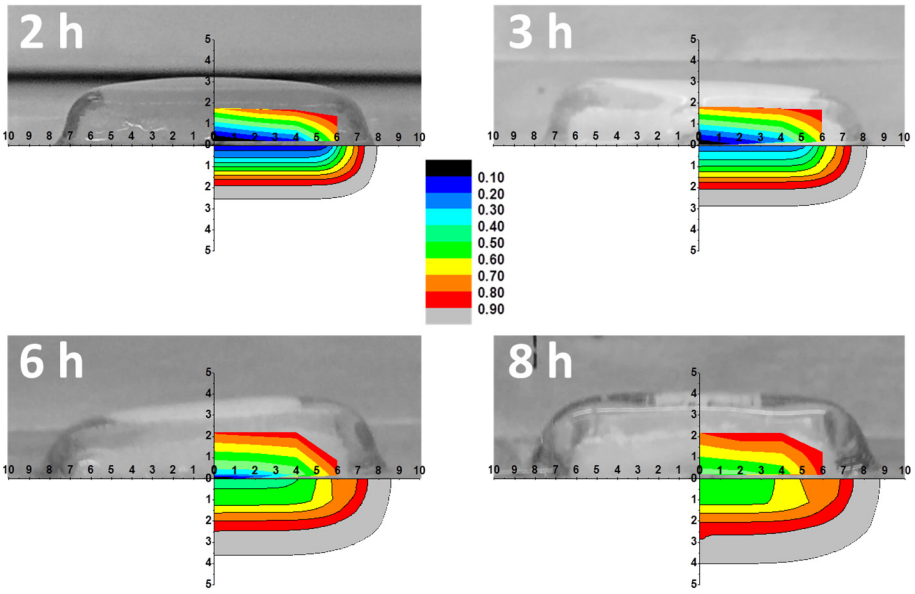

***Figure 18**. Semi-overall dissolution: comparison between experimental and modeling results in terms of tablets pictures (top part of the graphs), experimental water mass fraction from texture analysis (top right part of the graphs) and modeling water mass fraction (bottom right part of the graphs). All the spatial dimensions are in mm; color scale is referred to water content mass fraction (black = dry matrix; light gray = fully hydrated matrix).*

From these graphs, it is possible to see that the internal tablet hydration level, as well as the final swollen tablet shape, are quantitatively well predicted by the model thanks to the comparison with the texture analysis results and the swollen matrix pictures, respectively. This confirms, once again, the validity of the proposed model, that is able to predict in a satisfactorily manner all the phenomena involved in a tablet dissolution process, as well as the effectiveness of the experimental methods employed in the characterization of the swollen tablets.

2.5.4 Commercial-like tablets

The tablets in this case are made, as shown in **Figure 19** (left), of HPMC 45%, Micro Crystalline Cellulose (MCC) 15%, lactose (LAC) 30%, theophylline (TP) 10%. To model such kind of system two main assumptions were done:

- LAC was considered as a diffusant with the same transport characteristics as TP (hypothesis supported by the close self-diffusion coefficients of these molecules in water (Ribeiro et al., 2006, Grassi et al., 2001));
- MCC was combined with the HPMC, forming a pseudo-component (PC) with average characteristics weighted to their amount (**Figure 19**) (it is likely that the MCC particles do not diffuse within the system but move solidly with the HPMC matrix).

Therefore, the system under investigation is made by four components: water (i = 1), TP (i = 2), pseudocomponent (MCC+HPMC) (i= 3), and LAC (i = 4). The components characteristics in terms of initial mass fractions, densities, and molecular weights are reported in **Table 4**.

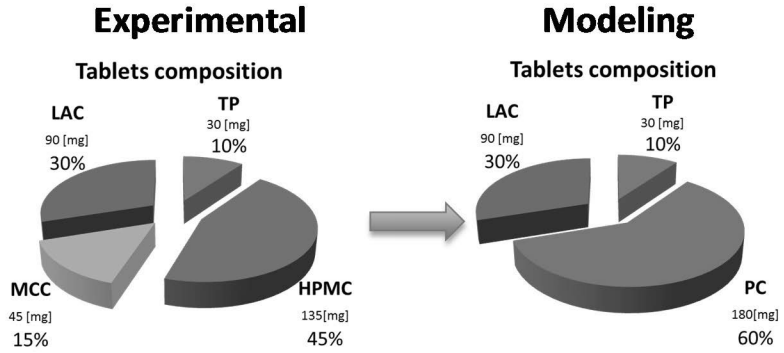

***Figure 19**. On the left, the real tablet composition. On the right, the simulated tablet composition, with the definition of the pseudo-component (PC).*

The densities in

Table 1 are calculated from the particle densities and from the tablets porosity reported in Viridén et al. (Viridén et al., 2011).

Table 4. *Mass fraction, density, and molecular weight for each tablet component*

From experiments/literature				
		Batch A		**Batch B**
ω_{10}	Initial water mass fraction [−]		0.00	
ω_{20}	Initial drug mass fraction [−]		0.10	
ω_{30}	Initial pseudo-component mass fraction [−]		0.60	
ω_{40}	Initial lactose mass fraction [−]		0.30	
ρ_{10}	Water density [kg/m^3]		1000.00	
ρ_{20}	Drug density [kg/m^3]	1209.90		1199.50
ρ_{30}	Pseudo-component density [kg/m^3]	1134.80		1125.00
ρ_{40}	Lactose density [kg/m^3]	1250.50		1239.70
M_1	Water molecular weight [g/mol]		18.00	
M_2	Drug molecular weight [g/mol]		180.16	
M_3	Pseudo-component molecular weight [g/mol]	130750.00		103000.00
M_4	Lactose molecular weight [g/mol]		342.30	
From experiments/hypotheses				
$\omega_{1,eq}$	Equilibrium water mass fraction [−]		0.97	
$\omega_{2,eq}$	Equilibrium drug mass fraction [−]		0	
From literature/optimization				
$D_{1,eq}$	Water effective diffusivity in the fully swollen matrix [m^2/s]		8×10^{-9}	
$D_{2,eq}$, $D_{4,eq}$	Drug and Lactose effective diffusivity in the fully swollen matrix [m^2/s]		3.5×10^{-10}	
β_1	Water Fujita-type equation coefficient [−]		3.53 (Gao and Fagerness, 1995, Caccavo et al., 2015b)	
β_2	Drug Fujita-type equation coefficient [−]		4 (Caccavo et al., 2015b)	

2.5.4.1 Whole matrix results

Figure 20 shows the experimental and calculated masses of the model substance TP and HPMC (the heterogeneous batch B and homogenous batch A) in the dissolving tablets. The experiments were performed in two different experimental setups, (i) a USP II dissolution apparatus equipped with an external stationary basket and (ii) a rotating disc with the tablets glued onto the rotating disc. The rotating disc setup fits into the NMR probe and make it possible to simultaneously study the TP and HPMC release and water content in the formulation. Experimentally it was found that the drug release kinetics, under the same dissolution conditions, was similar for formulation A and B, whereas the polymer release kinetic had a completely different behavior in both setups. Formulation A showed clearly a faster erosion than formulation B. It has earlier been shown that formulations containing homogenous HPMC batches, with same degree of substitution and molecular weight, erode faster than heterogeneous batches (Viridén et al., 2009b, Viridén et al., 2010). This has been explained with formation of strong hydrophobic transient crosslinks between the HPMC chains for batches with a high degree of heterogeneity in the substitution pattern (Viridén et al., 2009b, Viridén et al., 2010), which also results in formation of a thicker gel layer and marked influence on the drug release for drugs with low solubility (Viridén, 2011). However, for drugs with relative high solubility as TP (11.2 mg/ml @ 37 °C in phosphate buffer (Viridén et al., 2011)) the effect on drug release rate and polymer heterogeneity is lower: as soon as the water penetrate inside the matrix and form a gel the drug will promptly dissolve and freely diffuse toward the dissolution medium.

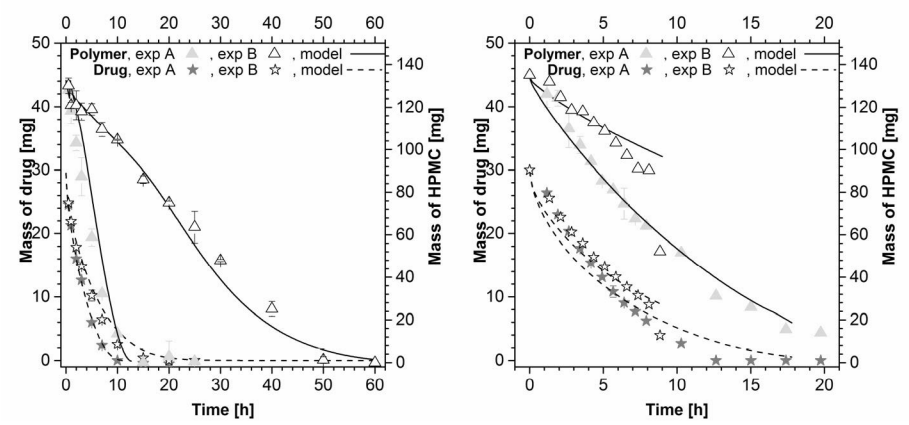

***Figure 20**. Polymer and drug masses in the tablet during the hydration. Symbols: experimental data; curves: model calculations. On the left, results for USP experiments; on the right, results for NMR experiments.*

The experimental release data for formulation A in the USP II setup was used to tune the model to obtain the diffusion coefficients of water and TP/LAC in the system, as well as the erosion constant k_{er}. The diffusion coefficients depends on the composition and, once determined, they can be applied to describe different systems, for example for tablets with different sizes and shapes. The best fitting parameters were determined to be $D_{1,eq} = 8 \times 10^{-9}$ m^2/s for water and $D_{2,eq} = D_{4,eq} = 3.5 \times 10^{-10}$ m^2/s for TP and LAC, and with an erosion constant of $k_{er_{USP}}^{BatchA} = 280 \times 10^{-9}$ m/s. The masses of TP and polymer in the tablets during the release were calculated for the B formulation, and for both formulations A and B in the NMR setup, by using these obtained diffusion coefficients, while the erosion constant was left as the only remaining fitting parameter. Formulation B was characterized by a lower erosion constant ($k_{er_{USP}}^{BatchB} = 55 \times 10^{-9}$ m/s) than obtained for formulation A ($k_{er_{USP}}^{BatchA} = 280 \times 10^{-9}$ m/s), as expected since the erosion for formulation B was slower than for A. In the NMR rotating disc setup the erosion was faster, giving an increase in the obtained erosion rates for both formulation A and B ($k_{er_{NMR}}^{BatchA} = 380 \times 10^{-9}$ m/s and $k_{er_{NMR}}^{BatchB} = 100 \times 10^{-9}$ m/s, respectively). The erosion constants fitted for the NMR are significantly higher than the ones obtained in the USP setup. This shows that the erosion phenomena is a function of the composition of the formulation but also of the fluid dynamics in the dissolution setup, and it appears that the shear forces in the NMR release cell are larger than in the USP II setup. This is coherent with the higher speed of rotation employed and the smaller container dimension that surely leads to higher shear stresses on the swollen tablet with respect to the USP dissolution conditions. It might be argued that the experiments for batch B in the USP dissolutions show a larger polymer release with the respect to the NMR tests, despite the modeling erosion constants are higher in the last case. However, it has to be considered that the surface area exposed to erosion is lower in NMR systems since the bottom part of the tablet is glued on the disc and not exposed, therefore it cannot exchange matter with the release medium.

In conclusion, a good agreement between the experimental data and the calculated polymer and TP release from both formulation A and B were obtained, and the masses of the TP and polymer in the dissolving tablets can be calculated by using the model after adapting it to the flow conditions in the setup, once the diffusion coefficients are obtained.

2.5.4.2 Distributed results

The NMR images for batch A and B at different times can be seen in **Figure 21** and **Figure 22**.They are presented as the water mass fraction distribution inside the swollen tablets at different dissolution times. The left part of **Figure 21** and **Figure 22** shows the original NMR images with the rotating disc (at the bottom part) and the swollen tablet (at the upper part) for formulation A and B, respectively. The right part of **Figure 21** and **Figure 22**

shows the mass fraction distributions. The upper part of the water mass fraction presents experimental images, whereas the bottom part shows the predicted water mass fraction distributions. Due to limitations imposed by the NMR technique, the reported water content (experimental and calculated) is only shown in the range of 60-100% w/w.

The results for homogeneous batch A at two different times are presented in **Figure 21**, which show the water concentration profile along the radial "r" direction and the axial "z" direction with a 97% w/w water content at the erosion boundaries and with a decreasing concentration going toward the tablet core. It is worth noting that in this system the most hydrated layer, with a water content between 90 and 97% w/w, is extremely thin in both the experimental and predicted results due to the high erosion rate achieved in this experimental setup. The experimental and modeling results are in fairly good agreement and well comparable, despite the several approximations made. At 2.70 h there is an almost perfect match in predictions of degree of swelling and water concentrations, as can also been seen in **Figure 21** (left side). At 7.20 h the match between the predicted and the experimental water contents at different positions in the hydrated layer are less good (**Figure 21**, right side). The swelling behavior for batch A in the radial direction at 7.20 h shows a rather good agreement between the experiments and predictions (**Figure 21**, right). However, in axial direction at r=0 the degree of swelling is larger experimentally than for the predicted values. External forces, such as gravity, that may act and deform the swollen matrix were not included in the employed model. These forces become more relevant at higher hydration levels, when the formed gel layer is weaker and more prone to be deformed.

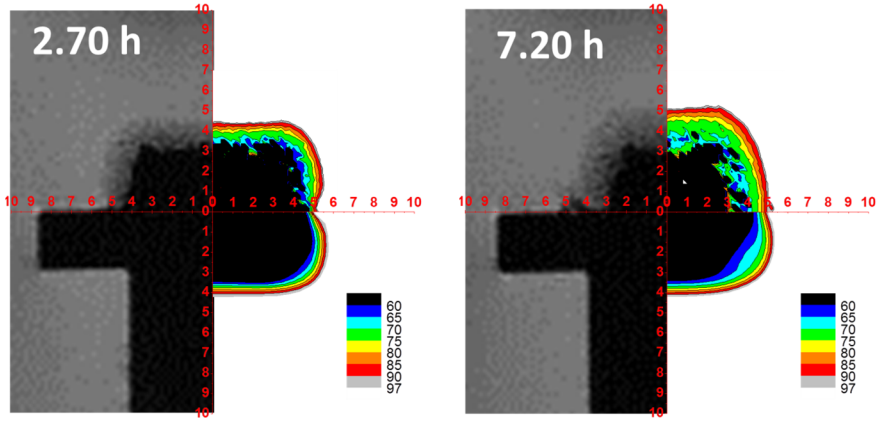

***Figure 21**. NMR images (top left of each figure), experimental water fraction distribution (top right of each figure), calculated water fraction distribution (bottom right of each figure). Experiments carried out on formulation A at two immersion times (right side: 2.70 h and left side 7.20 h).*

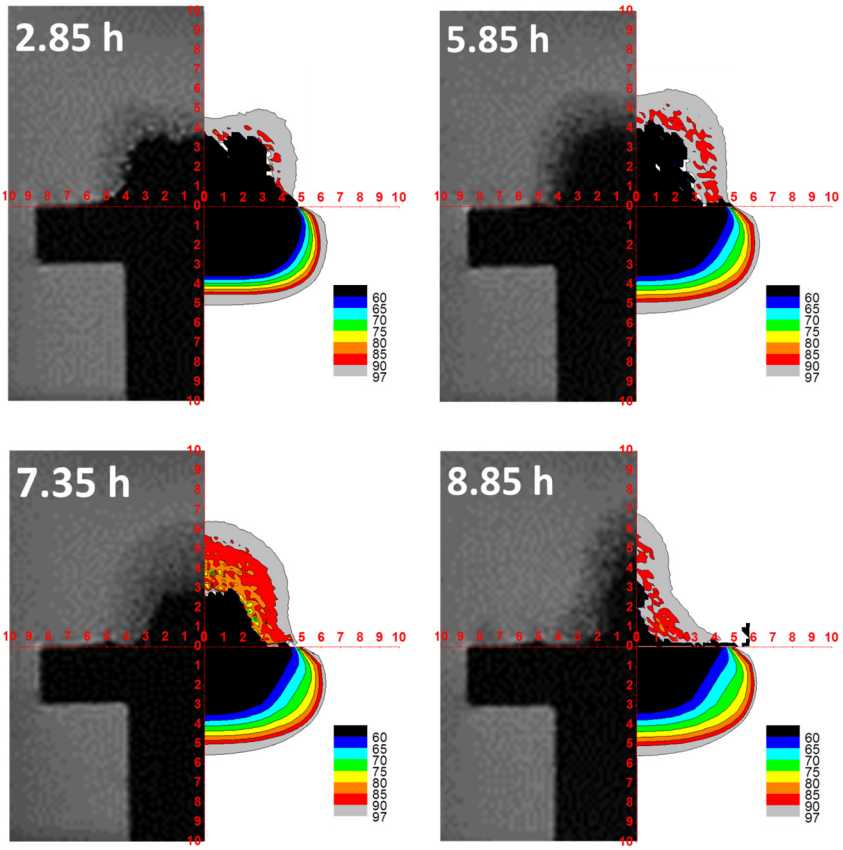

***Figure 22**. NMR images (top left of each figure), experimental water fraction distribution (top right of each figure), calculated water fraction distribution (bottom right of each figure). Experiments carried out with HPMC from batch B, four immersion times (2.85, 5.85, 7.35 and 8.85 h).*

The simulation results, which could more or less predict the swelling and water distribution for the homogenous batch A, were compared with the heterogeneous batch B MRI results, see **Figure 22**. The heterogeneous batch B shows experimentally a completely different dissolution behavior in terms of hydration and swelling compared to batch A. Therefore, the predictions failed with respect to both shape and water distribution in the swollen gel layer, and more specific these differences were observed:

1) The predicted size in radial direction was larger than shown by the experimental data and somewhat smaller in axial direction at all times. The swelling at the edge between the two planes is overestimated compared to the experimental results. This was due to the drop formation caused by gravitation and deformation of the gel layer, as seen in

(Tajarobi et al., 2009, Viridén, 2011) and discussed above. The drop shape deformation increased with time as the gel becomes larger and more diluted (**Figure 22**).

2) The predicted water concentration gradient in the gel layer changes gradually, whereas the experimental concentration gradient is completely different with formation of two regions in the gel layer, one with water content above 85% without any clear dependence of the position and one region with water content below 60 %. The thick gel layer for batch B, containing a high amount of water is an effect of the hydrophobic transient interactions, giving higher viscosities at lower polymer concentrations (Viridén et al., 2009a), and thus it can better withstand the applied shear forces (Körner et al., 2009). The discontinuous experimental concentration profile for formulation B, with almost two regions with different water content separated by a step change, compared to the predicted extremely uniform hydration profile cannot be explained with a simple diffusion process driven by the gradient of the molar fraction (Fick's law).

3) For batch B the black regions, with a water content below 60%, is smaller than the predicted region at all times and diminish faster than for the predictions. This indicates a faster water penetration than expected.

One suggestion to the discrepancies between experimental and predictions data for the hydration/swelling might be that the mechanism is better described by the so called "pure Case II sorption", where the diffusion of the dissolution media into the matrix is considerably quicker than the speed of the relaxation of the polymer chains. This leads to a separation between the external gel layer and the internal almost unpenetrated glassy core (Alfrey et al., 1966, Camera-Roda and Sarti, 1986, Tritt-Goc et al., 2005). The modeling approach employed, despite being able to describe the drug and HPMC release, was found to be insufficient to describe the water uptake and swelling for batch B. The difference between the experimental and predictions for formulation B indicates that relaxation behavior should be significantly different for homogenous and heterogeneous HPMC batches.

2.6 Summary

In this chapter a mechanistic model for drug release from hydrogel-based systems has been developed and validated against experimental data (Caccavo et al., 2015b, Caccavo et al., 2015a).

HPMC-based tablets, loaded with Theophylline have been studied. Differently to what is normally done in dissolution tests, in this work besides the evaluation of the drug release via spectrophotometric analysis, it has been determined also the water and polymer residue by gravimetric analysis. This has been done on the entire tablets, as well as on portion of them, obtaining internal profiles of the components. The partially swollen tablets have been also subjected to indentation tests, which after an opportune calibration have allowed obtaining information on the water distribution inside the system.

The 2D-axisymmetric model has been built on the water and drug mass transport equations; the polymer has been obtained from the mass fraction constraint. The deformations have been describe with an ALE moving mesh method, whose boundaries move in relation to the amount of water and drug entering or leaving the system. The comparison between the detailed experimental results and the modeling results has showed a good agreement, in terms of masses, shape and components distribution, demonstrating that the main features had been correctly described.

Such a formulated model has been applied to describe commercial-like tablets (in which excipients are present), with two type of HPMC with different substitution pattern (i.e. different degree of cross-links) and tested in non-standard apparatus (NMR cell) (Caccavo et al., submitted). Despite after a proper tuning the model had been able to describe the drug and polymer release, the shape and the water distribution inside the system (experimentally taken from MRI technique) were not correctly described.

This application demonstrated the limits of a "mass transport only" approach. In the analyzed case the forces acting on the swelling tablet (shear, centrifugal, gravitational) could have a relevant impact, but most of all the different degree of cross-links of the HPMC plays the major role. This could dramatically change the water absorption behavior, being able to generate gels with different mechanical properties (i.e. stiffness, time of relaxation etc.) that in turn influence the mass transport. Such a relation between stiffness of the gel (stresses) and mass transport is not contemplated in a "mass transport only" approach, where it is supposed that the deformation is only driven by local mass variations, without accounting for the mechanical response. In other words the mass transport can drive deformation but stresses (internal or imposed) cannot.

2.7 Nomenclature

In **Table 5** the nomenclature employed during the mass transport based model developed to describe hydrogel-based systems.

Table 5. *Nomenclature of the mass transport based model*

Nomenclature	
A	Infinitesimal surface $[m^2]$
D_i	Pseudo-diffusion coefficient $[m^2/s]$
$D_{i,eq}$	Effective diffusion coefficient of the i^{th} species in the fully swollen matrix $[m^2/s]$
dr	Radial displacement [m]
dz	Axial displacement [m]
$H(r)$	Tablet semi-thickness, function of the radial position, during the dissolution process [m]
$\mathbf{j_i}$	Diffusive mass flux of the i^{th} species $[kg/(m^2\ s)]$
k_{er}	Erosion constant $[m/s]$
M	Average molar mass $[g/mol]$
M_i	Molar mass of the i^{th} species $[g/mol]$
R	Reference radial coordinate of the mesh/material frame [m]
r	Radial coordinate of the spatial frame [m]
r_0	Initial tablet radius [m]
r_i	Source term of the i^{th} species $[kg/(m^3\ s)]$
t	Time [s]
$\mathbf{v}$	Mass average velocity $[m/s]$
$\mathbf{v_{er}}$	Erosion velocity $[m/s]$
$\mathbf{v_{swe}}$	Swelling velocity $[m/s]$
x_i	Mole fraction of the i^{th} species $[-]$
Z	Reference axial coordinate of the mesh/material frame [m]
z	Axial coordinate of the spatial frame [m]
z_0	Initial tablet semi-thickness [m]
β_i	Fujita-type equation concentration dependence parameter of the i^{th} species $[-]$
Γ_i	i^{th} boundaries [m]
ρ	System density $[kg/m^3]$
ρ_i	Density of the i^{th} species $[kg/m^3]$

Ω	Computational domain $[m^2]$
ω_i	Mass fraction of the i^{th} species $[-]$
$\omega_{i,0}$	Initial mass fraction of the i^{th} species $[-]$
$\omega_{i,eq}$	Equilibrium mass fraction of the i^{th} species $[-]$
$\langle\omega_i\rangle(r)$	Average mass fraction on the axial direction function of the radial position $[-]$

Chapter Three

Analysis and modeling hydrogels: the poroviscoelasticy

In this chapter the mechano-diffusive behavior of hydrogels, where the water mass transport is strictly coupled with the system mechanics, will be treated.

Stress-relaxation tests, capable of highlighting the hydrogel poroviscoelastic behavior will be performed.

A poroviscoelastic model, within the monophasic approach, will be developed, implemented and validated against experimental results.

Part of this work has been reported in:

- **CACCAVO, D.** & LAMBERTI, G. **2017**. PoroViscoElastic model to describe hydrogels' behavior. Materials Science and Engineering: C, 76, 102–113.
- **CACCAVO, D.**, CASCONE, S., POTO, S., LAMBERTI, G. & BARBA, A. A., **in press**. Mechanical and transport phenomena in agarose-based hydrogels studied by compression-relaxation tests. Carbohydrate Polymers, doi: 10.1016/j.carbpol.2017.03.027.

3.1 Introduction to poroviscoelasticity

Hydrogels couple solvent mass transport to system deformation and vice versa. This phenomenon is generally called poroelasticity, which is also a characteristic of other materials (i.e. biological tissues, soils etc.). The poroelasticity is produced by "long range" motion of water molecules, which results in the swelling or shrinking of the hydrogel.

Another peculiarity of hydrogels is that the constituent polymeric network can have viscoelastic characteristics (i.e. like polymeric melts), which eventually translate in an overall hydrogel viscoelastic behavior. The viscoelasticity is generated by conformational changes of the structure, i.e. cross-links reformation or "short-range" motion of water molecules, with the change of the hydrogel's shape at constant volume.

Depending on the time interval of interest and on the characteristic times of relaxation and diffusion, hydrogels can behave viscoelastically, poroelastically or poroviscoelastically.

A comprehensive analysis and characterization of hydrogel-based systems should therefore be able to discriminate between the poro and the visco elastic regime to be able to emphasize, in the system application, the one of interest. The simplest conceivable experimental procedure to enlighten the hydrogel behavior is a stress-relaxation test, where a certain deformation is prescribed and the stress evolution is recorded. This can be performed by unconfined/confined compression tests (Ström et al., 2015, Li et al., 2012, Wang et al., 2014) or by indentation tests (Hu et al., 2012) with several indenters (Chan et al., 2012, Delavoipiere et al., 2016).

Despite experimental tests give irreplaceable results, a deep and complete analysis can not exclude a mathematical description of the phenomena, which is able to bring minimal aspects out. As shown in the paragraph 1.3.2.1, the developed models to describe this peculiar behavior can be traced back to the multiphasic and to the monophasic (multicomponent) approaches. Despite the multiphasic approach has the major number of publications on its side (Birgersson et al., 2008, Doi, 2009, Feng et al., 2010, Kurnia et al., 2012b, Kurnia et al., 2012a, Lai et al., 1991), the resulting models require non-physical based parameters and several Partial Differential Equations (PDEs) to describe the system, which often lead to the development of simplified model versions. On the other side, the monophasic approach, recently extended to hydrogels (Hong et al., 2008), benefits from stronger thermodynamic bases and requires less PDEs to describe the system (and to be numerically solved). Within the monophasic approach, several modeling works dealt with hydrogel poroelasticity (Chester and Anand, 2010, Hong et al., 2009, Hong et al., 2010, Kang and Huang, 2010, Lucantonio et al., 2013, Zhang et al., 2009), instead only few modeling works analyzed the complete hydrogel poroviscoelastic behavior. Among them some did it only from a theoretical point of view (Hu and Suo, 2012), others within the field of linear

theory of elasticity (Wang et al., 2014), some other solving the equation in 1D/2D cases (Wang and Hong, 2012, Zhao et al., 2011) and one solved the complete 3D poroviscoelastic model with ad hoc FEM code (Chester, 2012).

3.2 Aim

Aim of this part of the PhD thesis is to develop a 3D model, coherently with the monophasic theory, to depict the poroviscoelastic behavior of hydrogels, within the field of nonlinear solid mechanics (large deformations).

Further aim is to implement and solve the developed model in a commercial software (COMSOL Multiphysics 5.0). To fulfill these goals the mass and linear momentum balance equations, supported by constitutive equations from non-equilibrium thermodynamics, are derived. The polymer network is considered as viscoelastic, describable with a Standard Linear Solid model and its time depended elastic response is computed using the affine network theory (Gaussian chains distribution). The polymer-solvent interaction is accounted for the Flory-Huggins mixing theory. The resulting PDEs, scaled down to a 2D-axisymmetric problem, are recasted in their weak forms and implemented in COMSOL Multiphysics 5.0, to be solved with the Finite Element Method (FEM). A parametric study is performed in order to assess the relative importance of the model parameters on hydrogels' behavior.

Firmly convinced that a combined experimental-modeling approach is the only track to reach a deep comprehension of the phenomena analyzed, further aim of this work is the investigation of agarose gels behavior in terms of water mass transport and stress-relaxation behavior as model system to test the developed model.

3.3 Materials and Methods

3.3.1 Materials

Agarose (CAS Number 9012-36-6), characterized by a transition temperature (gel point) of 36°C, used in this work was purchased by Sigma Aldrich, Milano, Italy. Deionized water was used as immersion medium during both the mechanical and the gravimetric tests.

Phenol (≥99%, CAS number 108-95-2) and sulfuric acid (ACS reagent, 95-98%, CAS number 7664-93-9) used in the colorimetric method were purchased by Sigma Aldrich, Milano, Italy.

3.3.2 Samples preparation method

Solutions of agarose were prepared adding the required amounts of water which was heated up to 80°C and continuously stirred to facilitate the agarose powder dispersion. The solutions, initially opaque, were kept at 90°C for

about 1 hour, until it became completely clear. In this work different polymer concentrations were investigated, up to 4.5% w/w of polymer.

To prepare the gel samples, the hot solutions were poured in a cylindrical aluminum mold (diameter 20 mm, height 10 mm) and covered to avoid the water evaporation. After 15 minutes at room temperature, the gel was formed and the covering was removed. The gel was carefully removed from the mold and weighted to determine its initial mass (m_0).

In order to verify the polymer concentration of the samples, a gravimetric analysis was performed on different samples, which, after their production, were weighted and dried in oven overnight at 105°C, to allow the complete evaporation of water. Then, the samples were weighted again and by the ratio between their dry mass and their initial mass, the percentage of polymer was calculated.

3.3.3 Mechanical tests

The mechanical tests were performed at room temperature using a Texture Analyzer (TA.XT Stable Micro System, UK) equipped with a 5 kg loading cell. An aluminum cylindrical probe (diameter 30 mm) was selected in order to ensure the covering of the whole gel surface. The initial position of the texture probe was at 15 mm respect to the bottom of a Petri disc, which is the origin point of the axis **z** (as shown in **Figure 23**). The gels, prepared according to the procedure previously describes, were placed into the Petri disc (diameter 90 mm), where 70 mL of deionized water were previously placed. The water covered completely the gel sample, in order to avoid sample dehydration during the test due to evaporation. The sample was manually centered under the probe and the mechanical test (stress-relaxation) started. The stress-relaxation test can be divided into three different stages: i) the pre-test stage, ii) the compression stage, and iii) the relaxation stage.

During the pre-test stage, the texture probe moved from its initial position, which corresponds to a displacement 0 (the origin of the axis **s**, on the probe surface, as shown in **Figure 23**) until the device detected a trigger force of 0.02 N, which means that the probe touched the sample surface. The trigger force value was chosen to be higher than the force measured when the probe touches the water surface and adequately low to avoid the compression of the sample during this stage. Then, the compression stage started. During this stage the probe moves, according to the **s** axis in **Figure 23**, with a constant velocity of 0.3 mm/s up to a distance of 1 mm (10% axial gel deformation) squeezing the gel sample and recording the force measured. Finally, the relaxation stage consisted in the probe holding for 1200 s in the final position of the compression stage. During this stage the force opposed by the gel sample, which was relaxing the stress gained in the previous stage, was measured.

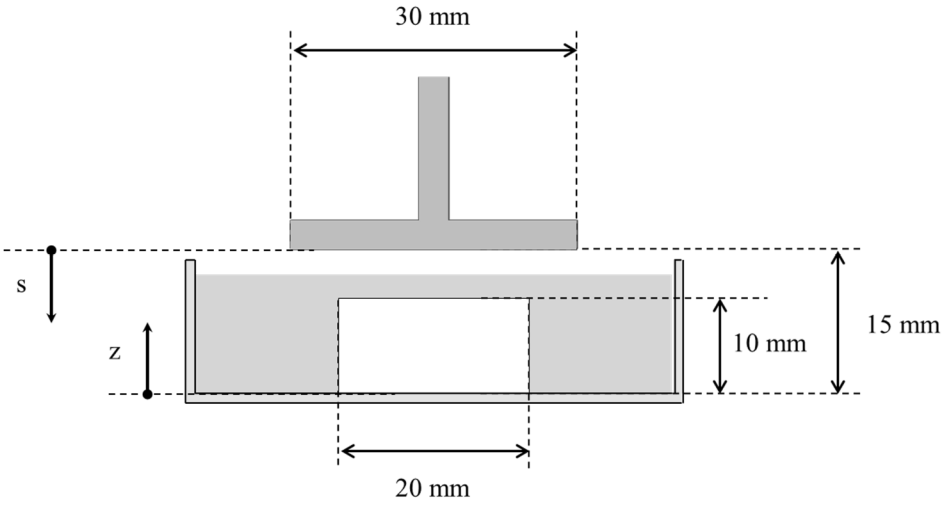

***Figure 23**. Schematic of the compression-relaxation test with the reference frame adopted.*

3.3.4 Determination of water up-take - water losses

In order to measure gel–water up-take or water losses, during the mechanical test, a gravimetric assay was applied. The gel samples, immediately after the runs, were withdrawn from the immersion water and weighted. By the difference between the sample weight after the stress-relaxation test and immediately after its preparation (m_0), it was possible to evaluate the amount of water exchanged with the external environment (Δm_1 in **Table 6**).

3.3.5 Quantification of polymer erosion

At the end of the stress relaxation test, a sample of the immersion water was withdrawn to determine the polymer content and to quantify the erosion phenomenon which took place during the mechanical test. A colorimetric method (Nielsen, 2014) was applied to determine the agarose dissolved. Briefly, this method consists in different steps:

i) withdrawing of 2 mL of the solution containing agarose and placement in a test tube;
ii) adding of 50 µL of a phenol solution (80% w/w of phenol in water);
iii) adding of 5 mL of sulfuric acid to the test tube;
iv) waiting 10 min at room temperature;
v) mixing (shaking) of the test tube;
vi) immersing the tube in a water bath at 20-25°C for 10 min to cool down the sample.

The sample resulted in a yellow-red color, which can be analyzed by a spectrophotometer. In this work a spectrophotometer Lambda 25 (Perkin

Elmer, Italy) was used to determine the agarose concentration at λ=490 nm.

3.4 Modeling

3.4.1 Balance equations

When dealing with solids it is convenient to use material coordinates (Lagrangian approach) that refer to a particular state of the matter (i.e. stress free) with respect to which one may measure strain and develop constitutive equations. The mass transport instead is normally referred to the spatial coordinates (Eulerian approach), where the matter can enter and leave a certain control volume. Coupling the mass transport with solid mechanics requires the choice of a single reference frame and, since dealing with non-linear solids in spatial coordinates is problematic, all the following equations (mechanics and mass transport), where not differently specified, refer to the hydrogel initial state (reference state, material coordinates $\bar{X}$).

3.4.1.1 Mass balance

The water mass balance can be written as:

$$\frac{\partial c_1}{\partial t} = -\bar{\nabla} \cdot \bar{h}_1 \tag{3.1}$$

where c_1 is the molar water concentration and $\bar{h}_1$ is the water molar flux.

3.4.1.2 Linear momentum balance

In this balance the *quasistatic* approach can be used, considering that the time scales associated with diffusion are considerably longer than those associated with inertia, so that the inertial terms can be neglected:

$$\bar{\nabla} \cdot \bar{\bar{P}} = \bar{0} \tag{3.2}$$

Where $\bar{\bar{P}}$ is the first Piola-Kirchoff stress tensor (or nominal stress tensor), which relates the force in the deformed configuration to an oriented area vector in the reference configuration.

3.4.1.3 Volumetric constraint

In hydrogels a variation of the water content has to results in a system deformation and vice versa an imposed volumetric deformation has to generate a water content change. The two components, water and polymer, are considered incompressible, whereas the hydrogel, due to water content variation, is compressible. Therefore, the volumetric constraint relates the water concentration to the system deformation and vice versa:

$$J = 1 + \Omega_1 (c_1 - c_{10}) \tag{3.3}$$

where J is the volumetric deformation from the initial to the current state (also known as $\det(\bar{\bar{F}})$, where $\bar{\bar{F}}$ is the deformation gradient tensor), Ω_1 is the water molar volume and c_{10} is the initial water molar concentration.

3.4.2 Constitutive equations

The mass and the momentum balance equations have to be supported by constitutive equations to relate, for example, the deformations with the stresses etcetera. In this work, similarly to what is commonly done with hyperelastic materials (Holzapfel, 2000), and driven by the theory of Gurtin et al. (Gurtin et al., 2010), the free-energy imbalance (or dissipation inequality) approach was used to derive the constitutive equations:

$$\frac{\partial A}{\partial t} - \bar{\bar{P}}: \dot{\bar{\bar{F}}} - \mu_1 \dot{c}_1 + \bar{h}_1 \cdot \bar{\nabla}\mu_1 \leq 0 \tag{3.4}$$

This imbalance can be seen as the application of the first two principles of thermodynamics. It states that, for an isothermal process, changes in the net free energy of the system (A is the Helmholtz free energy density that corresponds to the strain-energy density function) are influenced by the conventional power expended on the system ($\bar{\bar{P}}: \dot{\bar{\bar{F}}}$), and by the energy carried into the system by solvent transport ($-\mu_1 \dot{c}_1 + \bar{h}_1 \cdot \bar{\nabla}\mu_1$). Due to dissipations, not all this power can be converted in a net free energy variation, which translates in an inequality. Once the hydrogel's free-energy is known, from equation (3.4) it is possible to derive the constitutive equations.

The Helmholtz free energy density, A, of a neutral polymer network (subscript "2") in an aqueous solution (subscript "1") can be written as the additive decomposition of the free energy density of elastic stretch of the polymer network (related to the system deformation) and the free energy density of mixing, due to the interaction of polymer and water. According to the theory developed by Flory and Rehner, the more general form of the free energy of a neutral hydrogel can be described as:

$$A = A^{el} + A^{mix} \tag{3.5}$$

The elastic contribution can be obtained from the theory of rubber elasticity, whereas the mixing contribution can be obtained from the Flory-Huggins mixing theory.

At this point, a further conceptual complication rises since the elastic free energy from rubber elasticity refers to the dry state (subscript "D") as reference state ($A_D^{el} = 0$ at dry state). At that state the mixing energy term presents a singular point (at dry state $A_D^{mix} = -\infty$). Nevertheless this numerical issue is harmless in practice since hydrogels includes many water molecules. The problem is solvable obtaining the expressions of the hydrogel free energy with respect to the dry state and then operating a change of reference frame, from the dry to the initial hydrogel conditions (reference frame).

3.4.2.1 The change of reference frame

Aim of the change of the reference frame is to avoid referring to the dry polymer as initial state. This allows circumventing the numerical problem related to the singularity of the Flory-Huggins mixing theory in that state and/or allows choosing as reference state hydrogels at known concentration of solvent. To perform the change of reference frame (**Figure 24**) it is assumed that the dry polymer network equilibrates with a solvent of chemical potential μ_{10}, under no mechanical loads, such that the deformation from the dry to the reference state is homogenous:

$$\bar{\bar{F}}_0 = \bar{\nabla}_{\bar{X}_D}\bar{\chi}_0 = \lambda_0\bar{\bar{I}} \tag{3.6}$$

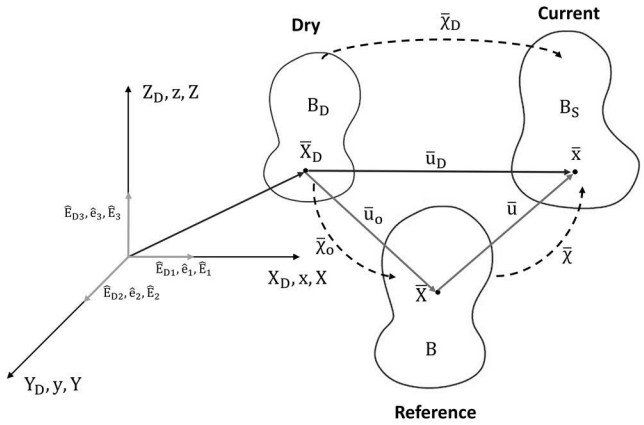

Figure 24. *Sketch of the dry, the reference and the current frames. B_D represents the sketch of the body at dry ("D") state. B represent the body at the reference state. B_S represent the body at the current (spatial "S") state.*

The variables referring to the dry state (denoted by the subscript "D") can be rewritten as made of the contribution of the initial homogeneous deformation (denoted by the subscript "0") and the contribution given by the variation with respect to the reference state:

$$\begin{aligned} &\bar{\bar{F}}_D = \bar{\bar{F}}_O\bar{\bar{F}} \\ &J_D = det\left(\bar{\bar{F}}_D\right) = J_0\,J \\ &c_{1D} = J_0\,c_1 \\ &A_D = J_0 A \end{aligned} \tag{3.7}$$

Where $\bar{\bar{F}}_i$ represent the deformation gradients ($i = D$ from dry to current, $i = 0$ from dry to reference, $i =$ " " from reference to current), J_i the volumetric deformation, $c_{1,i}$ the solvent concentration. A_D represent the free energy density with respect to the dry state and A is the free energy density with respect to the reference state.

3.4.2.2 Basic of the rubber elasticity theory

The theory of rubber elasticity, from which elastic constitutive equations can be derived, is based on statistical thermodynamics (branch of statistical mechanics), which relates microscopic behaviors and motions occurring inside the material with the macroscopic properties of the material. This is performed applying the classical mechanical laws to the "statistical ensemble", which is a large collection of virtual independent copies (basic element) of the system in various states.

The basic element for rubber material is the "individual chain", which is a portion of the network structure extending from a cross linkage to the next one occurring along a given primary molecule. The dimension of a polymer most widely used to characterize its spatial configurational character is the distance $\bar{r}$ from one end group to the other of the chain molecule: this vector is called the chain displacement or the end-to-end vector.

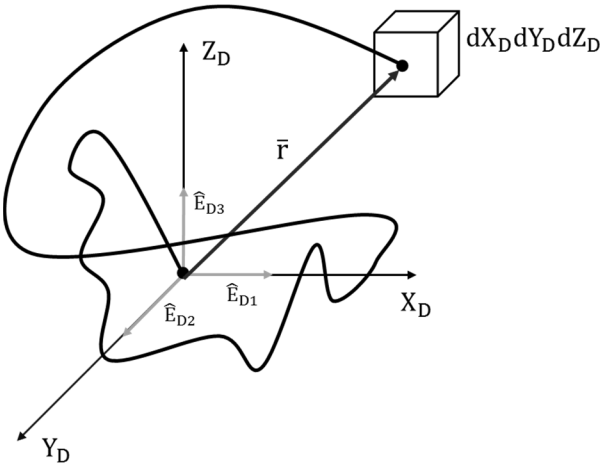

***Figure 25**. The chain displacement vector and the spatial configuration of a polymer chain taking the origin of coordinates at one end of the chain.*

Since cross-linking is a random process, the chains created by cross-linking will occur in random configurations. Their end-to end vectors will be distributed according to the probability density function $W(X_D, Y_D, Z_D)$. If one end of a freely jointed polymer chain is placed at the origin of a coordinate system, and the chain is permitted to assume any configuration at random, $W(X_D, Y_D, Z_D)$ expresses the probability that the other end occurs in the volume element of size $dX_D dY_D dZ_D$ (Flory, 1953), as represented in **Figure 25**.

The most used probability density function ($W(X_D, Y_D, Z_D)$) is the Gaussian distribution function, on which the classical rubber elasticity theory has been built. Once the distribution function of the chains has been chosen, network models have to be developed to relate the microscopic deformation to

macroscopic deformation (i.e affine network model, phantom network model etc.) (Rubinstein and Colby, 2003, Mark and Erman, 2007, Mark, 2007, Holzapfel, 2000, Treloar, 2005) .

For completeness it has to be said that the Gaussian-based models fails at high level of stretch ($\mathrm{r}/\mathrm{n}l \geq 0.40$ (Boyce and Arruda, 2000)), where the force-extension relation becomes non-linear with an upturn due to finite chain extensibility. In these cases a non-Gaussian treatment of the single chain, which takes into account the finite extensibility of the chain, and thus leads to a more realistic form of distribution function has to be considered. This involves considerable sacrifices of both simplicity and generality and, for these reasons, the non-Gaussian approaches will not be considered in this thesis. However, readers interested in applying these models can find useful the following references (Argon, 2013, Arruda and Boyce, 1993, Bischoff et al., 2001, Boyce and Arruda, 2000, Treloar, 2005).

3.4.2.2.a Gaussian distribution and affine network models

In the following, an example on how it is possible to derive the elastic Helmholtz free energy from statistical thermodynamics. The Gaussian distribution is representative of sufficiently long chains that behave as a linear spring whose expression is the following,

$$W(r) = \left(\frac{3}{2\pi\langle {r_{un}}^2\rangle}\right)^{\frac{3}{2}} exp\left(-\frac{3r^2}{2\langle {r_{un}}^2\rangle}\right). \tag{3.8}$$

The average dimensions of a chain are suitably represented by the mean-square end-to-end distance $\langle r^2\rangle$. The unperturbed dimensions are represented by a subscript "un"[1]. The unperturbed mean-square end-to-end distance $\langle r_{un}^2\rangle$ is defined through the relation:

$$\langle r_{un}^2\rangle = \int r^2 W(r) dr \tag{3.9}$$

The Helmholtz free energy of the chain is obtained as

$$A_{chain}^{el,TOT} = c(T) - k_B T ln(W(r)) = A^*(T) + \frac{3k_B T r^2}{2\langle {r_{un}}^2\rangle} \tag{3.10}$$

Where $c(T)$ is a constant that is a function of the temperature only, and $A^*(T) = c(T) + k_B T\ ln\left(\left(\frac{3}{2\pi\langle {r_{un}}^2\rangle}\right)^{\frac{3}{2}}\right)$

The total free energy of the network relative to the undeformed state is obtained by summing equation (3.10) over all chains of the network:

[1] In other texts (i.e. MARK, J. E. 2007. *Physical Properties of Polymers Handbook*, Springer New York.) the unperturbed state is indicated with the subscript "0".

$$\Delta A^{el,TOT} = \frac{3k_BT}{2\langle r_{un}{}^2\rangle}\sum_{\nu}(r^2 - \langle r_{un}{}^2\rangle) = \frac{3k_BT\nu}{2}\left(\frac{\langle r^2\rangle}{\langle r_{un}{}^2\rangle} - 1\right) \qquad (3.11)$$

In this expression the term c(T) has disappeared because the process can be considered isothermal, and ν represents the number of network chains. The average of the mean squared end-to-end chain vectors in the deformed network $\langle r^2\rangle$ can be defined as $\langle r^2\rangle = \sum_\nu r^2/\nu$.

The relationship between $\langle r^2\rangle$ and $\langle r_{un}{}^2\rangle$ is required for further development of the theory. A molecular model is needed for such a relationship (the affine and the phantom network models are the two simplest molecular models employed in relating the deformation of the chain to macroscopic deformation) and, in this example the affine network model will be used. According to the affine network model, local deformations are the same as the macroscopically imposed deformation. The junction points in the affine network model are assumed to be embedded in the network.

Given the three principal stretch ratios:

$$\lambda_{X_D} = \frac{X_D}{X_{un}};\ \lambda_{Y_D} = \frac{Y_D}{Y_{un}};\ \lambda_{Z_D} = \frac{Z_D}{Z_{un}} \qquad (3.12)$$

the average chain dimensions are represented, respectively, in the undeformed and deformed state in this way:

$$\langle r_{un}{}^2\rangle = \langle X_{un}{}^2\rangle + \langle Y_{un}{}^2\rangle + \langle Z_{un}{}^2\rangle \qquad (3.13)$$

$$\langle r^2\rangle = \langle X_D{}^2\rangle + \langle Y_D{}^2\rangle + \langle Z_D{}^2\rangle \qquad (3.14)$$

Assuming an isotropic network, the equation (3.13) becomes:

$$\langle X_{un}{}^2\rangle = \langle Y_{un}{}^2\rangle = \langle Z_{un}{}^2\rangle = \frac{\langle r_{un}{}^2\rangle}{3} \qquad (3.15)$$

In the affine network model, components of each chain vector transform linearly with macroscopic deformation:

$$\begin{aligned}\langle X_D{}^2\rangle &= \lambda_{X_D}{}^2\langle X_{un}{}^2\rangle\\ \langle Y_D{}^2\rangle &= \lambda_{Y_D}{}^2\langle Y_{un}{}^2\rangle\\ \langle Z_D{}^2\rangle &= \lambda_{Z_D}{}^2\langle Z_{un}{}^2\rangle\end{aligned} \qquad (3.16)$$

and the elastic free energy (equation (3.11)) could be written as,

$$\Delta A^{el,TOT} = \frac{\nu k_BT}{2}\left(\lambda_{X_D}{}^2 + \lambda_{Y_D}{}^2 + \lambda_{Z_D}{}^2 - 3\right) \qquad (3.17)$$

The constitutive equations for hyperelastic materials define the relationship between the applied stresses and the resulting deformations and vice versa. This relationship is obtained by means of *the strain energy density function,* that corresponds to the free energy per unit volume of the dry network V_D (a free energy density).

$$\Delta A^{el} = \frac{\nu k_B T}{2V_D} \left({\lambda_{X_D}}^2 + {\lambda_{Y_D}}^2 + {\lambda_{Z_D}}^2 - 3\right) \tag{3.18}$$

Where the elastic modulus G is expressed in the following way:

$$G = \frac{\nu k_B T}{V_D} = \frac{\rho RT}{M_s} \tag{3.19}$$

In the last equality, ρ is the network density and M_s is the number-average molar mass of a network strand.

Equation (3.18) has been derived not considering volume variations, instead a more general form obtained by a rigorous statistical mechanical analysis (Flory, 1953), can be:

$$\Delta A^{el} = \frac{G}{2}\left[\left({\lambda_{X_D}}^2 + {\lambda_{Y_D}}^2 + {\lambda_{Z_D}}^2 - 3\right) - 2ln\frac{V}{V_D}\right] \tag{3.20}$$

Where V and V_D are the initial and final volume of the networks and their ratio can be defined as $V/V_D = \lambda_{X_D}\,\lambda_{Y_D}\,\lambda_{Z_D}$, therefore:

$$\Delta A^{el} = \frac{G}{2}\left[\left({\lambda_{X_D}}^2 + {\lambda_{Y_D}}^2 + {\lambda_{Z_D}}^2 - 3\right) - 2\,ln\left(\lambda_{X_D}\,\lambda_{Y_D}\,\lambda_{Z_D}\right)\right] \tag{3.21}$$

In the following the symbol Δ is dropped and the subscript, indicating the reference state will be used (i.e. $\Delta A^{el} = A_D^{el}$).

3.4.2.3 The (visco)elastic contribution

In this work, the affine network model (which is based on the Gaussian distribution of end-to-end distances of the network chains) has been chosen to describe the polymer network elastic contribution. However other possibilities based on different network models (based on Gaussian or Non-Gaussian distribution hypotheses) are possible (Chester, 2012, Chester and Anand, 2010, Horkay and McKenna, 2007). In general, following this model, the deformation can be related to the free energy density with respect to the dry state:

$$A_D^{el} = \frac{G}{2}\left[\lambda_{X_D}^2 + \lambda_{Y_D}^2 + \lambda_{Z_D}^2 - 3 - 2\,ln\left(\lambda_{X_D}\lambda_{Y_D}\lambda_{Z_D}\right)\right] \tag{3.22}$$

In terms of principal stretches λ_{X_D}, λ_{Y_D}, λ_{Z_D} or, in terms of deformation gradient ($\bar{\bar{F}}_D$):

$$A_D^{el} = \frac{G}{2}\left[\bar{\bar{F}}_D : \bar{\bar{F}}_D - 3 - 2\ln\left(\det(\bar{\bar{F}}_D)\right)\right] \tag{3.23}$$

where G is an elastic modulus.

In this work to describe the intrinsic viscoelasticity of the network structure a simple Standard Linear Solid (SLS) model has been considered. This is composed by a purely elastic branch (a in **Figure 26**) and a Maxwell element branch (b in **Figure 26**) in parallel. The springs elasticity is represented by the

elastic moduli G_1 and G_2, whereas the dashpot has viscosity η or, analogously, the Maxwell element is characterized by a relaxation time $\tau = \eta/G_2$.

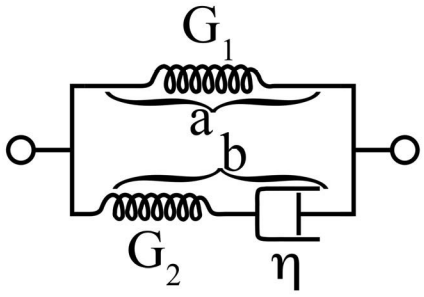

Figure 26. *Standard Linear Solid (SLS) rheological model. With "a" and "b" the pure elastic branch and the Maxwell element branch are indicated, respectively.* G_1 *and* G_2 *represent the elastic moduli of the springs and* η *the viscosity of the dashpot.*

For this model the total deformation gradient is equal to the deformation gradient of the branches: $\bar{\bar{F}}_D = \bar{\bar{F}}_{D_a} = \bar{\bar{F}}_{D_b}$ whereas the total stress is given by the sum of both the branches: $\bar{\bar{P}} = \bar{\bar{P}}_a + \bar{\bar{P}}_b$. The elastic Helmholtz free energy can be obtained summing the elastic contributions of the branches $A_D^{el} = A_{D_a}^{el} + A_{D_b}^{el}$. The elastic deformation of the Maxwell element is $\bar{\bar{F}}_{D_b}^{el} = \bar{\bar{F}}_{D_b}\left(\bar{\bar{F}}^{visc}\right)^{-1}$, where $\bar{\bar{F}}^{visc}$ is the internal variable (Holzapfel, 2000) representing the dashpot deformation that does not need to refer to a particular state. Using the affine network model (equation (3.23)):

$$\begin{aligned} A_D^{el} = \frac{G_1}{2}\left[\bar{\bar{F}}_D : \bar{\bar{F}}_D - 3 - 2\ln\left(\det(\bar{\bar{F}}_D)\right)\right] \\ + \frac{G_2}{2}\left[\bar{\bar{F}}_D\left(\bar{\bar{F}}^{visc}\right)^{-1} : \bar{\bar{F}}_D\left(\bar{\bar{F}}^{visc}\right)^{-1} - 3\right. \\ \left. - 2\ln\left(\det\left(\bar{\bar{F}}_D\left(\bar{\bar{F}}^{visc}\right)^{-1}\right)\right)\right] \end{aligned} \tag{3.24}$$

That is the elastic free energy of a polymeric network with a behavior describable with an SLS model and using the dry state as reference state ($\bar{\bar{F}}_D = \bar{\bar{F}}^{visc} = \bar{\bar{I}}$ at reference state, therefore $A_D^{el} = 0$).

3.4.2.4 The mixing contribution

The mixing contribution to the free energy can be attributed to the solvent-polymer interaction and can be obtained applying the Flory-Huggins mixing theory. Unfortunately there is no explicit molecular model for the free energy of mixing in gel (crosslinked polymer plus solvent); therefore it is assumed that the free energy of mixing in gel has the same functional dependence of the mixing free energy of a polymer solution (linear polymer plus solvent). Despite this equation has been derived for uncrosslinked polymer solutions, it

has been proved to be potentially able to describe the behavior of ideal elastomeric gels (Li et al., 2012):

$$A^{mix,TOT} = RT[n_1 ln(\phi_1) + n_2 ln(\phi_2) + n_1 \chi_{12} \phi_2] \tag{3.25}$$

Where R is the the gas constant, T the temperature n_1 and ϕ_1 are the number of moles and the volume fraction of solvent, n_2 and ϕ_2 are the moles of dry polymers and the polymer volume fraction, and χ_{12} is the Flory-Huggins interaction parameter. The pure solvent is the reference state.

It is possible to define, the polymer and the solvent volume fraction, using the solvent molar volume (Ω_1) and the solvent concentration with respect to the dry state (c_{1D}):

$$\phi_1 = \frac{\Omega_1 c_{1D}}{1 + \Omega_1 c_{1D}} [=] \frac{volume\ of\ solvent}{volume\ of\ solvent + volume\ of\ polymer} \tag{3.26}$$

$$\phi_2 = \frac{1}{1 + \Omega_1 c_{1D}} [=] \frac{volume\ of\ polymer}{volume\ of\ solvent + volume\ of\ polymer} \tag{3.27}$$

Bearing in mind that n_2 has to be equated to zero owing to the absence of "free" polymer moles in the network structure (Flory, 1953), and substituting the equations (3.26) and (3.27) in the equation of the free energy of mixing:

$$A_D^{mix,TOT} = RT \left[n_1 ln \left(\frac{\Omega_1 c_{1D}}{1 + \Omega_1 c_{1D}} \right) + \frac{n_1 \chi_{12}}{1 + \Omega_1 c_{1D}} \right] \tag{3.28}$$

To obtain the free energy density the solvent moles has to be replaced with the solvent concentration with respect to the dry state (c_{1D}):

$$A_D^{mix} = RT \left[c_{1D} ln \left(\frac{\Omega_1 c_{1D}}{1 + \Omega_1 c_{1D}} \right) + \frac{c_{1D} \chi_{12}}{1 + \Omega_1 c_{1D}} \right] \tag{3.29}$$

3.4.2.5 The total free energy density

The hydrogel free energy density with respect to the dry states reads:

$$\begin{aligned} A_D(\bar{\bar{F}}_D, c_{1D}, \bar{\bar{F}}^{visc}) &= A_D^{el} + A_D^{mix} \\ &= \frac{G_1}{2} \left[\bar{\bar{F}}_D : \bar{\bar{F}}_D - 2\, ln\left(det\left(\bar{\bar{F}}_D\right)\right) \right] \\ &+ \frac{G_2}{2} \left[\bar{\bar{F}}_D \left(\bar{\bar{F}}^{visc}\right)^{-1} : \bar{\bar{F}}_D \left(\bar{\bar{F}}^{visc}\right)^{-1} - 3 \right. \\ &\left. - 2\, ln\left(det\left(\bar{\bar{F}}_D \left(\bar{\bar{F}}^{visc}\right)^{-1}\right)\right) \right] \\ &+ RT \left[c_{1D} ln \left(\frac{\Omega_1 c_{1D}}{1 + \Omega_1 c_{1D}} \right) + \frac{c_{1D} \chi_{12}}{1 + \Omega_1 c_{1D}} \right] \end{aligned} \tag{3.30}$$

Operating the change of reference frame, from the dry to the initial hydrogel conditions (reference frame), it is possible to avoid the numerical singularity.

$$
\begin{aligned}
A(\bar{\bar{F}}, c_1, \bar{\bar{F}}^{visc}) &= A^{el} + A^{mix} \\
&= \frac{1}{J_0}\left\{\frac{G_1}{2}\left[\bar{\bar{F}}_0\bar{\bar{F}} : \bar{\bar{F}}_0\bar{\bar{F}} - 3 - 2\,ln\left(det(\bar{\bar{F}}_0\bar{\bar{F}})\right)\right]\right. \\
&+ \frac{G_2}{2}\left[\bar{\bar{F}}_0\bar{\bar{F}}\left(\bar{\bar{F}}^{visc}\right)^{-1} : \bar{\bar{F}}_0\bar{\bar{F}}\left(\bar{\bar{F}}^{visc}\right)^{-1} - 3\right. \\
&\left.\left. - 2\,ln\left(det\left(\bar{\bar{F}}_0\bar{\bar{F}}\left(\bar{\bar{F}}^{visc}\right)^{-1}\right)\right)\right] \\
&+ RT\left[J_0 c_1 ln\left(\frac{J_0\Omega_1 c_1}{1 + J_0\Omega_1 c_1}\right) + \frac{J_0 c_1 \chi_{12}}{1 + J_0\Omega_1 c_1}\right]\Bigg\}
\end{aligned}
\tag{3.31}
$$

Where J_0 is the volumetric deformation ($J_0 = det(\bar{\bar{F}}_0)$) that characterize the homogeneous deformation (of stretch: λ_0) from the dry to the reference configuration.

3.4.2.6 The constitutive equations

Before using the equation (3.31) in the free-energy imbalance equation (3.4), to derive the constitutive equations some considerations have to be done. When constraints are imposed on deformation (in this case the volumetric constraint) a numerical solution via a single-field based method (i.e. standard displacement-based) exhibits numerical difficulties, commonly referred as locking phenomena. To overcome these numerical difficulties it is common practice to consider one (two-field based) or more (multi-field based) additional fields, which are treated as independent variables, with the aim of achieving nonlocking and stable numerical solution (Holzapfel, 2000). In this work the Lagrange-multiplier method (two-field based) has been used, similarly to (Hong et al., 2008, Kang and Huang, 2010, Lucantonio et al., 2013), where the constraint is algebraically added through a Lagrange-multiplier "p", which assumes the (physical) meaning of hydrostatic pressure, to the Helmholtz free energy density obtaining a relaxed "R" version of it:

$$
\begin{aligned}
&A_R\left(\bar{\bar{F}}, \mathrm{c}_1, \bar{\bar{F}}^{visc}, p\right) \\
&\qquad = A\left(\bar{\bar{F}}, \mathrm{c}_1, \bar{\bar{F}}^{visc}\right) - p\left[J - \left(1 + \Omega_1(c_1 - c_{10})\right)\right]
\end{aligned}
\tag{3.32}
$$

therefore, using the relaxed version of the free energy instead of the free energy, at the cost of an additional field variable "p", the volumetric constraint is enforced and the numerical solution stabilized.

Differentiating the relaxed version of the free energy with respect to time:

$$
\begin{aligned}
&\frac{\partial A_R\left(\bar{\bar{F}}, \mathrm{c}_1, \bar{\bar{F}}^{visc}, p\right)}{\partial t} \\
&\qquad = \frac{\partial A_R}{\partial \bar{\bar{F}}} : \frac{\partial \bar{\bar{F}}}{\partial t} + \frac{\partial A_R}{\partial c_1}\frac{\partial c_1}{\partial t} + \frac{\partial A_R}{\partial \bar{\bar{F}}^{visc}} : \frac{\partial \bar{\bar{F}}^{visc}}{\partial t} \\
&\qquad + \frac{\partial A_R}{\partial p}\frac{\partial p}{\partial t}
\end{aligned}
\tag{3.33}
$$

where the last term on the RHS is zero by the definition of volumetric constraint. Substituting equation (3.33) into equation (3.4) and rearranging:

$$\left(\frac{\partial A_R}{\partial \bar{\bar{F}}} - \bar{\bar{P}}\right) : \frac{\partial \bar{\bar{F}}}{\partial t} + \left(\frac{\partial A_R}{\partial c_1} - \mu_1\right)\frac{\partial c_1}{\partial t} + \frac{\partial A_R}{\partial \bar{\bar{F}}^{visc}}\frac{\partial \bar{\bar{F}}^{visc}}{\partial t} + \bar{h}_1 \cdot \bar{\nabla}\mu_1 \leq 0 \tag{3.34}$$

In order to satisfy this inequality in any conditions:

$$\begin{aligned} &\frac{\partial A_R}{\partial \bar{\bar{F}}} = \frac{\partial A}{\partial \bar{\bar{F}}} - pJ\bar{\bar{F}}^{-T} = \bar{\bar{P}} \\ &\frac{\partial A_R}{\partial c_1} = \frac{\partial A}{\partial c_1} + p\Omega_1 = \mu_1 \\ &\frac{\partial A_R}{\partial \bar{\bar{F}}^{visc}}\frac{\partial \bar{\bar{F}}^{visc}}{\partial t} \leq 0 \\ &\bar{h}_1 \cdot \bar{\nabla}\mu_1 \leq 0 \end{aligned} \tag{3.35}$$

The first two are the constitutive equations for the stress ($\bar{\bar{P}}$) and for the water chemical potential (μ_1), whereas the last two give indications on the kinetic laws for the dashpot deformation gradient ($\bar{\bar{F}}^{visc}$) and the water flux ($\bar{h}_1$). To satisfy the free energy imbalance, the kinetic equations have to be of the type:

$$\begin{aligned} &\frac{\partial \bar{\bar{F}}^{visc}}{\partial t} = -\frac{1}{\eta}\frac{\partial A_R}{\partial \bar{\bar{F}}^{visc}} = -\frac{1}{\eta}\frac{\partial A}{\partial \bar{\bar{F}}^{visc}} \\ &\bar{h}_1 = -\bar{\bar{D}} \cdot \bar{\nabla}\mu_1 \end{aligned} \tag{3.36}$$

Where η and $\bar{\bar{D}}$ are the dashpot viscosity and the mobility tensor, both positively defined.

3.4.2.6.a The mobility tensor

In general, $\bar{\bar{D}}$ may depend on the independent variables (i.e. water concentration, deformation/stress) and/or on the orientation (anisotropic transport). This further complicates the math without adding indispensable concepts to the model development.

The concept of diffusion, in the following, is used in the broadest term: the driving force is the water chemical potential gradient, which is made of a concentration dependent term (usual diffusion concept) and a pressure dependent term (usual permeation concept). Therefore, the employed diffusivity, which relates the chemical potential gradient to the water flux, can differ of order of magnitude with respect to usual diffusion coefficients.

In this work it has been considered an isotropic diffusion behavior in the current configuration with constant diffusivity. Therefore, the mobility tensor $\bar{\bar{D}}_S$ can be expressed in this way:

$$\bar{\bar{D}}_S = D_s\,\bar{\bar{I}} \tag{3.37}$$

Where $D_s = D/(\Omega_1 RT)$ and D is the diffusion coefficient.

The solvent flux defined as the solvent moles per unit time crossing per unit area in the current state, can assume the following form:

$$\bar{h}_{1S} = -\bar{\bar{D}}_S \bar{\nabla}_x \mu_1 = -D_s \bar{\bar{I}} \cdot \bar{\nabla}_x \mu_1 = -D_s \bar{\nabla}_x \mu_1 \tag{3.38}$$

In order to define this flux with respect to the reference coordinates, it is necessary to use the transformation law for surface integrals (Gurtin et al., 2010):

$$\begin{aligned} \int_{\partial P_S} -\bar{h}_{1S}(\bar{x},t) \cdot \bar{n}\, da &= \int_{\partial P} -\bar{h}_{1m}(\bar{X},t) \cdot \bar{\bar{F}}^C \cdot \bar{m}\, dA \\ &= \int_{\partial P} -\bar{h}_1(\bar{X},t) \cdot \bar{m}\, dA \end{aligned} \tag{3.39}$$

Where $\mathrm{P_S}$ and P represent a region of the current and the reference configuration, $\bar{h}_{1m}$ is the mapping of $\bar{h}_{1S}$ onto the material coordinates and $\bar{h}_1 = \bar{h}_{1m} \cdot \bar{\bar{F}}^C$ is the referential solvent flux. Recalling that $\bar{\nabla}_x \mu_1 = \bar{\bar{\mathrm{F}}}^{-\mathrm{T}} \bar{\nabla}_X \mu_1$ (Holzapfel, 2000), $\bar{h}_{1m}$ can be writtens as:

$$\bar{h}_{1m}(\bar{X},t) = \bar{h}_{1S}(\chi(\bar{X},t),t) = -D_m \bar{\bar{F}}^{-T} \bar{\nabla}_X \mu_1 \tag{3.40}$$

Where D_m is the mobility tensor in the material coordinate (which is the mapping of D_s onto the material coordinates), which in this case is equal to D_S (this last being independent on spatial variables): $D_m = D/(\Omega_1 RT)$. Therefore:

$$\bar{h}_1 = \bar{h}_{1m} \cdot \bar{\bar{\mathrm{F}}}^{\mathrm{C}} = -\, D_m \bar{\bar{\mathrm{F}}}^{\mathrm{C}} \bar{\bar{\mathrm{F}}}^{-\mathrm{T}} \bar{\nabla}_X \mu_1 = -J\, D_m \bar{\bar{\mathrm{F}}}^{-1} \bar{\bar{\mathrm{F}}}^{-\mathrm{T}} \bar{\nabla}_X \mu_1 \tag{3.41}$$

Finally, recalling the referential flux definition $\bar{h}_1 = -\bar{\bar{D}} \cdot \bar{\nabla}_X \mu_1$, it results:

$$\bar{\bar{D}} = J \frac{D}{\Omega_1 RT} \bar{\bar{\mathrm{F}}}^{-1} \bar{\bar{\mathrm{F}}}^{-\mathrm{T}} \tag{3.42}$$

Readers interested in more complex model of diffusion can find interesting the references (Lucantonio et al., 2013, Chester and Anand, 2010).

3.4.3 Initial and boundary conditions

The initial conditions describe a hydrogel at known concentration of water (c_{10}), not yet deformed ($\bar{u} = \bar{0}$) and relaxed ($\bar{\bar{F}}^{visc} = \bar{\bar{F}}_0$). :

$$@t = 0: \begin{cases} c_1 = c_{10} \\ \bar{u} = \bar{0} \\ \bar{\bar{F}}^{visc} = \bar{\bar{F}}_0 \end{cases} \tag{3.43}$$

Where $\bar{u}$ is the displacement field. Considering the initial condition as a stress free state:

$$@t = 0: \bar{\bar{P}} = 0 \Rightarrow p_0 = \frac{G_1}{\lambda_0^3}\left(1 - \frac{1}{{\lambda_0}^2}\right) \tag{3.44}$$

Being $\lambda_0 = J_0^{1/3}$ and $J_0 = 1/(1 - \Omega_1 c_{10})$, also equation (3.44) can be related to the initial water concentration; therefore the initial conditions, with this approach, are fully specified once the initial water concentration is known.

The boundary conditions (BCs) are case specific and will be specified in the following. However a peculiar BC is the one on the boundaries in contact with the external medium. As in (Lucantonio et al., 2013), in this work it is assumed the equilibrium between the internal and external water at the interface:

$$\mu_1 = \mu_1^{ext} \tag{3.45}$$

Which translate in an implicit Dirichlet condition on c_1. The chemical potential of the water surrounding the gel, μ_1^{ext}, (for a pure substance) can be computed by: $\mu_1^{ext} = {\mu_1}^{0,ext}(T^0, p^0) + RT \ln(p^{ext}/p^{0,ext})$, where the superscript zero indicates the value at the reference standard state. Choosing as reference state the pure liquid water (${\mu_1}^{0,ext}(T^0, p^0) = 0$), coherently with what it has been done within the Flory-Huggins theory, it results that at standard state ($p^{ext} = p^{0,ext}$), $\mu_1^{ext} = 0$. Of course this approach can be easily extended to more complicate cases (i.e. water solutions, humidity etcetera), using proper equations to compute the water chemical potential. It can be said that the pure liquid water chemical potential practically constitute an upper limit for the external chemical potential. Indeed, a part from cases in which the external water is pressurized ($p^{ext} > p^{0,ext}$), an addition of solutes (that could also be impurities) sensibly reduce the value of the chemical potential, therefore normally $\mu_1^{ext} \leq 0$.

3.4.3.1 Admissible initial water concentrations

It has been said that the once the initial water concentration is known, the initial conditions are fully specified. However not all the values of the initial water concentration are realistic values. To highlight this concept let's imagine that the initial state has been obtained equilibrating a dry network with a water solution at known chemical potential μ_1^{ext}, so that the chemical potential of the relaxed hydrogel will be $\mu_{10} = \mu_1^{ext}$. The chemical potential of the relaxed hydrogel, analogously to the water chemical potential used so far, is given by the sum of the water concentration contribution ($\mu_{10}(c_{10}) = \partial A/\partial c_1$) and the network stress contribution ($\mu_{10}(p_0) = p_0\Omega_1$). Therefore, given the external chemical potential (μ_1^{ext}) the higher the stiffness of the gel (G_1), the higher the network stress contribution $\mu_{10}(p_0)$ and the lower the water concentration contribution $\mu_{10}(c_{10})$ and, therefore, the lower the amount of water absorbable. Accordingly, the implicit upper limit for the initial water concentration (c_{10}) is given by the constraint: $\mu_{10}(c_{10}, p_0) = \mu_1^{ext} \leq 0$.

3.4.4 Implementation

The model has been implemented in 2D-axysimmetric geometry, through the weak formulations, in COMSOL MULTIPHYSICS 5.0, and solved in the Lagrangian frame.

The choice of study axysimmetric problems considerably reduces the computational effort required and at the same time it increases the numerical solution quality (finer meshes can be used). Of course the problem has to be axysimmetric in geometry and loadings. It has to be considered that solving the problem in a 2D-axysimmetric requires a change of variable, from Cartesian (X, Y, Z) to Cylindrical (R, θ, Z) coordinates, which reduces to (R, Z) in the axysimmetric hypothesis.

The mass balance (equation (3.1)) in the 2D-axysimmetric weak form reads:

$$0 = -2\pi \int_A \frac{\partial c_1}{\partial t} \tilde{c}_1 R \, dA - 2\pi \int_{\partial A} \overline{h_1} \, \tilde{c}_1 \cdot \bar{m} \, R \, dL + \\ +2\pi \int_A \overline{h_1} \cdot \bar{\nabla} \tilde{c}_1 R \, dA \tag{3.46}$$

Where $\tilde{c}_1$ represent the test function (Lagrange quadratic shape functions).

The linear momentum balance (equation (3.2)) has the form:

$$0 = -2\pi \int_A (\bar{\bar{P}} : \bar{\nabla} \tilde{\bar{u}}) \, R \, dA + 2\pi \int_{\partial A} \bar{\bar{P}} \cdot \tilde{\bar{u}} \cdot \bar{m} \, R \, dL \tag{3.47}$$

where $\bar{u}$ is the displacement field and $\tilde{\bar{u}}$ is its test function (Lagrange quadratic shape functions). $\bar{m}$ is the normal unit vector to the domain boundary.

As previously said the use of a two-field method introduced an additional field variable "p", which is computed through (equation (3.3)):

$$0 = -2\pi \int_A \left[J - \left(1 + \Omega_1 (c_1 - c_{10})\right) \right] \tilde{p} \, R \, dA \tag{3.48}$$

where $\tilde{p}$ is the test function (discontinuous Lagrange linear shape functions). The interpolation (shape) functions has been chosen to be of lower order (linear) and discontinuous to improve the computational efficiency, as suggested in (Holzapfel, 2000).

The (five) kinetic equations describing the dashpot deformation have been implemented with the physic "Domain ODEs and DAEs" solving for distribute ODEs (Ordinary Differential Equations) on the domain using the default shape function (Lagrange quadratic shape functions).

The implicit Dirichlet condition on c_1 has been implemented through the "weak form boundary PDE" physics, which analogously to (Lucantonio et al., 2013), solves for the water concentration on the boundary (subscript "B") c_{B1} that satisfies equation (3.45). This is then used as Dirichlet condition for the mass balance equation (equation (3.46)).

$$0 = 2\pi \int_{\partial A} (\mu_1 - \mu_1^{ext}) \tilde{c}_{B1} R \, dL \tag{3.49}$$

$\tilde{c}_{B1}$ is the test function (Lagrange quadratic shape functions).

The domain has been meshed with triangular elements and boundary layers. The solution have been obtained with an implicit time-stepping scheme to solve the time-dependent problem: Backward Differentiation Formula (BDF) with free time stepping. At each time step, the nonlinear system of equations has been tackled with a Fully Coupled approach and Newtonian (constant) iterations. The resulting linear system of equations has been solved with the direct solver MUMPS.

The simulations have been have been carried out with the help of a workstation based on the processor Intel® Core™ i7-4820K with a clock rate of 3.70 GHz and a RAM of 64 GB. The results obtained are mesh-size independent and the calculation time have been of order of minutes.

3.5 Results and discussion

In the following the parametric study results of a free swelling test and of an unconfined stress-relaxation test will be shown. Then the model will be used to simulate the agarose gel behavior subjected to unconfined stress-relaxation tests. In all the cases, the problem has been tackled in 2D-axisymmetric geometry (**Figure 27**), with a computational domain of side 1x1 cm, representing the gel samples of radius and height of 1 cm.

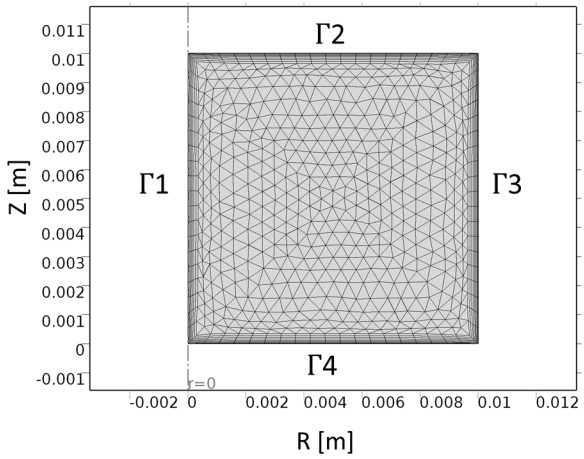

***Figure 27**. Computational meshed domain. With Γ are indicated the domain boundaries.*

3.5.1 Parametric study

3.5.1.1 Free swelling test

The free swelling of dry polymeric network is the simplest conceivable experiment, which can be performed immerging the system in water; nevertheless, the resulting behavior is of great interest in several applications (i.e. as drug release system). In this work it has been simulated the free swelling of an almost dry system (initial water mass fraction: $\omega_{10} = 0.01$) immerged in pure water ($\mu_1^{ext} = 0$) to highlight the effect of the model parameters on the system behavior. The Flory-Huggins interaction parameter (χ_{12}) has been fixed to the realistic value of 0.2 (affinity between solvent and polymer) as in (Lucantonio et al., 2013, Hong et al., 2008).

The boundary conditions that particularize the problem are:

$$\begin{aligned} &\forall \bar{X} \in \Gamma 2, \Gamma 3: \begin{cases} \mu_1 = \mu_1^{ext} \\ \bar{u} = free \end{cases} \\ &\forall \bar{X} \in \Gamma 4: \begin{cases} \bar{\nabla}\mu_1 = \bar{0} \\ u_Z = 0 \end{cases} \\ &\forall \bar{X} \in \Gamma 1: \begin{cases} \bar{\nabla}\mu_1 = \bar{0} \\ u_R = 0 \end{cases} \end{aligned} \tag{3.50}$$

Where the boundary Γ2 and Γ3 represent the side of the cylinder in contact with the pure water ($\mu_1 = \mu_1^{ext}$) and that can freely deform. The boundaries Γ4 and Γ1 represents respectively a plane and an axis of symmetry, therefore by definition there is no flux of water through these boundaries. They are also constrained in Z and R directions respectively, to avoid translation.

In **Figure 28** the effect of the elastic moduli on the amount of water adsorbed and on the swollen shape evolution along with the water mass fraction in time is depicted.

The modulus G_1, which represents the elastic modulus of the relaxed hydrogel, considerably affects the amount of water absorbable (**Figure 28**, top left). A stiffer network at long-time limit (higher G_1) produces, for a given deformation, higher internal stresses that result in a higher pressure field. This increases the internal water chemical potential that can equate to the external chemical potential with lower amount of water. This constitute a first important result: stiffer gels (highly cross-linked polymer networks) equilibrate with a given external water solution absorbing less water than softer gels.

The relaxed modulus G_1 affect not only the total amount of water absorbable but also the kinetic of the process and the system deformation (**Figure 28**, bottom left). At time zero the hydrogel is depicted as a blue cylinder, where the color is representative of the water mass fraction ($\omega_{10} = 0.01$). As the time passes, the system tends to the equilibrium absorbing water and deforming.

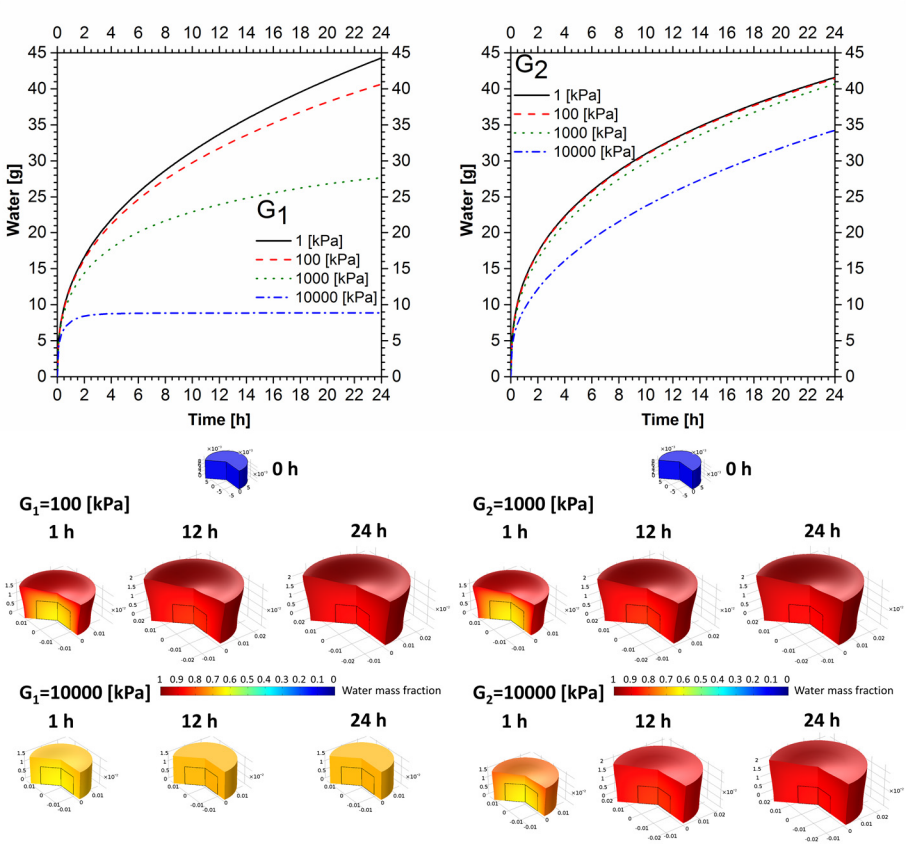

***Figure 28**. Free swelling parametric study: effect of the elastic moduli, G1 (left) and G2 (right). On the top the amount of water absorbed during a swelling test, on the bottom the shape of the hydrogel and the water mass fraction ranging from 0 (blue) to 1 (red). Where not differently specified G1=100 [kPa], G2=1000 [kPa], $D=1\times10^{-7}[m^2/s]$, $\tau=10000$ [s].*

It is clear that the water concentration that satisfy the boundary condition $\mu_1 = \mu_1^{ext}$ is greater in the case of G_1 smaller (100 [kPa]), red color ($0.9 \leq \omega_1 \leq 1$), with respect to the stiffer case (10000 [kPa]), yellow color ($0.6 \leq \omega_1 \leq 0.7$). The possibility to absorb greater amount of water in softer gels produces pronounced non-homogeneous deformations, whereas the time depended deformation of stiffer gels resemble steps of homogeneous deformations.

The modulus G_2, which summed to G_1 (when the dashpot is undeformed: $\bar{\bar{F}}^{visc} = \bar{\bar{I}}$) represents the elastic modulus of the unrelaxed system, affects the kinetic of hydration but not the equilibrium hydration value. Indeed, in **Figure 28** (top right), the water absorption curves tend to the same final value but

with a retardation effect due to the short time limit stiffness of the hydrogel (higher G_2). Higher the transient initial stiffness slower the absorption phenomenon. This is because stiffer gels equilibrates with a given external solvent needing smaller water concentration values, since the pressure term in the chemical potential is more relevant. As the contribution of G_2 fades out all the systems go toward the same equilibrium water concentration value with the same kinetic. The retardation effect of different short time limit stiffness, in term of shape and water mass fraction, is depicted in **Figure 28** (bottom right). At $t < \tau$, when the contribution of the Maxwell's element spring is still relevant, the difference in stiffness translate in a different deformation and water content. At $t \gg \tau$, all the systems tend to equilibrate with the same water concentration (being G_1 equal), however the deformation of short time limit stiffer gels (higher G_2) will be more homogeneous since they reach the maximum allowed concentration in a smother way. Summarizing, the hydrogel stiffness influences the free swelling behavior in different ways: the long time limit stiffness (G_1) influences the kinetic of hydration and the water equilibrium concentration value, while the short time limit stiffness (G_2) plays a role mainly in the kinetic of hydration.

To relate these results to practical applications, the reader can think at the two classes of hydrogel: chemical cross-linked and physical cross-linked. In the first case, the hydrogel is a system in which the long time limit stiffness prevails on the short time limit stiffness (G_1 prevails on G_2), since the possibility to relax the network is limited by the strong chemical links. This means that, working with the same polymer and modifying only the amount of cross-linker, therefore modifying the degree of cross-links (G_1), it is possible to tune the amount of water absorbable by the system or, in turn, the degree of swelling. In the case of physical cross-linked hydrogels the transient weaker links between the structure allow an almost complete relaxation of the stress, due to breakage and reformation (in the limiting case of complete reorganization of the network structure ($G_1 \rightarrow 0$) the behavior can be defined poro-visco-plastic). This means that the short time limit stiffness prevails on the long time limit stiffness (G_2 prevails on G_1) and the hydrogel will tend to absorb the same amount of water at the equilibrium, but reaching this point with different kinetic depending on the number of transient cross-links (G_2): the softer the gel, the faster the water up-take.

In **Figure 29** the effects of the diffusion coefficient and the relaxation time on the amount of water adsorbed and on the swollen shape evolution along with the water mass fraction in time are depicted. As expected the effect of the diffusivity on the kinetic of water absorption is massive (**Figure 29** top left). Increasing the diffusivity value the absorption kinetic increases since, given the water chemical potential gradient, the water flux increases. The diffusivity does not influence the equilibrium water concentration but its effect is relevant on the time dependent deformation (**Figure 29** bottom left). At lower values of diffusivity, the chemical potential gradient (and the water

concentration gradient) are sharper, generating pronounced non-homogeneous deformations; while in the case of higher diffusivity, the gradients are smoothed out by easier water movements, producing deformations that are more homogeneous.

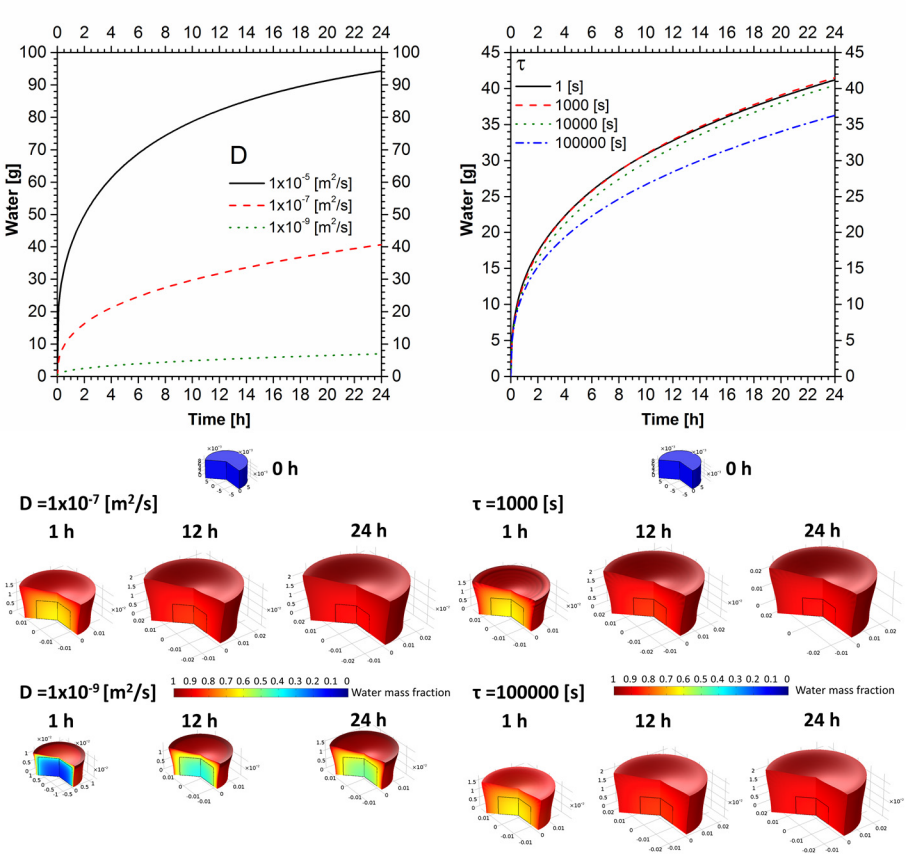

***Figure 29**. Free swelling parametric study: effect of the diffusion coefficient D (left) , and the relaxation time, τ (right). On the top the amount of water absorbed during a swelling test, on the bottom the shape of the hydrogel and the water mass fraction ranging from 0 (blue) to 1 (red). Where not differently specified G1=100 [kPa], G2=1000 [kPa], $D=1\times10^{-7}[m^2/s]$, τ=10000 [s].*

The effect of the relaxation time of the network structure on the water absorption is depicted in **Figure 29** (top right). This parameter tunes the time relaxation of the Maxwell's element: higher τ means that the relaxation is slower and hence the system stiffness is higher for longer time. This result in

a slower absorption kinetic and in deformations more homogeneous (**Figure 29** bottom right).

3.5.1.2 Unconfined stress-relaxation test

The unconfined stress-relaxation test is a simple experiment that can highlight viscoelastic behaviors. This consists in an application of a given deformation, which is then kept constant while the stress evolution is recorded. In polymeric materials the relaxation is due to rearrangement of the network structure (viscoelasticity) while in hydrogels, the relaxation can be generated by rearrangement of the network structure (viscoelasticity) and by the long-range motion of the water (poroelasticity).

In this work it has been simulated the stress-relaxation behavior of a hydrogel (initial water mass fraction: $\omega_{10} = 0.8$) in equilibrium with the surrounding solvent ($\mu_1^{ext} = \mu_{10}$) to highlight the effect of the model parameters on the system behavior. The Flory-Huggins interaction parameter (χ_{12}) has been fixed to the realistic value of 0.2.

The boundary conditions that particularize the problem are:

$$\begin{aligned}
&\forall \bar{X} \in \Gamma 2, : \begin{cases} \bar{\nabla}\mu_1 = \bar{0} \\ u_R = 0 \\ u_Z = \begin{cases} @t < t^*, -v^* \cdot t \\ @t \geq t^*, -1\ [mm] \end{cases} \end{cases} \\
&\forall \bar{X} \in \Gamma 3: \begin{cases} \mu_1 = \mu_{1,ext} \\ \bar{u} = free \end{cases} \\
&\forall \bar{X} \in \Gamma 4: \begin{cases} \bar{\nabla}\mu_1 = \bar{0} \\ u_Z = 0 \end{cases} \\
&\forall \bar{X} \in \Gamma 1: \begin{cases} \bar{\nabla}\mu_1 = \bar{0} \\ u_R = 0 \end{cases}
\end{aligned} \tag{3.51}$$

Where Γ2 represents the boundary in contact with a probe which deforms the gel: the compression is achieved lowering the probe at $v^* = 0.3$ [mm/s] until it has moved of 1 mm (10% of deformation) at $t = t^* = 3.33$ [s]. At $t > t^*$ the probe is immobile, at the new position reached. The boundary Γ3 is the one in contact with the external environment, Γ4 represents the bottom of the instrument and Γ1 is the axis of symmetry.

In **Figure 30** it is reported the effect of the elastic moduli (G_1 and G_2) on the axial stress and on the water mass loss percentage. The axial stress reported is the average value, of the Cauchy stress ($\bar{\bar{\sigma}} = J^{-1}\bar{\bar{P}} \cdot \bar{\bar{F}}^T$), computed on the boundary Γ2, which would be the value measured by a real instrument.

In **Figure 30** on the left side, the effect of the relaxed modulus G_1 is reported. On the upper part the effect on the axial stress is shown, where the massive impact of this modulus is clear. Increasing G_1 the stress-relaxation curves translate toward higher stress values, influencing both the maximum and the relaxed stress values. The relaxed modulus G_1 affect also the amount of water expelled by the system: increasing G_1 the internal stresses increase,

increasing the pressure and therefore the internal water chemical potential. This results in a greater amount of water expelled, given a certain deformation, as G_1 increases.

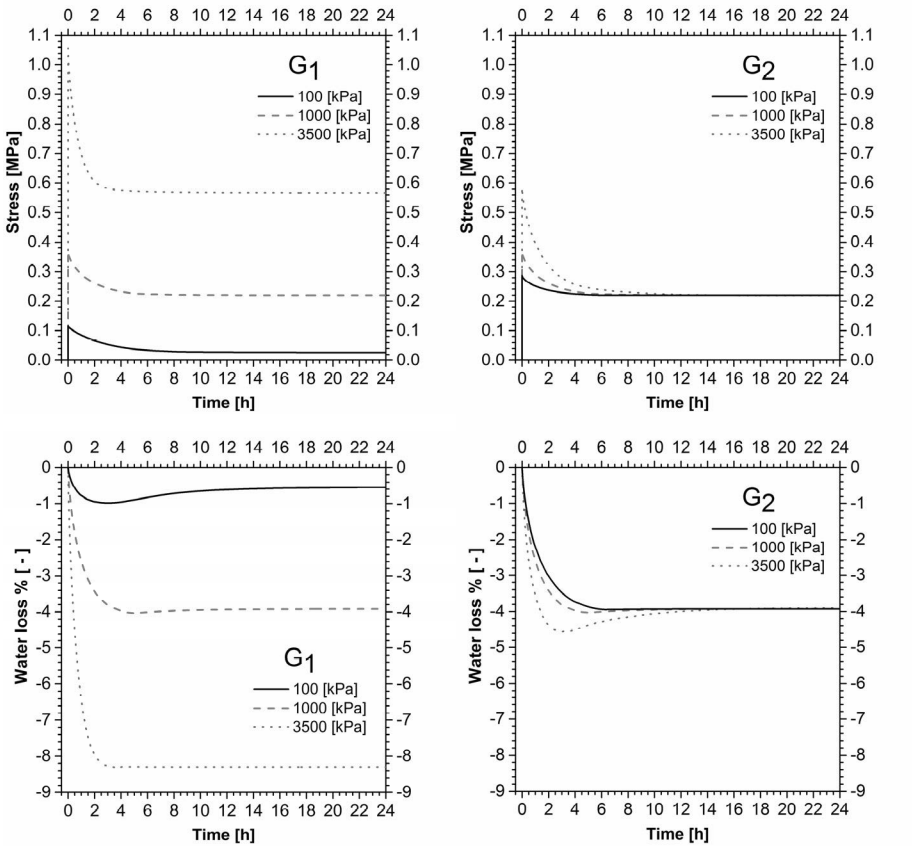

***Figure 30**. Stress-relaxation parametric study: effect of the elastic moduli (G_1 left, G_2 right) on the axial stress (top) and the water loss (bottom). Where not differently specified G_1=1000 [kPa], G_2=1000 [kPa], $D=1\times10^{-7}$ [m^2/s], τ=1000 [s]*

In **Figure 30** on the right side, the effect of the short-time elasticity G_2 is reported. On the upper part the effect on the axial stress of G_2 is shown: the transient elasticity affect the maximum stress value (peak value), while the relaxed value is not affected since at $t \to \infty$ the Maxwell branch is completely relaxed. The same effect can be seen on the water expelled: in the short time limit ($t < \tau$) the system is stiffer and the stress generated and the water chemical potential are higher. This cause the loss of great amount of water, which than tend to return inside the system due to its relaxation (stiffness reduction).

In **Figure 31** it is reported the effect of the diffusion coefficient and of the relaxation time on the axial stress and on the water mass loss percentage. In particular, on the left part of **Figure 31** the effect of the diffusion coefficient is reported. At very high values (i.e. $1 \times 10^{-5}\,[m^2/s]$) the chemical equilibrium can be established in few seconds (the characteristic diffusion time is of order of seconds: $t_D = L^2/D$, where L is the diffusion length), therefore the increase of stress, which translates in an increase of the internal water chemical potential (non-equilibrium condition), is promptly compensated by the water movement. Therefore, the drop of the stress value at low time is due to poroelastic effect (the network relaxation is not yet started $t \approx t_D \ll \tau$), as it can be confirmed by the water loss diagram (**Figure 31** bottom left).

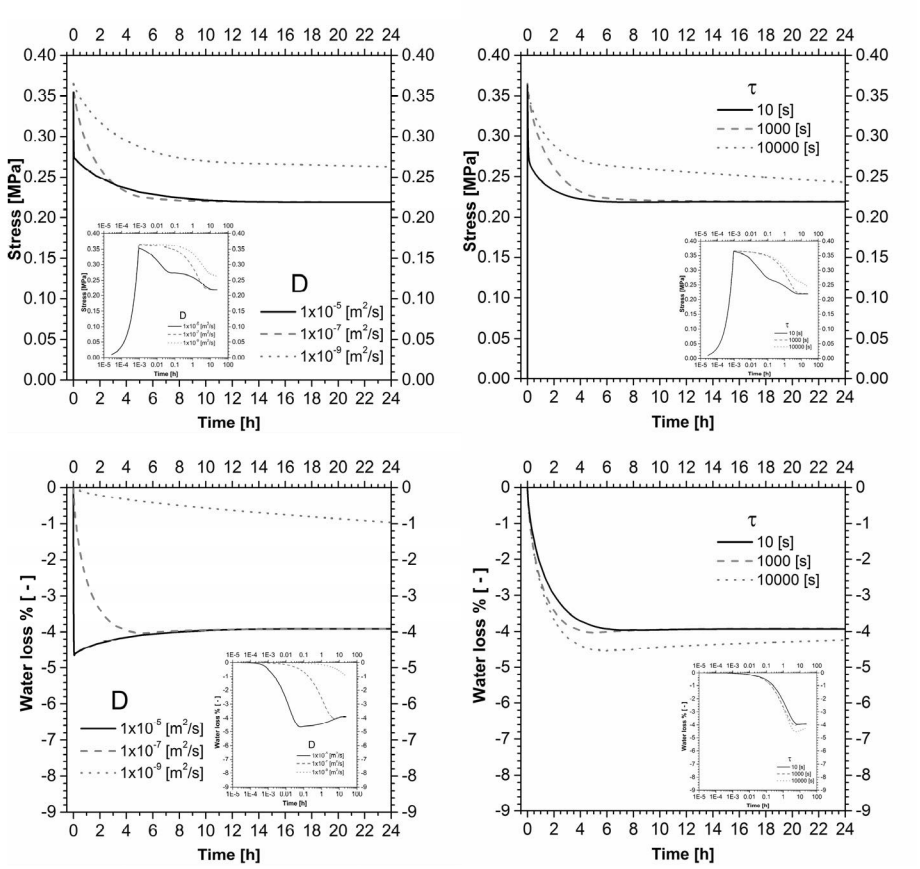

***Figure 31**. Stress-relaxation parametric study: effect of the diffusivity (left) and of the relaxation time (right) on the axial stress (top) and the water loss (bottom). Where not differently specified G_1=1000 [kPa], G_2=1000 [kPa], D=1×10^{-7} [m^2/s], τ=1000 [s]. The insets show the same results on a logarithmic scale abscissa*

After the initial drop, the axial stress continue slightly to decrease whereas the water increases: this is, once again, due to the network viscoelasticity that relaxes the structure (stress decrease) and allows higher equilibrium water concentration (water inlet).

At very high diffusion times, $t_D \gg \tau$ (i.e. $1 \times 10^{-9}\ [m^2/s]$), the stress-relaxation behavior, in the time range analyzed, is only due to the intrinsic structure viscoelasticity, the axial stress considerably decrease around the relaxation time (inset in **Figure 31** top left), whereas the water movement is still limited (<1% w/w). As the diffusion time become comparable with the structure relaxation time, $t_D \approx \tau$ (i.e. $1 \times 10^{-7}\ [m^2/s]$), the stress-relaxation behavior is of poroviscoelastic nature characterized by the water diffusion in a relaxing structure.

The effect of the structure relaxation time τ is depicted on the right part of **Figure 31**. When $\tau \ll t_D$ (**Figure 31** top right and its inset), (i.e. $\tau = 10\ [s]$) the stress relaxation curve shows a first steep decrease due to the viscoelasticity of the structure (around $t = \tau = 10\ [s] \approx 3 \times 10^{-3}[h]$), followed by another step of relaxation due to poroelasticity ($t = t_D = 1000\ [s] \approx 0.3\ [h]$), demonstrated by the consistent outlet of water (**Figure 31** bottom right and its inset) around t_D. When $\tau \gg t_D$, (i.e. $\tau = 10000\ [s]$), the relaxation, is initially controlled by poroelasticity: it starts along with the water outlet ($t = t_D$), as it can be seen comparing the insets of the right part of **Figure 31**. When the time become comparable with the relaxation time $t = \tau$ ($\tau = 10000\ [s] \approx 2.8\ [h]$) another step of relaxation starts, this time generated by the structure relaxation. When $\tau \approx t_D$, ($\tau = 1000\ [s]$) the time of structure relaxation is comparable with the time of diffusion and it is not possible to distinguish different steps of relaxation.

The analysis of these stress relaxation simulation data can give useful information to setup experimental tests and/or to design new systems based on hydrogels. It has been shown that stiffness (long and short time) can differently tune the amount of water expelled: deformed chemical crosslinked gels (G_1 prevails on G_2) would release much water than physical gels (G_2 prevails on G_1) that, instead, after an initial water release would rearrange the structure, reduce the internal stresses and reabsorb the water. Moreover, tuning the amount of stable (chemical) or transient (physical) crosslinks, therefore tuning G_1 and G_2, it is possible to tune the stress relaxation response in terms of peak force and relaxed final force, to obtain the desired behavior. It has also been shown that is possible to tune the relaxation behavior and the water movement varying the hydrogel permeability (easiness of water movement) and the relaxation time (related to the bond energy of the transient crosslinks) separating or joining the poroelastic and the viscoelastic effect. Indeed, in the practical cases, one can need a relaxation accompanied by water release (poroelasticity) or a relaxation without water release (viscoelasticity) and it has been demonstrated that, chosen a time scale of interest, it is possible to separate the effects.

3.5.2 Stress-relaxation behavior of agarose gels

3.5.2.1 Water up-take and polymer erosion

The gravimetric analysis, to determine the variation of the water and polymer masses, was performed on all the runs, which differs for the initial polymer concentration, ω_{20} in **Table 6**.

The initial total mass of the gel sample is reported as m_0 in **Table 6**. The variation of the water mass, prior and after the stress-relaxation tests, Δm_1, is reported in **Table 6**. Considering that these values were obtained weighting the samples, which were immerged in water, and taking into account that the order of magnitude of Δm_1 is the same as a single drop of water (50 mg), which can be a realistic value of the amount of water retained on the surface of the sample, deeper considerations on these data would be speculations. However it is possible to assert that some water actually leaves the system, but in a very low amount (a pure volumetric deformation would release around 300 mg of water for the deformation imposed), however there is not a specific trend. The variation of the polymer mass, Δm_2, which could be due to the system erosion shows that this phenomenon, in the time range considered, is negligible. In all the cases the polymer release is less than 0.5% w/w.

Therefore the gravimetric analyses demonstrated that the deformation does not produce a consistent movement of water (the poroelastic effect should be marginal) and the gels in the experimental condition do not dissolve in the water medium.

***Table 6**. For each sample (average value from five tests ± standard deviation): initial total mass, m_0; water mass change, Δm_1; initial polymer mass fraction, ω_{20}; polymer mass change, Δm_2.*

Run	$\boldsymbol{\omega_{20}}$, [%]	$\boldsymbol{m_0}$, [mg]	$\boldsymbol{\Delta m_1}$, [mg]	$\boldsymbol{\Delta m_2}$, [mg]
1	0.97±0.03	3412±26	-63±20	0.10±0.07
2	2.14±0.09	3797±92	-30±13	0.40±0.52
3	3.58±0.15	3693±96	-91±101	0.16±0.04
4	4.64±0.33	3765±155	-19±13	0.50±0.05

3.5.2.2 Results of mechanical tests

In **Figure 32** the stress-relaxation behavior of the gel analyzed is shown. With the thick black solid lines the average values are reported, the thin lines represent individual tests. The first vertical tract is representative of the compression part, where the probe is lowered from 10 mm (according to the

axis **z** in **Figure 23** - 0% of deformation, top surface of the undeformed hydrogel) to 9 mm (10% of deformation).

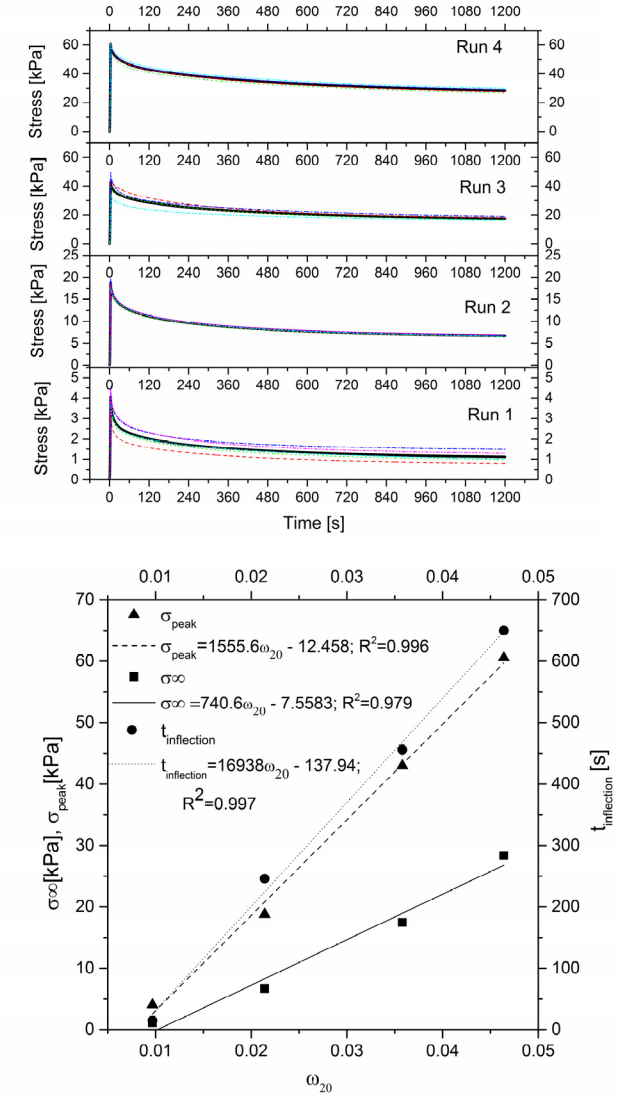

***Figure 32**. Results of mechanical compression-relaxation tests. On the left the stress relaxation curves for each run. The duration of each test is 1200 [s] = 20 [min], the observed stress values [kPa] are reported on the ordinate using different levels. The data for each test are reported as thin lines, the average values from five tests are reported as thick lines. On the right the characteristic point of the relaxation curves ($\sigma_\infty, \sigma_{peak}, t_{inflection}$) against the polymer concentration.*

The stress decreasing portion instead is representative of the relaxation part, where the probe remains at 9 mm and the force evolution is recorded.

It is clear that increasing the polymer concentration (going from Run 1 to Run 4) the system becomes stiffer, responding to the same deformation (10%) with higher stress values. In the time range analyzed both the peak stress (σ_{peak}), which is the maximum value of the stress, and the relaxed stress value (σ_∞), which is the stress value at the end of the test (ideally at infinite time, when the gel is completely relaxed), increase along with the polymer concentration (**Figure 32** right). This is an expected result since increasing the amount of polymer, the agarose gel, which is a physical gel, can form more cross—links (hydrogen-bonds) that tighten the polymeric structure. The relaxation time of the system, represented in this section by the inflection time ($t_{inflection}$) of the curve $\sigma(\log(t))$, also tends to increase along with the polymer concentration: gels with more polymer relax the stress slower than gels with less polymer. This is not an obvious result since, as it has been discussed in the introduction, the relaxation can be due to poroelastic phenomena or viscoelastic phenomena. However considering the low amount of water released at the end of the test (at $t = 1200\ [s]$) and looking at the time scale of relaxation recorded ($t << 1200\ [s]$), which is far smaller than the characteristic diffusion time ($t_D = L^2/D = 0.01^2/2 \times 10^{-9} = 50000[s]$), it is most probably that the viscoelastic relaxation prevails on the poroelastic relaxation. Therefore the different kinetic of relaxation can be mainly attributed to the time needed to rearrange the polymeric structure (i.e. breakage and reformation of the hydrogen-bonds), which takes longer when more cross-links are involved.

The experimental results in terms of characteristic points, $\sigma_{peak}, \sigma_\infty, t_{inflection}$, show a good linear trend when plotted against the gel polymer concentration (**Figure 32** right) in the range investigated. These relations could be used to predict the characteristic points of the stress-relaxation curve for agar gels at polymer concentration between 1 and 4.5 %w/w subjected to a deformation of 10%.

3.5.2.3 Model data fitting

In **Figure 33** the comparison between three out of four experimental results of the stress relaxation test and the model simulation are reported. The model calculations are the results of an inverse problem optimization to estimate the model parameters (G_1, G_2, τ), going to reduce the error between the experimental and the modeling stress relaxation curve.

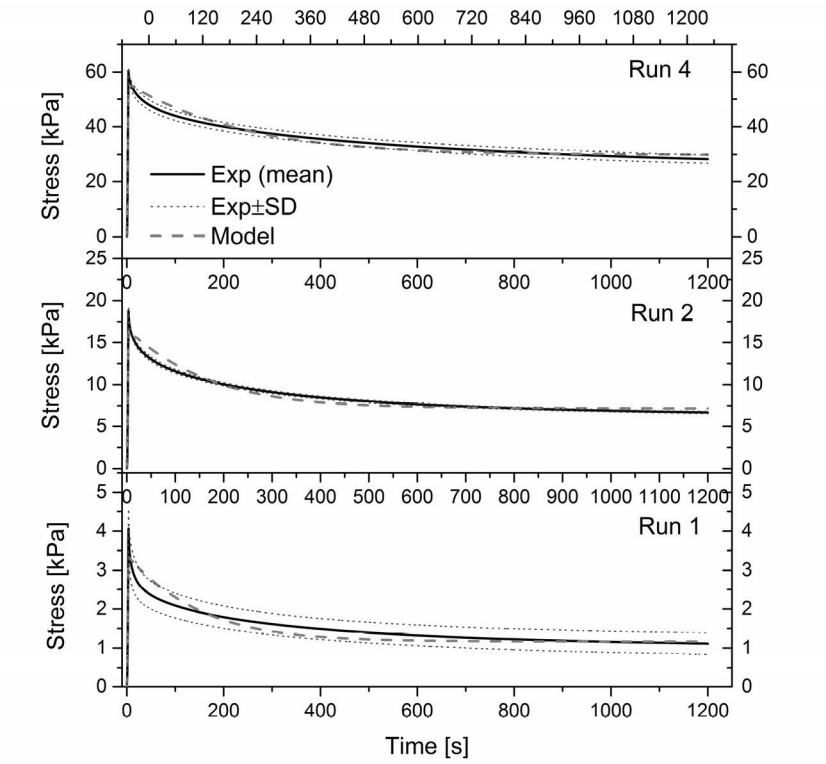

***Figure 33**. Data fitting using the model for runs 1, 2 and 4. Experimental data are reported as tick solid black lines (average values from five tests, taken from Figure 3) and thin blue dot lines (average ± standard deviation); calculated data are reported as thick red dashed lines.*

Despite the modeling description could be satisfactory, the agreement is not perfect due to the oversimplified rheological model. Indeed a simple SLS model has been considered, which uses a single Maxwell element, therefore a single viscoelastic relaxation time. In general, polymers as well hydrogel and agar gels (Labropoulos et al., 2001), present a spectra of viscoelastic relaxation times, which are better described as the number of Maxwell elements increase. Despite it is relatively easy to add more Maxwell elements to the model, this would add parameters (two each additional Maxwell element) but not relevant concept to this work.

In **Figure 34** are reported the optimized model parameters (G_1, G_2, τ) against the initial gel polymer concentration. As it can be seen, the modeling elastic moduli and the relaxation time increase along with the polymer concentration, in agreement with the consideration done on the experimental data (section 4.2). The higher the amount of polymer, the higher the number of cross-link, the higher the elastic moduli. Despite a spectra of relaxation time would better describe the experiments, the single modeling relaxation time is

able to catch the trend assumed in section 4.2: the higher the number of cross-link the slower the viscoelastic relaxation phenomena, the higher the relaxation time.

In the concentration range analyzed, the parameters show a reasonable linear trend, which has been exploited to obtain linear relation between parameters and polymer concentration (**Figure 34**) so that, knowing the initial concentration of the sample, it is possible to estimate the model parameters.

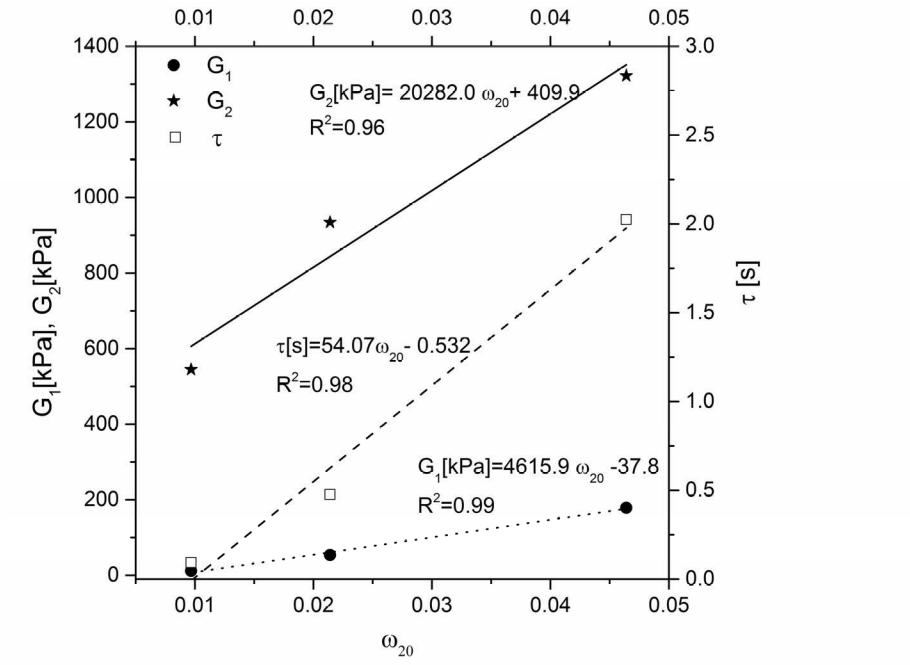

***Figure 34**. The parameters of the model (G_1, G_2, τ) versus the initial polymer mass fraction in the gel, along with linear fitting of the data (curve and equations).*

3.5.2.4 Model simulation

The linear relations between model parameters and initial polymer concentration have been used to derive G_1, G_2, and τ for Run 3 ($\omega_{20} = 3.58\% w/w$) and to predict at zero tunable parameters the system response. As it can be seen in **Figure 35** the model prediction (green dot line) fairly describe the experimental results (black solid line), with the same limitations discussed in section 4.3, and being well comparable with the results of an optimization procedure (red dash line) where case specific parameters have been derived. Therefore the generalization proposed in **Figure 34** is verified and can be safely used to predict the model parameters within the range of polymer concentration investigated.

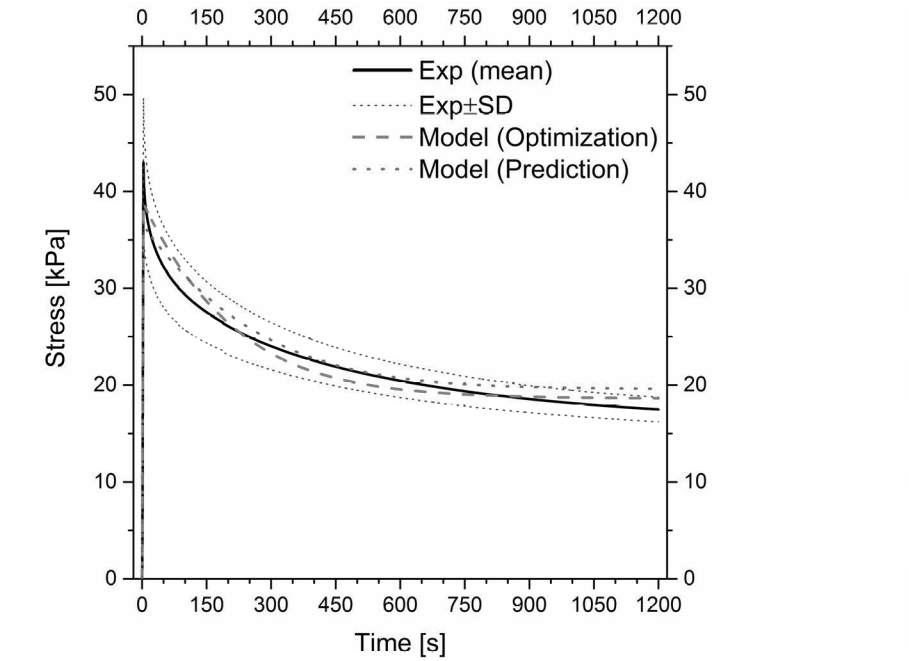

***Figure 35**. Stress-relaxation curve for Run 3 ($\omega_{20} = 3.58\%w/w$). Experimental data are reported as tick solid black lines (average values from five tests) and thin blue dot lines (average ± standard deviation); with the thick green line the model prediction is reported, whereas with the red dashed line the result of the model optimization is shown.*

Once the model parameters have been obtained, and therefore the model properly tuned, the gel could be virtually analyzed in many ways, i.e. varying the deformation, the probe type (indentation), confining the gel (confined compression tests) and so forth.

It is important to emphasize that G_1, G_2, and τ are material specific parameters and directly related to the polymeric structure (i.e. number of cross-links). Chemical gels, where the number of cross-links are fixed, could be describable with a single value of these parameters in a wide range of solvent concentration (reminding to use a concentration dependent diffusion coefficient). Therefore after a single stress-relaxation test it would be possible to describe swelling/shrinking tests. Instead, as demonstrated in this study, physical gels are quite sensitive to a change of solvent/polymer concentration, varying the degree of crosslinking and therefore the elastic moduli and the relaxation time of the structure, which are no more constants but at least function of the polymer concentration: $G_1(\omega_2), G_2(\omega_2)$ and $\tau(\omega_2)$. This complicates the model extension to swelling/shrinking tests that involve large variation of the water/polymer content, since the functionality of these parameters with the amount of polymer have to be known. However the same

approach used in this study could be used: perform several stress-relaxation tests, at different polymer concentration, to obtain the sought functionality.

3.6 Summary

In this chapter a 3D monophasic model able to describe the hydrogel poroviscoelastic behavior has been developed within the field of non-linear solid mechanics and deriving the constitutive equations from non-equilibrium thermodynamics.

In particular the polymer network hyperviscoelasticity has been considered as describable by an SLS model in which the springs are hyperelastic accordingly to the affine network model of rubber elasticity. The water movement is driven by its chemical potential gradients, which account for the polymer-solvent interaction (Flory-Huggins theory) and for the hydrostatic pressure. This last, mathematically generated as a Lagrange multiplier, relates the water content to the system deformation (accordingly to the volumetric constraint), being influenced by the polymer chains stresses as well as by the water content. The diffusion in the system, for the sake of simplicity, has been considered isotropic with constant diffusivity.

The model has been implemented through the weak formulation in a commercial FEM-based software (COMSOL Multiphysics® 5.0) in a 2D-axisymmetric version. The performed parametric study have highlighted the model ability to describe the hydrogel's poroviscoelasticity and displayed the relative importance of the model/gel parameters on the resultant behavior.

A model gel, the agarose, has been experimentally analyzed with stress-relaxation tests accompanied by gravimetric analysis. The system has shown, in the time range analyzed, poor poroelastic properties, and marked viscoelastic ones. The developed poroviscoelastic model has been used to derive the agarose gels characteristic parameters and then used to predict the gel behavior, showing a good reliability.

Thanks to the general approach employed, this model constitute the base to describe hydrogels. It can be "easily" extended to non-Gaussian treatment of the polymeric chains, to more complex mobility tensors as well as to multicomponent systems, allowing to describe hydrogel-based systems (i.e. hydrogel loaded with drugs). Therefore the proposed model is very useful for designing and optimizing hydrogels for several uses.

3.8 Nomenclature

In **Table 7** the nomenclature used during the development of the poroviscoelastic model.

Table 7. *Nomenclature of the poroviscoelastic model*

Nomenclature	
A	Helmholtz free energy density $[J/mol]$
c_1	Water concentration $[mol/m^3]$
D	Diffusion coefficient $[m^2/s]$
$\bar{\bar{D}}$	Mobility tensor $[mol^2/(s \cdot m \cdot J)]$
$\bar{\bar{F}}$	Deformation gradient tensor $[-]$
G	Elastic modulus $[Pa]$
$\bar{h}_1$	Water molar flux $[mol/(s \cdot m^2)]$
$\bar{\bar{I}}$	Identity tensor $[-]$
J	Volumetric deformation $(\det(\bar{\bar{F}}))$ $[-]$
p	Hydrostatic pressure $[Pa]$
$\bar{\bar{P}}$	First Piola-Kirchhoff stress tensor $[Pa]$
R	Gas constant $[J/(mol \cdot K)]$ (or radial coordinate)
t	Time $[s]$
T	Temperature $[K]$
$\bar{u}$	Displacement field $[m]$
Γ	Domain boundary
η	Dashpot viscosity $[Pa \cdot s]$
λ	Stretch ratio $[-]$
μ_1	Water chemical potential $[J/mol]$
$\bar{\bar{\sigma}}$	Cauchy stress tensor $[Pa]$
τ	Relaxation time $[s]$
χ_{12}	Flory-Huggins interaction parameter $[-]$
$\bar{\chi}$	Motion function $(\bar{x} = \bar{\chi}(\bar{X}, t))$ $[-]$
ω_1	Water mass fraction $[-]$
Ω_1	Water molar volume $[m^3/mol]$
SUBSCRIPTS	
0	Initial condition
D	Dry state
S	Spatial (deformed) state
x	Derivation with respect to the spatial coordinates
X	Derivation with respect to the material coordinates
SUPERSCRIPTS	
0	Standard State
el	Elastic contribution
mix	Mixing contribution
$visc$	Referred to the dashpot
ext	Referred to the external condition

Chapter Four

Toward a complete approach: the multicomponent poroviscoelastic model

In this chapter how it is possible to extend the poroviscoelastic model to hydrogel-based system for controlled release applications will be demonstrated. The presence of another diffusing species will be accounted for, opportunely modifying the transport and constitutive model equations. This will be implemented and, as an example, the drug release from a swelling system will be reported.

4.1 Introduction

The high interest in controlled release hydrogel-based systems, as seen in the section 1.3.2.1 and in chapter 2, has led to develop mathematical models mainly based on a "mass transport" only approach. However, as shown in the introduction (section 1.2.1) and in the chapters 2 and 3, the mechanics of the hydrogel has an impact on the water absorption (and vice versa), which surely translate in an influence on an active ingredient release.

The difficulties related to the development and implementation of a "full" monophasic model, with multiple diffusing species, should be evident from the previous chapter and indeed, to the author's knowledge, no traces of such models are present in literature. However, thanks to the comprehensive approach used in this thesis in the development of the poroviscoelastic model, it is possible to treat hydrogels with multi diffusing species, i.e. hydrogels loaded with active ingredients, thus filling this important void in literature.

4.2 Aim

Aim of this chapter is to show how to extend the poroviscoelastic model (polymer plus water) developed in the previous chapter to controlled release hydrogel-based systems (polymer plus water plus active ingredient). During the development/extension of the poroviscoelastic model with multiple diffusing species, for sake of simplicity, several limiting hypotheses will be done, discussed and pointed out as needed future improvements.

4.3 Modeling

4.3.1 Balance equations

The water "1" and the active ingredient (AI) "3" (i.e. drug) mass balances are:

$$\begin{cases} \dfrac{\partial c_1}{\partial t} = -\bar{\nabla} \cdot \bar{h}_1 \\ \dfrac{\partial c_3}{\partial t} = -\bar{\nabla} \cdot \bar{h}_3 \end{cases} \tag{4.1}$$

Where c_i and $\bar{h}_i$ are the molar concentration and molar flux of the ith species.

The linear momentum balance is:

$$\bar{\nabla} \cdot \bar{\bar{P}} = \bar{0} \tag{4.2}$$

Where $\bar{\bar{P}}$ is the first Piola-Kirchoff stress tensor.

All the species are treated as incompressible substances, whereas the hydrogels is compressible due to the water and the active ingredient content variation. This translates in the volumetric constraint:

$$J = 1 + \Omega_1(c_1 - c_{10}) + \Omega_3(c_3 - c_{30}) \tag{4.3}$$

Where J is the volumetric deformation from the initial to the current state, Ω_i and c_{i0} are the molar volume and the initial molar concentration of the ith species.

4.3.2 Constitutive equations

The free-energy imbalance (or dissipation inequality) for multiple diffusing species, two in this case, can be written as (Gurtin et al., 2010):

$$\frac{\partial A}{\partial t} - \bar{\bar{P}}: \dot{\bar{\bar{F}}} - \mu_1 \dot{c}_1 + \bar{h}_1 \cdot \bar{\nabla}\mu_1 - \mu_3 \dot{c}_3 + \bar{h}_3 \cdot \bar{\nabla}\mu_3 \leq 0 \tag{4.4}$$

A is the Helmholtz free energy density (that corresponds to the strain-energy density function), $(\bar{\bar{P}}: \dot{\bar{\bar{F}}})$ is the conventional power expended on the system, $(-\mu_i \dot{c}_i + \bar{h}_i \cdot \bar{\nabla}\mu_i)$ is the energy carried into the system by species transport.

Analogously to the "simple" poroviscoelastic case, once the expression of the Helmholtz free energy is known, the constitutive equations can be derived from equation (4.4).

Considering a neutral gel, the free energy obeys to the theory of Flory and Rehner:

$$A = A^{el} + A^{mix} \tag{4.5}$$

4.3.2.1 The (visco)elastic contribution

Let us consider that the elastic contribution, analogously to the previous case, is viscohyperelastic in nature and describable with a Standard Linear Solid model (coupled to the affine network theory for the elastic contribution) (**Figure 26**):

$$\begin{aligned} A_D^{el} = \frac{G_1}{2}\left[\bar{\bar{F}}_D : \bar{\bar{F}}_D - 3 - 2\ln\left(\det(\bar{\bar{F}}_D)\right)\right] \\ + \frac{G_2}{2}\left[\bar{\bar{F}}_D\left(\bar{\bar{F}}^{visc}\right)^{-1} : \bar{\bar{F}}_D\left(\bar{\bar{F}}^{visc}\right)^{-1} - 3\right. \\ \left. - 2\ln\left(\det\left(\bar{\bar{F}}_D\left(\bar{\bar{F}}^{visc}\right)^{-1}\right)\right)\right] \end{aligned} \tag{4.6}$$

Where G_1 and G_2 are elastic moduli, $\bar{\bar{F}}_D$ the deformation gradient with respect to the dry state, $\bar{\bar{F}}^{visc}$ is the internal variable representing the dissipative mechanism of the materials (Holzapfel, 2000).

4.3.2.2 The mixing contribution

For sake of simplicity, let us consider that the Active Ingredient (AI) do not interact with the other components (water and polymer). Under this

assumption, the AI contribution to the free energy of mixing is only of entropic nature[2]:

$$A^{mix} = RT[c_1 ln(\phi_1) + c_2 ln(\phi_2) + c_3 \ln(\phi_3) + c_1 \chi_{12} \phi_2] \quad (4.7)$$

Where R is the the gas constant, T the temperature c_1 and ϕ_i are the molar concentration and the volume fraction of the i^{th} species. χ_{12} is the Flory-Huggins interaction parameter.

To sum the elastic free energy density to the mixing free energy density they have to refer to the same state, therefore the mixing contribution have to be formulated per volume of dry polymer.

Considering that the volume fractions can be expressed as:

$$\begin{cases} \phi_1 = \dfrac{\Omega_1 c_{1D}}{1 + \Omega_1 c_{1D} + \Omega_3 c_{3D}} \\ \phi_2 = \dfrac{1}{1 + \Omega_1 c_{1D} + \Omega_3 c_{3D}} \\ \phi_3 = \dfrac{\Omega_3 c_{3D}}{1 + \Omega_1 c_{1D} + \Omega_3 c_{3D}} \end{cases} \quad (4.8)$$

Where Ω_i and c_{iD} are the molar volume and the molar concentration (with respect to the dry state) of the i^{th} component. Bearing in mind there are no "free" polymer moles in the network structure (Flory, 1953), the equation (4.7) can be rewritten as:

$$A_D^{mix} = RT \left[c_{1D} \ln \left(\frac{\Omega_1 c_{1D}}{1 + \Omega_1 c_{1D} + \Omega_3 c_{3D}} \right) + c_{3D} \ln \left(\frac{\Omega_3 c_{3D}}{1 + \Omega_1 c_{1D} + \Omega_3 c_{3D}} \right) + c_{1D} \frac{\chi_{12}}{1 + \Omega_1 c_{1D} + \Omega_3 c_{3D}} \right] \quad (4.9)$$

4.3.2.3 The total free energy density

The total free energy density is the sum of the elastic and mixing contribution:

$$A_D = A_D^{el} + A_D^{mix} \quad (4.10)$$

However, despite the derivation of the elastic free energy density oblige to derive the expression using the dry state as reference state, it is not possible to work with respect to this state using equation (4.10) since the mixing terms shows a singular behavior at the dry state.

[2] Depending on the type of polymer/solvent/AI the interactions could be present and relevant, giving rise to enthalpic terms with the additional parameters χ_{ij}. In this chapter, which has demonstrative aims, these interactions are neglected, however a rigorous approach should include them.

A change of reference frame has to be performed, analogously to the section 3.4.2.1, in this case it is assumed that the dry polymer network equilibrates with a solvent of chemical potential μ_{10} and with a AI of chemical potential μ_{30}, under no mechanical loads, such that the deformation from the dry to the reference state is homogenous. It results that:

$$\begin{aligned} A(\bar{\bar{F}}, c_1, c_3, \bar{\bar{F}}^{visc}) &= A^{el} + A^{mix} \\ &= \frac{1}{J_0}\left\{\frac{G_1}{2}\left[\bar{\bar{F}}_0\bar{\bar{F}} : \bar{\bar{F}}_0\bar{\bar{F}} - 3 - 2\,ln\left(det(\bar{\bar{F}}_0\bar{\bar{F}})\right)\right]\right. \\ &+ \frac{G_2}{2}\left[\bar{\bar{F}}_0\bar{\bar{F}}\left(\bar{\bar{F}}^{visc}\right)^{-1} : \bar{\bar{F}}_0\bar{\bar{F}}\left(\bar{\bar{F}}^{visc}\right)^{-1} - 3\right. \\ &\left. - 2\,ln\left(det\left(\bar{\bar{F}}_0\bar{\bar{F}}\left(\bar{\bar{F}}^{visc}\right)^{-1}\right)\right)\right] \\ &+ RTJ_0\left[c_1 ln\left(\frac{J_0\Omega_1 c_1}{1 + J_0\Omega_1 c_1 + J_0\Omega_3 c_3}\right)\right. \\ &+ c_3 ln\left(\frac{J_0\Omega_3 c_3}{1 + J_0\Omega_1 c_1 + J_0\Omega_3 c_3}\right) \\ &\left.\left. + \frac{c_1\chi_{12}}{1 + J_0\Omega_1 c_1 + +J_0\Omega_3 c_3}\right]\right\} \end{aligned} \tag{4.11}$$

As in the previous chapter, before using equation (4.11) into equation (4.4) to derive the constitutive equation, the volumetric constraint (equation (4.3)) is algebraically added through a Lagrange-multiplier "p", enforcing it and obtaining a relaxed "R" version of the system free energy density:

$$\begin{aligned} A_R(\bar{\bar{F}}, c_1, c_3, \bar{\bar{F}}^{visc}, p) &= A^{el} + A^{mix} \\ &= \frac{1}{J_0}\left\{\frac{G_1}{2}\left[\bar{\bar{F}}_0\bar{\bar{F}} : \bar{\bar{F}}_0\bar{\bar{F}} - 3 - 2\,ln\left(\det(\bar{\bar{F}}_0\bar{\bar{F}})\right)\right]\right. \\ &+ \frac{G_2}{2}\left[\bar{\bar{F}}_0\bar{\bar{F}}\left(\bar{\bar{F}}^{visc}\right)^{-1} : \bar{\bar{F}}_0\bar{\bar{F}}\left(\bar{\bar{F}}^{visc}\right)^{-1} - 3\right. \\ &\left. - 2\,ln\left(det\left(\bar{\bar{F}}_0\bar{\bar{F}}\left(\bar{\bar{F}}^{visc}\right)^{-1}\right)\right)\right] \\ &+ RTJ_0\left[c_1 ln\left(\frac{J_0\Omega_1 c_1}{1 + J_0\Omega_1 c_1 + J_0\Omega_3 c_3}\right)\right. \\ &+ c_3 ln\left(\frac{J_0\Omega_3 c_3}{1 + J_0\Omega_1 c_1 + J_0\Omega_3 c_3}\right) \\ &\left.\left. + \frac{c_1\chi_{12}}{1 + J_0\Omega_1 c_1 + +J_0\Omega_3 c_3}\right]\right\} \\ &- p(J - 1 - \Omega_1(c_1 - c_{10}) - \Omega_3(c_3 - c_{30})) \end{aligned} \tag{4.12}$$

4.3.2.4 The constitutive equations

Substituting equation (4.12) into equation (4.4) and rearranging:

$$\left(\frac{\partial A_R}{\partial \bar{\bar{F}}} - \bar{\bar{P}}\right) : \frac{\partial \bar{\bar{F}}}{\partial t} + \left(\frac{\partial A_R}{\partial c_1} - \mu_1\right)\frac{\partial c_1}{\partial t} + \bar{h}_1 \cdot \bar{\nabla}\mu_1 + \left(\frac{\partial A_R}{\partial c_3} - \mu_3\right)\frac{\partial c_3}{\partial t} + \bar{h}_3 \cdot \bar{\nabla}\mu_3 + \frac{\partial A_R}{\partial \bar{\bar{F}}^{visc}}\frac{\partial \bar{\bar{F}}^{visc}}{\partial t} \leq 0 \tag{4.13}$$

In order to satisfy this inequality in any conditions:

$$\begin{aligned}
&\frac{\partial A_R}{\partial \bar{\bar{F}}} = \frac{\partial A}{\partial \bar{\bar{F}}} - pJ\bar{\bar{F}}^{-T} = \bar{\bar{P}} \\
&\frac{\partial A_R}{\partial c_1} = \frac{\partial A}{\partial c_1} + p\Omega_1 = \mu_1 \\
&\frac{\partial A_R}{\partial c_3} = \frac{\partial A}{\partial c_3} + p\Omega_3 = \mu_3 \\
&\frac{\partial A_R}{\partial \bar{\bar{F}}^{visc}}\frac{\partial \bar{\bar{F}}^{visc}}{\partial t} \leq 0 \\
&\bar{h}_1 \cdot \bar{\nabla}\mu_1 \leq 0 \\
&\bar{h}_3 \cdot \bar{\nabla}\mu_3 \leq 0
\end{aligned} \tag{4.14}$$

The first three are the constitutive equations for the stress tensor and the water and the AI chemical potential. The last three gives indication on the thermodynamic valid kinetic expression for the internal variable and the water and AI molar flux. These last can have the form:

$$\begin{aligned}
&\frac{\partial \bar{\bar{F}}^{visc}}{\partial t} = -\frac{1}{\eta}\frac{\partial A_R}{\partial \bar{\bar{F}}^{visc}} = -\frac{1}{\eta}\frac{\partial A}{\partial \bar{\bar{F}}^{visc}} \\
&\bar{h}_1 = -\bar{\bar{D}}_1 \cdot \bar{\nabla}\mu_1 \\
&\bar{h}_3 = -\bar{\bar{D}}_3 \cdot \bar{\nabla}\mu_3
\end{aligned} \tag{4.15}$$

Where $\bar{\bar{D}}_i$ are the mobility tensors. In this case it has been considered isotropic diffusion in the current frame (see paragraph 3.4.2.6.a):

$$\bar{\bar{D}}_i = J\frac{D_i}{\Omega_i RT}\bar{\bar{F}}^{-1}\bar{\bar{F}}^{-T} \tag{4.16}$$

but with diffusion coefficients function of the polymer concentration, according to the free-volume theory (Caccavo et al., 2016):

$$D_i = D_i^* \times \exp\left(-\beta_i\left(\frac{\phi_2}{1-\phi_2}\right)\right) \tag{4.17}$$

Where D_i^* is the diffusion of the ith component in the pure solvent ($\phi_2 = 0$) and β_i is a parameters that tune the dependence of the diffusivity with the polymer concentration.

4.3.3 The initial conditions

The initial conditions describe a hydrogel at known concentration of water (c_{10}) and AI (c_{30}), not yet deformed ($\bar{u} = \bar{0}$) and relaxed ($\bar{\bar{F}}^{visc} = \bar{\bar{F}}_0$):

$$@t = 0: \begin{cases} c_1 = c_{10} \\ c_3 = c_{30} \\ \bar{u} = \bar{0} \\ \bar{\bar{F}}^{visc} = \bar{\bar{F}}_0 \end{cases} \tag{4.18}$$

Where $\bar{u}$ is the displacement field. Considering the initial condition as a stress free state:

$$@t = 0: \bar{\bar{P}} = 0 \Rightarrow p_0 = \frac{G_1}{\lambda_0^3}\left(1 - \frac{1}{{\lambda_0}^2}\right) \tag{4.19}$$

4.3.4 Implementation

The model has been implemented in 2D-axysimmetric geometry, through the weak formulations, in COMSOL MULTIPHYSICS 5.0, and solved in the Lagrangian frame.

The weak form equations implemented have the form:

$$\begin{aligned} 0 &= -2\pi \int_A \frac{\partial c_1}{\partial t} \tilde{c}_1 R \, dA - 2\pi \int_{\partial A} \overline{h_1}\, \tilde{c}_1 \cdot \bar{m} \, R \, dL + \\ &\quad + 2\pi \int_A \overline{h_1} \cdot \bar{\nabla} \tilde{c}_1 R \, dA \\ 0 &= -2\pi \int_A \frac{\partial c_3}{\partial t} \tilde{c}_3 R \, dA - 2\pi \int_{\partial A} \overline{h_3}\, \tilde{c}_3 \cdot \bar{m} \, R \, dL + \\ &\quad + 2\pi \int_A \overline{h_3} \cdot \bar{\nabla} \tilde{c}_3 R \, dA \\ 0 &= -2\pi \int_A (\bar{\bar{P}} : \bar{\nabla} \tilde{\bar{u}}) \, R \, dA + 2\pi \int_{\partial A} \bar{\bar{P}} \cdot \tilde{\bar{u}} \cdot \bar{m} \, R \, dL \\ 0 &= -2\pi \int_A \left[J - \left(1 + \Omega_1 (c_1 - c_{10}) + \Omega_3 (c_3 - c_{30})\right)\right] \tilde{p} \, R \, dA \end{aligned} \tag{4.20}$$

The (five) kinetic equations describing the dashpot deformation (equation (4.15) first) have been implemented with the physic "Domain ODEs and DAEs" solving for distribute ODEs (Ordinary Differential Equations) on the domain.

The domain has been meshed with triangular elements and boundary layers. The solution have been obtained with an implicit time-stepping scheme to solve the time-dependent problem: Backward Differentiation Formula (BDF) with free time stepping. At each time step, the nonlinear system of equations has been tackled with a Fully Coupled approach and Newtonian (automatic) iterations. The resulting linear system of equations has been solved with the direct solver MUMPS.

The simulations have been have been carried out with the help of a workstation based on the processor Intel® Core™ i7-4820K with a clock rate of 3.70 GHz and a RAM of 64 GB. The results obtained are mesh-size independent and the calculation time have been of order of minutes.

4.4 Results and discussion

In the following are reported the results of a parametric study describing the hydration of a cylindrical hydrogel matrix (radius and height of 1 cm), initially dry ($\omega_{10} = 0.01$) and loaded with 10%w/w ($\omega_{30} = 0.1$) of active ingredient (theophylline). Refer to **Figure 27** for the computational domain. The case is analogous to the free swelling case reported in section 3.5.1.1, with the addition of the drug loading.

At time zero the system is immersed in a large excess of pure water ($\mu_1^{ext} = 0$), where the drug concentration is negligible so that the perfect sink condition is verified ($\mu_3^{ext} \to -\infty$ or $c_3^{ext} = 0$). Therefore, the boundary conditions are:

$$\begin{aligned} &\forall \bar{X} \in \Gamma 2, \Gamma 3: \begin{cases} \mu_1 = \mu_1^{ext} \\ c_3 = 0 \\ \bar{u} = free \end{cases} \\ &\forall \bar{X} \in \Gamma 4: \begin{cases} \bar{\nabla}\mu_1 = \bar{0} \\ \bar{\nabla}\mu_3 = \bar{0} \\ u_Z = 0 \end{cases} \\ &\forall \bar{X} \in \Gamma 1: \begin{cases} \bar{\nabla}\mu_1 = \bar{0} \\ u_R = 0 \end{cases} \end{aligned} \tag{4.21}$$

The boundary condition on the water chemical potential was applied using equation (3.49), while a direct Dirichlet condition for the drug mass transport equation ($c_3 = 0$) was preferred, due to numerically instabilities caused by the application of drug chemical potential tending to minus infinite. The boundaries Γ4 and Γ1 represents respectively a plane and an axis of symmetry, therefore by definition there is no flux of water through these boundaries. They are also constrained in Z and R directions respectively, to avoid translation.

The order of magnitude of the parameters employed in these simulations are the same as the one obtained for the agarose gels. However this last, being a physical gel, showed a polymer concentration dependence of the elastic moduli (variation of the number of cross-links), whereas in this case constant elastic moduli were employed.

In **Figure 36** the effects of the system elasticity on the water absorption and drug release are reported.

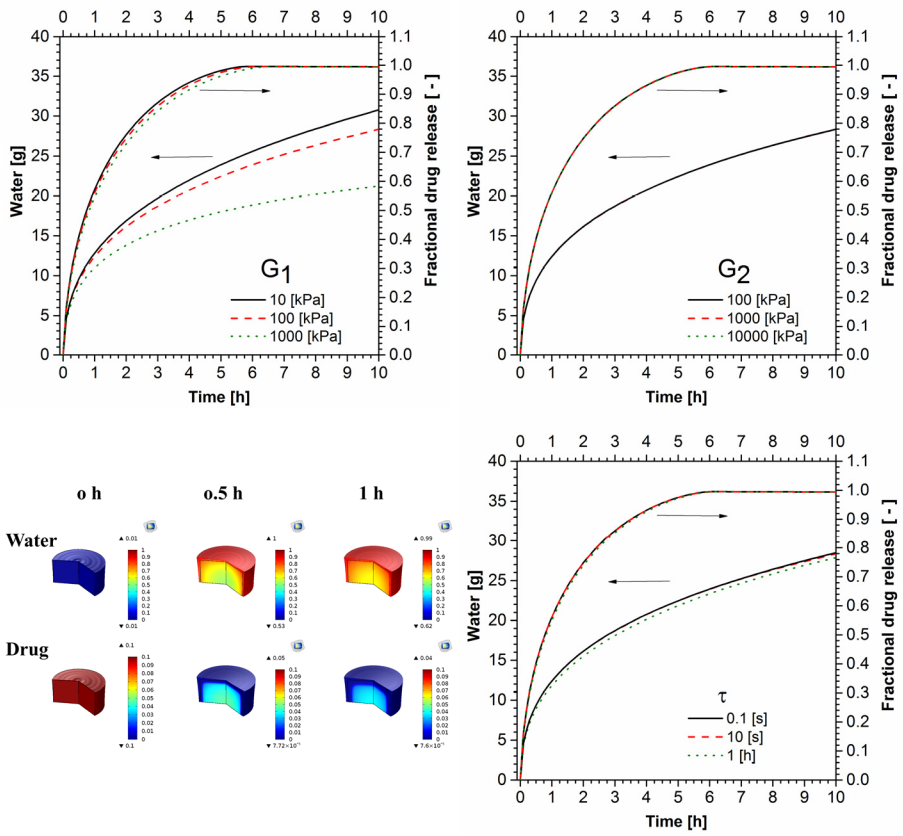

***Figure 36**. Free swelling and drug release parametric study: effect of the elastic moduli, G1 (top left) and G2 (top right), τ (bottom right) on the amount of water absorbed and on the drug released. On the bottom left the shape of the hydrogel and the water and drug mass mass fraction. The first range from 0 (blue) to 1 (red), the latter from 0 (blue) to 0.1 (red). Where not differently specified G1=100 [kPa], G2=1000 [kPa], τ=10 [s], D_1*=1×10^{-7}[m^2/s], D_3*=1×10^{-11}[m^2/s], β_1=0.5, β_3=0.5.*

The impact of G_2 and τ, in the range analyzed, is not relevant on both water absorption and drug release. This is because the diffusive processes of water and drug transport is manifested on a different (longer) time scale with respect to the viscoelasticity.

The permanent network elasticity (G_1) instead, have more marked influence on the water absorption that in turns translates in a slight modification of the drug release profile. The higher G_1, the lower the amount of water absorbed and the amount of drug released. The relation between G_1 and the amount of water absorbed has been discussed in paragraph 3.5.1.1 (**Figure 28**); briefly the stiffer is the polymer matrix the higher will be the pressure field that will allow to reach the chemical equilibrium ($\mu_1 = \mu_1^{ext}$)

with less solvent molecules. The AI chemical potential is influenced at the same way by the matrix stiffness, the higher the stiffness, the higher the pressure field and the lower the amount of molecule absorbable given a certain external chemical potential (this concept could be useful in the AI loading processes based on imbibition of dry matrix in drug solutions).

In **Figure 36** (top left), higher is the stiffness the slower is the drug release. It has to be considered the dual relationship of the AI with the water concentration. Firstly, the drug chemical potential is influenced by the water concentration (and vice versa) according to the entropic effect considered in the free energy of mixing. In **Figure 37** are reported the water and the drug chemical potentials, function of their concentrations. The plots have been obtained (in MATLAB) considering the terms $\partial A/\partial c_1 = \mu_1(c_1, c_3)$ and $\partial A/\partial c_3 = \mu_3(c_1, c_3)$. As it can be seen the water chemical potential (left), in the concentration range of interest, is scarcely influenced by the drug presence: the drug entropic effect is minimal due to its low amount. The drug chemical potential, instead, is affected by the water presence (once again only due to entropic/dilution effect): increasing the amount of water the drug chemical potential decreases. This reduces the drug chemical potential gradients and therefore should reduce the kinetic of drug movement, which is the opposite of what can be seen in **Figure 36** (top left).

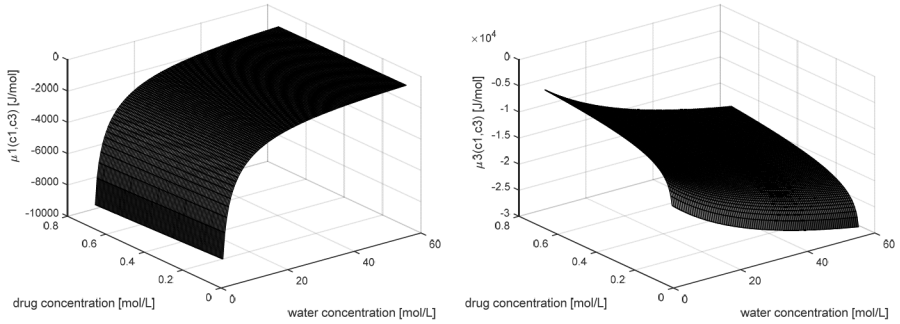

***Figure 37**. Water (left) and drug (right) chemical potentials function of their concentrations only (the term $p\Omega_i$ is not present). The concentration range goes from 0 to pure water for c_1 and from 0 to c_{30} (0.66 mol/L) for c_3.*

The second relation of the AI with the water amount is related to the diffusion coefficients, which are functions (equation (4.17)) of the polymer volume fraction. This last is strongly modified by the inlet/outlet of water and most probably the increase of the diffusion coefficient ($c_1 \uparrow, \phi_2 \downarrow, D_3 \uparrow$) totally compensate the decrease of drug chemical potential (moreover in these simulations the perfect sink condition is applied, always ensuring high driving forces).

In the bottom left part of **Figure 36** the shape of the swelling hydrogel is reported along the water and the drug mass fraction inside the matrix at different dissolution times.

In **Figure 38** the effect of the diffusion coefficients on the water absorption and drug release is reported.

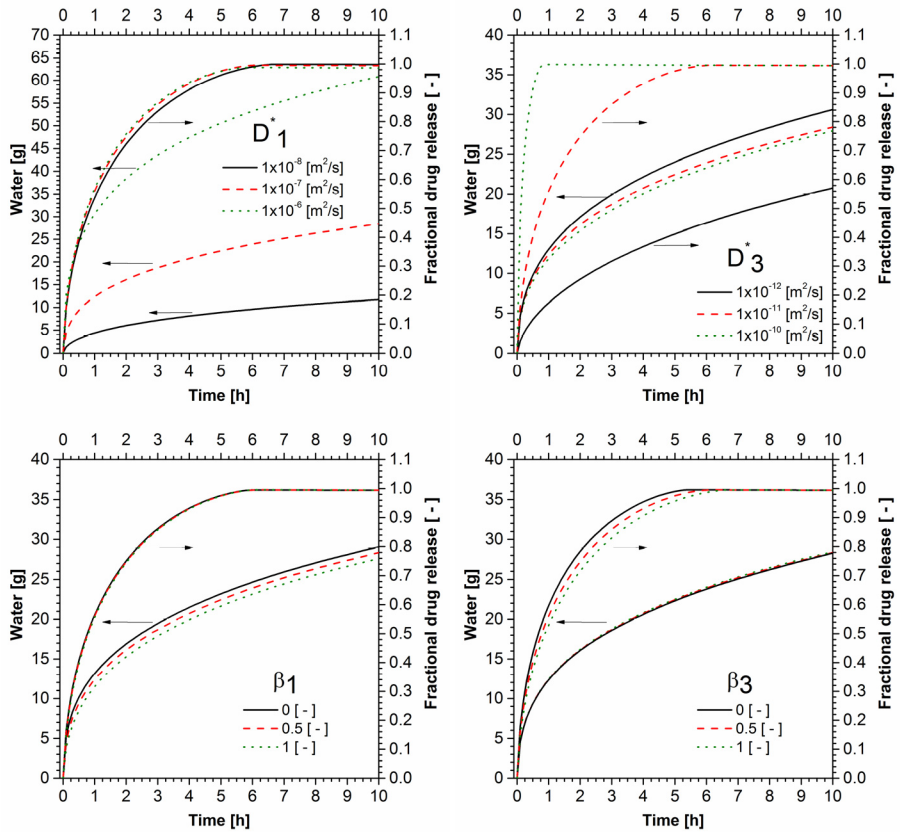

***Figure 38**. Free swelling and drug release parametric study: effect of the diffusion coefficients, D_1* (top left) and D_3* (top right), β_1 (bottom left), β_3 (bottom right), on the amount of water absorbed and on the drug released. Where not differently specified G1=100 [kPa], G2=1000 [kPa], τ=10 [s], $D_1^*=1\times10^{-7}$[m²/s], $D_3^*=1\times10^{-11}$[m²/s], β_1=0.5, β_3=0.5.*

Increasing the diffusion coefficient D_1^* the amount of water absorbed dramatically change, whereas the drug release is only slightly influenced: once again reducing the amount of water the drug release is retarded. The influence of β_1 (which tunes the diffusivity/concentration dependence) (**Figure 38** bottom left), in the range analyzed, is minimal. As expected increasing its value the initial absorbance of water is slowed down, whereas the effect on the drug release is absent.

Varying the diffusion coefficient D_3^* (**Figure 38** top right) the drug release is enormously affected, as expected. The higher the diffusion coefficient the faster the drug release. However also the water uptake seems to be influenced, absorbing more water as the amount of drug in the systems is higher. This

could be due to the slight decrease of the water chemical potential generated by the drug presence, which increases the water chemical potential gradients and therefore the water absorption kinetic. The effect of β_3 (**Figure 38** bottom right), affect only the drug release, slowing down the process as its value increases.

4.5 Summary

In this chapter the poroviscoelastic model has been reformulated to describe controlled release systems based on hydrogels. An Active Ingredient (AI) has been included as a non-interacting species, which simplify the development of the constitutive equations, and its diffusion has been studied along the water diffusion and the system mechanics. It has been proved the feasibility of such kind of approach implementing the model in COMSOL Multiphysics® and simulating the drug release from a swelling system, performing a parametric study. Despite additional work has to be done to refine the model, i.e. including the interaction terms between AI and water/polymer or using non-gaussian theory for the elastic contribution, the present approach, absent in literature, reveals quite robust and ready to be applied to practical cases. The applications are several, from drug delivery to tissue engineering to microfluidics, being this model able to couple the system solid mechanics with the species diffusion.

Chapter Five

Conclusion and perspectives

In this chapter the conclusion of this Ph.D. thesis will be reported along the possible future development of the work

5.1 Conclusion

In this Ph.D. thesis, the hydrogel and the hydrogel-based systems behavior has been extensively analyzed.

A first question to answer when approaching hydrogels is: "are they multiphasic or monophasic systems"? The answer cannot be taken for granted. Despite in most experimental cases the response is simply avoided, it become fundamental when the aim is to develop a mechanistic mathematical model of the system. The wide spreading of these materials, across several sectors (from the biomedical to the agro-food to the construction industry) has led several researchers, with different background, to deal with hydrogel-based systems, producing a vast and fragmented literature on the subject.

The most natural approach is to consider hydrogels as single-phase matter, in which several components can coexist, like it would be indisputably done for polymeric solutions (hydrosols). Another vision is to consider hydrogels as made of different phases, i.e. the water phase is separated from the polymeric phase, and these can exchange momentum. Despite this approach could seem odd to many experimental researchers, it is the most used in literature when modeling hydrogels.

In (Caccavo et al., 2017, Caccavo et al., 2016, Lamberti et al., 2016), briefly reported in the Introduction, a general framework for the hydrogels (and drug release) modeling is proposed. Several models from literature, multiphasic or monophasic, can be traced back to the proposed framework or, vice versa, depending on the chosen approach the framework can be particularized to give the multiphasic or the monophasic balance equations.

In this thesis, in light of its thermodynamic and numerical robustness, the monophasic approach, which is more consistent, has been chosen.

Another important question is related to the need of modeling/analyze the full behavior, mass transport plus mechanics, or just one aspect, mass transport only. The difficulties related to the solution/analysis of the full hydrogels behavior have led many researchers to describe hydrogel-based systems with a "mass transport only", to the best of my knowledge, approach. This is, in example, a must in drug delivery applications, where no one used a full model. During this PhD a mechanistic model for drug release from hydrogel-based system has been developed and validated against experimental data (Caccavo et al., 2015b, Caccavo et al., 2015a). HPMC-based tablets, loaded with Theophylline have been studied. Differently to what is normally done in dissolution tests, in this work besides the evaluation of the drug release via spectrophotometric analysis, the water and polymer residue have been determined by gravimetric analysis. This has been done on the entire tablets, as well as on portion of them, obtaining internal profiles of the components. The partially swollen tablets have been also subjected to indentation tests,

which after an opportune calibration have allowed obtaining information on the water distribution inside the system. A 2D-axisymmetric model has been built on the water and drug mass transport equations; the polymer has been obtained from the mass fraction constraint. The deformations have been described with an ALE moving mesh method, whose boundaries move in relation to the amount of water and drug entering or leaving the system. The comparison between the detailed experimental results and the modeling results has shown a good agreement, in terms of masses, shape and components distribution, demonstrating that the main features had been correctly described.

Such a formulated model has been applied to describe commercial-like tablets (in which excipients were present), with two type of HPMC with different substitution pattern (i.e. different degree of cross-links) and tested in non-standard apparatus (NMR cell) (Caccavo et al., submitted). Despite after a proper tuning the model has been able to describe the drug and polymer release, the shape and the water distribution inside the system (experimentally taken from MRI technique) have not been correctly described. This application demonstrated the limits of a "mass transport only" approach. In the analyzed case the forces acting on the swelling tablet (shear, centrifugal, gravitational) could have a relevant impact, but most of all the different degree of cross-links of the HPMC played the major role. This could dramatically change the water absorption behavior, being able to generate gels with different mechanical properties (i.e. stiffness, time of relaxation etc.) that in turn influence the mass transport. Such a relation between stiffness of the gel (stresses) and mass transport is not contemplated in a "mass transport only" approach, where it is supposed that the deformation is only driven by local mass variations, without accounting for the mechanical response. In other words the mass transport can drive deformation but stresses (internal or imposed) cannot.

In order to consider the hydrogel mechanics, the pure hydrogel behavior has been studied. Hydrogels normally couple solvent mass transport to system deformation and vice versa. This phenomenon is generally called poroelasticity and it is characteristic also of other materials (i.e. biological tissues, soils etc.). Another peculiarity of hydrogels is that the constituent polymeric network can have viscoelastic characteristics (i.e. like polymeric melts), which eventually translate in an overall hydrogel viscoelastic behavior. Depending on the time interval of interest and on the characteristic times of relaxation and diffusion, hydrogels can behave viscoelastically, poroelastically or poroviscoelastically (when the diffusion time is comparable with the relaxation time). A 3D model describing the poroviscoelastic behavior of hydrogels, still scarcely implemented in literature, has been developed within the field of non-equilibrium thermodynamics and non-linear solid mechanics (large deformations) and implemented in a commercial FEM-

based software (Caccavo and Lamberti, 2017). The results of such kind of model permit to discriminate between and to study the poroelastic and viscoelastic regime as well as it permits to study the poroviscoelastic behavior. Experimental unconfined stress-relaxation tests have been performed on agarose-gels at different concentrations with radius and height of 1 cm, and imposing a deformation of 10% (Caccavo et al., in press). In the time range analyzed (1200 s) the agarose-gel has shown a predominant viscoelastic behavior, releasing only little amount of water. The model, after an initial tuning of the parameters, has been able to fairly predict the experimental data. Characteristic of the developed approach is that, once the model parameters are derived, it is possible to describe the hydrogel subjected to different stimuli (mechanicals or chemicals).

The proposed poroviscoelastic model is extendable to multicomponent diffusion systems, which could be, in example, controlled release systems based on hydrogels. For the first time, to the author's knowledge, in the hydrogel-based systems modeling literature, in this thesis it has been shown how to extend the poroviscoelastic model to consider the presence of another diffusing species. The transport and constitutive model equations, opportunely modified, have been implemented in a commercial FEM-based software and, as an example, the drug release from a swelling system has been reported.

In conclusion, as a result of this work a deeper comprehension of hydrogel-based systems (HBSs) has been achieved, thanks to a combined experimental/modeling approach. It has been demonstrated that is not sufficient to analyze the drug release to characterize the behavior of HBSs. A complete investigation, considering the macroscopic behavior of the components as well as their distribution inside the system (microscopic behavior) should be preferred.

Along with the understanding of the hydrogel and hydrogel-based systems behavior, three important tools (mathematical models), have been produced. The 3D "mass balance only" model, which is able, with its pro e cons, to describe the active ingredient release from HBSs. The 3D poroviscoelastic model, which is able to describe the pure hydrogels behavior, coupling the solvent transport to the system large deformation. And in the end, for the first time in literature, the 3D poroviscoelastic model extended to other diffusing species, suitable for example in applications of active ingredient delivery. All these tools, properly tuned, can be of great aid in designing new systems based on hydrogels.

5.2 Perspectives

The future developments of this Ph.D. work are several, going from the improvements of the models to their applications in the different fields that exploit hydrogels.

Some work could be focused on the refinement of the proposed models. In particular, the poroviscoelastic models could be improved considering other (more realistic) elastic theories, for example the non-Gaussian theory of rubber elasticity. Moreover, a suitable equation to relate the elastic moduli with the polymer concentration, for physical gels, should be found and applied. Much complex rheological models could be considered. The mixing contribution could be further refined, upgrading the enthalpic terms and investigating the importance of the interaction parameter. The multicomponent poroviscoeleastic model, should be upgraded with the interaction terms of the active ingredient with water and polymer. The boundary conditions could be further investigated. Several independent experiments could be conceived to obtain the material/model parameters, i.e. like oscillatory rheology tests to determine the elastic moduli, free swelling tests to determine χ_{12}, and so forth.

Regarding the future applications (and practical importance) of this work, the model proposed could be applied to hydrogel-based system for active ingredient delivery (in biomedical and agro-food applications), for tissue engineering application (being here the mechanics relevant to the in situ application as well as to the cell differentiation and, the solvent/nutrient transport relevant for cell proliferation), in microfluidics applications (i.e. to design new stimuli responsive micro valves) etcetera. Therefore, the present work could be used as starting point to develop mechanistic models in almost all the sectors that use the hydrogel peculiar behavior.

Bibliography

ABRAHMSEN-ALAMI, S., KORNER, A., NILSSON, I. & LARSSON, A. 2007. New release cell for NMR microimaging of tablets. Swelling and erosion of poly(ethylene oxide). *Int J Pharm,* 342**,** 105-14.

ACHILLEOS, E. C., CHRISTODOULOU, K. N. & KEVREKIDIS, I. G. 2001. A transport model for swelling of polyelectrolyte gels in simple and complex geometries. *Computational and Theoretical Polymer Science,* 11**,** 63-80.

ACHILLEOS, E. C., PRUD'HOMME, R. K., KEVREKIDIS, I. G., CHRISTODOULOU, K. N. & GEE, K. R. 2000. Quantifying deformation in gel swelling: Experiments and simulations. *Aiche Journal,* 46**,** 2128-2139.

ALFREY, T., GURNEE, E. F. & LLOYD, W. G. 1966. Diffusion in glassy polymers. *Journal of Polymer Science Part C: Polymer Symposia,* 12**,** 249-261.

ALSOY, S. & DUDA, J. L. 2002. Influence of swelling and diffusion-induced convection on polymer sorption processes. *Aiche Journal,* 48**,** 1849-1855.

AMSDEN, B. 1998a. Solute diffusion in hydrogels.: an examination of the retardation effect. *Polymer gels and networks,* 6**,** 13-43.

AMSDEN, B. 1998b. Solute Diffusion within Hydrogels. Mechanisms and Models. *Macromolecules,* 31**,** 8382-8395.

ARGON, A. S. 2013. *The Physics of Deformation and Fracture of Polymers*, Cambridge University Press.

ARRUDA, E. M. & BOYCE, M. C. 1993. A three-dimensional constitutive model for the large stretch behavior of rubber elastic materials. *Journal of the Mechanics and Physics of Solids,* 41**,** 389-412.

BARBA, A. A., D'AMORE, M., CASCONE, S., CHIRICO, S., LAMBERTI, G. & TITOMANLIO, G. 2009a. On the behavior of HPMC/Theophylline matrices for controlled drug delivery. *Journal of Pharmaceutical Sciences,* 98**,** 4100-4110.

BARBA, A. A., D'AMORE, M., CHIRICO, S., LAMBERTI, G. & TITOMANLIO, G. 2009b. A general code to predict the drug release kinetics from different shaped matrices. *Eur J Pharm Sci,* 36**,** 359-68.

BETTINI, R., COLOMBO, P., MASSIMO, G., CATELLANI, P. L. & VITALI, T. 1994. Swelling and drug release in hydrogel matrices: polymer viscosity and matrix porosity effects. *European Journal of Pharmaceutical Sciences,* 2**,** 213-219.

BIRD, B. R., STEWART, W. E. & LIGHTFOOT, E. N. 2007. *Transport Phenomena*, Wiley & Sons Ltd.

BIRGERSSON, E., LI, H. & WU, S. 2008. Transient analysis of temperature-sensitive neutral hydrogels. *Journal of the Mechanics and Physics of Solids,* 56**,** 444-466.

BISCHOFF, J. E., ARRUDA, E. M. & GROSH, K. 2001. A new constitutive model for the compressibility of elastomers at finite deformations. *Rubber chemistry and technology,* 74**,** 541-559.

BOYCE, M. C. & ARRUDA, E. M. 2000. Constitutive models of rubber elasticity: a review. *Rubber chemistry and technology,* 73**,** 504-523.

CACCAVO, D., CASCONE, S., LAMBERTI, G. & BARBA, A. A. 2015a. Controlled drug release from hydrogel-based matrices: Experiments and modeling. *International Journal of Pharmaceutics,* 486**,** 144-52.

CACCAVO, D., CASCONE, S., LAMBERTI, G. & BARBA, A. A. 2015b. Modeling the drug release from hydrogel-based matrices. *Molecular Pharmaceutics,* 12**,** 474-83.

CACCAVO, D., CASCONE, S., LAMBERTI, G., BARBA, A. A. & LARSSON, A. 2016. Swellable Hydrogel-based Systems for Controlled Drug Delivery. *In:* SEZER, A. D. (ed.) *Smart drug delivery system.*

CACCAVO, D., CASCONE, S., LAMBERTI, G., BARBA, A. A. & LARSSON, A. 2017. Drug delivery from hydrogels: A general framework for the release modeling. *Current Drug Delivery,* 14 (2)**,** 179-189.

CACCAVO, D., CASCONE, S., POTO, S., LAMBERTI, G. & BARBA, A. A. in press. Mechanical and transport phenomena in agarose-based hydrogels studied by compression-relaxation tests. *Carbohydrate Polymers,* doi: 10.1016/j.carbpol.2017.03.027.

CACCAVO, D. & LAMBERTI, G. 2017. PoroViscoElastic model to describe hydrogels' behavior. *Materials Science and Engineering: C,* 76**,** 102–113.

CACCAVO, D., LAMBERTI, G., BARBA, A. A., ABRAHMSÉN-ALAMI, S., VIRIDÉN, A. & LARSSON, A. submitted. Effects of HPMC substituent pattern on water up-take, polymer and drug release; an experimental and modelling study. *European Journal of Pharmaceutical Sciences*.

CAMERA-RODA, G. & SARTI, G. C. 1986. Non-Fickian mass transport through polymers: A viscoelastic theory. *Transport Theory and Statistical Physics,* 15**,** 1023-1050.

CAMERA-RODA, G. & SARTI, G. C. 1990. Mass transport with relaxation in polymers. *AIChE Journal,* 36**,** 851-860.

CASCONE, S., LAMBERTI, G., TITOMANLIO, G., D'AMORE, M. & BARBA, A. A. 2014. Measurements of non-uniform water content in hydroxypropyl-methyl-cellulose based matrices via texture analysis. *Carbohydrate polymers,* 103**,** 348-354.

CHAN, E. P., HU, Y., JOHNSON, P. M., SUO, Z. & STAFFORD, C. M. 2012. Spherical indentation testing of poroelastic relaxations in thin hydrogel layers. *Soft Matter,* 8**,** 1492-1498.

CHESTER, S. A. 2012. A constitutive model for coupled fluid permeation and large viscoelastic deformation in polymeric gels. *Soft Matter,* 8**,** 8223-8233.

CHESTER, S. A. & ANAND, L. 2010. A coupled theory of fluid permeation and large deformations for elastomeric materials. *Journal of the Mechanics and Physics of Solids,* 58**,** 1879-1906.

CHIRICO, S., DALMORO, A., LAMBERTI, G., RUSSO, G. & TITOMANLIO, G. 2007. Analysis and modeling of swelling and erosion behavior for pure HPMC tablet. *Journal of Controlled Release,* 122**,** 181-188.

COLOMBO, P., BETTINI, R. & PEPPAS, N. A. 1999. Observation of swelling process and diffusion front position during swelling in hydroxypropyl methyl cellulose (HPMC) matrices containing a soluble drug. *Journal of Controlled Release,* 61**,** 83-91.

COMSOL 2013. Chapter 18. Deformed Geometry and Moving Mesh. *COMSOL Multiphysics Reference Manual VERSION 4.3b.*

DAVIDSON, G. R. & PEPPAS, N. A. 1986. Solute and penetrant diffusion in swellable polymers: VI. The Deborah and swelling interface numbers as indicators of the order of biomolecular release. *Journal of controlled release,* 3**,** 259-271.

DELAVOIPIERE, J., TRAN, Y., VERNEUIL, E. & CHATEAUMINOIS, A. 2016. Poroelastic indentation of mechanically confined hydrogel layers. *Soft Matter,* 12**,** 8049-8058.

DOI, M. 2009. Gel Dynamics. *Journal of the Physical Society of Japan,* 78**,** 052001.

DOW 2000. Using METHOCEL Cellulose Ethers for Controlled Release of Drugs in Hydrophilic Matrix Systems. U.S.A.

FENG, L., JIA, Y., CHEN, X., LI, X. & AN, L. 2010. A multiphasic model for the volume change of polyelectrolyte hydrogels. *The Journal of Chemical Physics,* 133**,** 114904(1-8).

FENG, L., JIA, Y., LI, X. & AN, L. 2011. Comparison of the multiphasic model and the transport model for the swelling and deformation of

polyelectrolyte hydrogels. *Journal of the Mechanical Behavior of Biomedical Materials,* 4**,** 1328-35.

FLORY, P. J. 1953. *Principles of Polymer Chemistry*, Cornell University.

FUJITA, H. 1961. Diffusion in polymer-diluent systems. *Fortschritte Der Hochpolymeren-Forschung.* Springer Berlin Heidelberg.

GALDI, I. & LAMBERTI, G. 2012. Drug release from matrix systems: analysis by finite element methods. *Heat and Mass Transfer,* 48**,** 519-528.

GAO, P. & FAGERNESS, P. E. 1995. Diffuision in HPMC gels. I. Determination of drug and water diffusivity by pulsed-field-gradient spin-echo NMR. *Pharmaceutical Research,* 12**,** 955-964.

GRASSI, G., HASA, D., VOINOVICH, D., PERISSUTTI, B., DAPAS, B., FARRA, R., FRANCESCHINIS, E. & GRASSI, M. 2010. Simultaneous Release and ADME Processes of Poorly Water-Soluble Drugs: Mathematical Modeling. *Molecular Pharmaceutics,* 7**,** 1488-1497.

GRASSI, G., LAPASIN, R., GRASSI, M. & COLOMBO, I. 2007a. *Understanding Drug Release and Absorption Mechanisms A Physical and Mathematical Approach*.

GRASSI, M., COLOMBO, I. & LAPASIN, R. 2001. Experimental determination of the theophylline diffusion coefficient in swollen sodium-alginate membranes. *Journal of Controlled Release,* 76**,** 93-105.

GRASSI, M., GRASSI, G., LAPASIN, R. & COLOMBO, I. 2007b. *Understanding Drug Release and Absorption Mechanisms: A Physical and Mathematical Approach*, Taylor & Francis.

GURTIN, M. E., FRIED, E. & ANAND, L. 2010. *The Mechanics and Thermodynamics of Continua,* New York, Cambridge University Press.

HIGUCHI, T. 1961. Rate of release of medicaments from ointment bases containing drugs in suspension. *Journal of Pharmaceutical Sciences,* 50**,** 874-875.

HOLZ, M., HEIL, S. R. & SACCO, A. 2000. Temperature-dependent self-diffusion coefficients of water and six selected molecular liquids for calibration in accurate 1H NMR PFG measurements. *Physical Chemistry Chemical Physics,* 2**,** 4740-4742.

HOLZAPFEL, G. A. 2000. *Nonlinear Solid Mechanics a Continuum Approach for Engineering,* Chichester, John Wiley & Sons Inc.

HONG, W., LIU, Z. & SUO, Z. 2009. Inhomogeneous swelling of a gel in equilibrium with a solvent and mechanical load. *International Journal of Solids and Structures,* 46**,** 3282-3289.

HONG, W., ZHAO, X. & SUO, Z. 2010. Large deformation and electrochemistry of polyelectrolyte gels. *Journal of the Mechanics and Physics of Solids,* 58**,** 558-577.

HONG, W., ZHAO, X., ZHOU, J. & SUO, Z. 2008. A theory of coupled diffusion and large deformation in polymeric gels. *Journal of the Mechanics and Physics of Solids,* 56**,** 1779-1793.

HORKAY, F. & MCKENNA, G. B. 2007. Chapter 29: Polymer Networks and Gels. *In:* MARK, J. E. (ed.) *Physical Properties of Polymers Handbook (Second Edition).* Springer.

HU, Y. & SUO, Z. 2012. Viscoelasticity and poroelasticity in elastomeric gels. *Acta Mechanica Solida Sinica,* 25**,** 441-458.

HU, Y., YOU, J.-O., AUGUSTE, D. T., SUO, Z. & VLASSAK, J. J. 2012. Indentation: A simple, nondestructive method for characterizing the mechanical and transport properties of pH-sensitive hydrogels. *Journal of Materials Research,* 27**,** 152-160.

JIN, Y., HOLZBECHER, E. & SAUTER, M. 2014. A novel modeling approach using arbitrary Lagrangian–Eulerian (ALE) method for the flow simulation in unconfined aquifers. *Computers & Geosciences,* 62**,** 88-94.

KANG, M. K. & HUANG, R. 2010. A Variational Approach and Finite Element Implementation for Swelling of Polymeric Hydrogels Under Geometric Constraints. *Journal of Applied Mechanics,* 77**,** 061004.

KAUNISTO, E., ABRAHMSEN-ALAMI, S., BORGQUIST, P., LARSSON, A., NILSSON, B. & AXELSSON, A. 2010. A mechanistic modelling approach to polymer dissolution using magnetic resonance microimaging. *J Control Release,* 147**,** 232-41.

KAUNISTO, E., TAJAROBI, F., ABRAHMSEN-ALAMI, S., LARSSON, A., NILSSON, B. & AXELSSON, A. 2013. Mechanistic modelling of drug release from a polymer matrix using magnetic resonance microimaging. *Eur J Pharm Sci,* 48**,** 698-708.

KIIL, S. & DAM-JOHANSEN, K. 2003. Controlled drug delivery from swellable hydroxypropylmethylcellulose matrices: model-based analysis of observed radial front movements. *Journal of Controlled Release,* 90**,** 1-21.

KÖRNER, A., PICULELL, L., ISELAU, F., WITTGREN, B. & LARSSON, A. 2009. Influence of Different Polymer Types on the Overall Release Mechanism in Hydrophilic Matrix Tablets. *Molecules,* 14**,** 2699.

KURNIA, J. C., BIRGERSSON, E. & MUJUMDAR, A. S. 2011. Computational Study of pH-sensitive Hydrogel-based Microfluidic Flow Controllers. *Journal of Functional Biomaterials,* 2**,** 195-212.

KURNIA, J. C., BIRGERSSON, E. & MUJUMDAR, A. S. 2012a. Analysis of a model for pH-sensitive hydrogels. *Polymer,* 53**,** 613-622.

KURNIA, J. C., BIRGERSSON, E. & MUJUMDAR, A. S. 2012b. Finite deformation of fast-response thermo-sensitive hydrogels – A computational study. *Polymer,* 53**,** 2500-2508.

LABROPOULOS, K. C., RANGARAJAN, S., NIESZ, D. E. & DANFORTH, S. C. 2001. Dynamic Rheology of Agar Gel Based Aqueous Binders. *Journal of the American Ceramic Society,* 84**,** 1217-1224.

LAI, W. M., HOU, J. S. & MOW, V. C. 1991. A Triphasic Theory for the Swelling and Deformation Behaviors of Articular Cartilage. *Journal of Biomechanical Engineering,* 113**,** 245-258.

LAMBERTI, G., BARBA, A. A., CASCONE, S., DALMORO, A. & CACCAVO, D. 2016. An Engineering Point of View on the Use of the Hydrogels for Pharmaceutical and Biomedical Applications. *In:* MAJEE, S. B. (ed.) *Emerging Concepts in Analysis and Applications of Hydrogels.* Intech.

LAMBERTI, G., CASCONE, S., CAFARO, M. M., TITOMANLIO, G., D'AMORE, M. & BARBA, A. A. 2013. Measurements of water content in hydroxypropyl-methyl-cellulose based hydrogels via texture analysis. *Carbohydrate Polymers,* 92**,** 765-768.

LAMBERTI, G., GALDI, I. & BARBA, A. A. 2011. Controlled release from hydrogel-based solid matrices. A model accounting for water up-take, swelling and erosion. *International Journal of Pharmaceutics,* 407**,** 78-86.

LI, H. 2009. *Smart Hydrogel Modelling*, Springer.

LI, J., HU, Y., VLASSAK, J. J. & SUO, Z. 2012. Experimental determination of equations of state for ideal elastomeric gels. *Soft Matter,* 8**,** 8121-8128.

LIN, C. C. & METTERS, A. T. 2006. Hydrogels in controlled release formulations: Network design and mathematical modeling. *Advanced Drug Delivery Reviews,* 58**,** 1379-1408.

LIU, Z., TOH, W. & NG, T. Y. 2015. Advances in Mechanics of Soft Materials: A Review of Large Deformation Behavior of Hydrogels. *International Journal of Applied Mechanics,* 07**,** 1530001.

LUCANTONIO, A., NARDINOCCHI, P. & TERESI, L. 2013. Transient analysis of swelling-induced large deformations in polymer gels. *Journal of the Mechanics and Physics of Solids,* 61**,** 205-218.

MAJEWICZ, T. G. & PODLAS, T. J. 2000. Cellulose Ethers. *Kirk-Othmer Encyclopedia of Chemical Technology.* John Wiley & Sons, Inc.

MARK, J. E. 2007. *Physical Properties of Polymers Handbook*, Springer New York.

MARK, J. E. & ERMAN, B. 2007. *Rubberlike Elasticity: A Molecular Primer*, Cambridge University Press.

MASARO, L. & ZHU, X. X. 1999. Physical models of diffusion for polymer solutions, gels and solids. *Progress in Polymer Science,* 24**,** 731-775.

MUHR, A. H. & BLANSHARD, J. M. V. 1982. Diffusion in gels. *Polymer,* 23**,** 1012-1026.

NEOGI, P. 1996. *Diffusion in Polymers*, Taylor & Francis.

NIELSEN, S. 2014. *Food analysis*, Springer Science & Business Media.

PEPPAS, N. A. 1985. Analysis of Fickian and non-Fickian drug release from polymers. *Pharm Acta Helv,* 60**,** 110-1.

PEPPAS, N. A., BURES, P., LEOBANDUNG, W. & ICHIKAWA, H. 2000. Hydrogels in pharmaceutical formulations. *European Journal of Pharmaceutics and Biopharmaceutics,* 50**,** 27-46.

PEPPAS, N. A. & SAHLIN, J. J. 1989. A simple equation for the description of solute release. III. Coupling of diffusion and relaxation. *International Journal of Pharmaceutics,* 57**,** 169-172.

RIBEIRO, A. C. F., ORTONA, O., SIMÕES, S. M. N., SANTOS, C. I. A. V., PRAZERES, P. M. R. A., VALENTE, A. J. M., LOBO, V. M. M. & BURROWS, H. D. 2006. Binary Mutual Diffusion Coefficients of Aqueous Solutions of Sucrose, Lactose, Glucose, and Fructose in the Temperature Range from (298.15 to 328.15) K. *Journal of Chemical & Engineering Data,* 51**,** 1836-1840.

RUBINSTEIN, M. & COLBY, R. H. 2003. *Polymer Physics*, OUP Oxford.

SIEPMANN, J., KRANZ, H., BODMEIER, R. & PEPPAS, N. A. 1999a. HPMC-Matrices for Controlled Drug Delivery: A New Model Combining Diffusion, Swelling, and Dissolution Mechanisms and Predicting the Release Kinetics. *Pharmaceutical Research,* 16**,** 1748-1756.

SIEPMANN, J. & PEPPAS, N. A. 2000. Hydrophilic Matrices for Controlled Drug Delivery: An Improved Mathematical Model to Predict the Resulting Drug Release Kinetics (the "sequential Layer" Model). *Pharmaceutical Research,* 17**,** 1290-1298.

SIEPMANN, J. & PEPPAS, N. A. 2001. Modeling of drug release from delivery systems based on hydroxypropyl methylcellulose (HPMC). *Advanced Drug Delivery Reviews,* 48**,** 139-157.

SIEPMANN, J., PODUAL, K., SRIWONGJANYA, M., PEPPAS, N. A. & BODMEIER, R. 1999b. A new model describing the swelling and drug release kinetics from hydroxypropyl methylcellulose tablets. *Journal of Pharmaceutical Sciences,* 88**,** 65-72.

SIEPMANN, J., SIEGEL, R. A. & RATHBONE, M. J. 2011. *Fundamentals and Applications of Controlled Release Drug Delivery*, Springer.

SIEPMANN, J. & SIEPMANN, F. 2008. Mathematical modeling of drug delivery. *Int J Pharm,* 364**,** 328-43.

SIEPMANN, J., STREUBEL, A. & PEPPAS, N. A. 2002. Understanding and Predicting Drug Delivery from Hydrophilic Matrix Tablets Using the "Sequential Layer" Model. *Pharmaceutical Research,* 19**,** 306-314.

STRÖM, A., LARSSON, A. & OKAY, O. 2015. Preparation and physical properties of hyaluronic acid-based cryogels. *Journal of Applied Polymer Science,* 132**,** n/a-n/a.

TAJAROBI, F., ABRAHMSÉN-ALAMI, S., CARLSSON, A. S. & LARSSON, A. 2009. Simultaneous probing of swelling, erosion and dissolution by NMR-microimaging—Effect of solubility of additives

on HPMC matrix tablets. *European Journal of Pharmaceutical Sciences,* 37**,** 89-97.

TRELOAR, L. R. G. 2005. *The Physics of Rubber Elasticity*, OUP Oxford.

TRITT-GOC, J., KOWALCZUK, J. & PISLEWSKI, N. 2005. Hydration of hydroxypropylmethyl cellulose: Effects of pH and molecular mass. *Acta Physica Polonica-Series A General Physics,* 108**,** 197-206.

VIRIDÉN, A. 2011. *Investigation of the functionality related characteristics of hydroxypropyl methylcellulose for the release from matrix tablets.* PhD, Chalmers University of Technology.

VIRIDÉN, A., ABRAHMSÉN-ALAMI, S., WITTGREN, B. & LARSSON, A. 2011. Release of theophylline and carbamazepine from matrix tablets – Consequences of HPMC chemical heterogeneity. *European Journal of Pharmaceutics and Biopharmaceutics,* 78**,** 470-479.

VIRIDÉN, A., LARSSON, A. & WITTGREN, B. 2010. The effect of substitution pattern of HPMC on polymer release from matrix tablets. *International Journal of Pharmaceutics,* 389**,** 147-156.

VIRIDÉN, A., WITTGREN, B., ANDERSSON, T., ABRAHMSÉN-ALAMI, S. & LARSSON, A. 2009a. Influence of Substitution Pattern on Solution Behavior of Hydroxypropyl Methylcellulose. *Biomacromolecules,* 10**,** 522-529.

VIRIDÉN, A., WITTGREN, B., ANDERSSON, T. & LARSSON, A. 2009b. The effect of chemical heterogeneity of HPMC on polymer release from matrix tablets. *European Journal of Pharmaceutical Sciences,* 36**,** 392-400.

VRENTAS, J. & DUDA, J. 1977. Diffusion in polymer–solvent systems. III. Construction of Deborah number diagrams. *Journal of Polymer Science: Polymer Physics Edition,* 15**,** 441-453.

VRENTAS, J., JARZEBSKI, C. & DUDA, J. 1975. A Deborah number for diffusion in polymer-solvent systems. *AIChE Journal,* 21**,** 894-901.

WANG, Q.-M., MOHAN, A. C., OYEN, M. L. & ZHAO, X.-H. 2014. Separating viscoelasticity and poroelasticity of gels with different length and time scales. *Acta Mechanica Sinica,* 30**,** 20-27.

WANG, X. & HONG, W. 2012. A visco-poroelastic theory for polymeric gels. *Proceedings of the Royal Society A: Mathematical, Physical and Engineering Science*.

XU, Y., JIA, Y., WANG, Z. & WANG, Z. 2013. Mathematical modeling and finite element simulation of slow release of drugs using hydrogels as carriers with various drug concentration distributions. *Journal of Pharmaceutical Sciences,* 102**,** 1532-1543.

ZHANG, J., ZHAO, X., SUO, Z. & JIANG, H. 2009. A finite element method for transient analysis of concurrent large deformation and mass transport in gels. *Journal of Applied Physics,* 105**,** 093522.

ZHAO, X., KOH, S. J. A. & SUO, Z. 2011. Nonequilibrium thermodynamics of dielectric elastomers. *International Journal of Applied Mechanics,* 03**,** 203-217.

… "*e quindi uscimmo a riveder le stelle*" …

I would like to thank my supervisor, prof. Gaetano Lamberti, for giving me the opportunity to carry out such an interesting work in his research group. Thanks for being close but distant enough in these years, letting me move the first steps in the scientific world. Thanks for having continuously stimulated my intellectual curiosity, keeping lit my interest in everything that was hydrogels related. This work has only been possible thanks to a great mentor, thank you!

I would like to thank my scientific committee: thanks to prof. Anna Angela Barba, who has closely supervised my activities; thanks to prof. Anette Larsson for all the suggestions and criticisms given during Skype meetings; thanks to prof. Juergen Siepmann for the stimulating comments on the ongoing work. It has been an honor to have such a scientific committee.

Many thanks go to the members of the Transport Phenomena and Processes group: Sara, Pietro, Lisa, Sabrina and Veronica, for all the scientific and recreational moments we shared in these years. Special thanks go to Pietro, who made lighter workdays with our lunches and to Sara, who has continuously helped and encouraged me (in her own way) during these years.

I would like to thank the most important people of my life: the family. *Grazie ai miei genitori, Luigi e Rita, per l'immenso amore dimostrato quotidianamente. Grazie a mia sorella, Vanna, per esserci sempre. Grazie ad Alessia, per aver saputo essermi vicina anche a distanza.*

Finally, I would like to thank all the people that believed and still believe in me…